Exact Solution of Surface-Volume-Surface Electric Field Integral Equation and Analysis of Its Spectral Properties

by

Md Osman Goni

A Thesis Submitted to the Faculty of Graduate Studies of

The University of Manitoba

in partial fulfillment of the requirements of the degree of

DOCTOR OF PHILOSOPHY

Department of Electrical and Computer Engineering

University of Manitoba

Winnipeg, Manitoba, Canada

Abstract

Exact solution of the Surface-Volume-Surface Electric Field Integral Equation (SVS-EFIE) is presented for the problem of radiation in the vicinity of homogeneous dielectric sphere. The solution is obtained via Galerkin Method of Moments (MoM) utilizing rotational and irrotational complete sets of orthogonal vector spherical harmonics as basis and test functions according to the Helmholtz decomposition. In this work, two types of formulations derived from single-source integral equation representation namely, SVS-EFIE-J and SVS-EFIE-M have been analyzed and solved with the MoM discretization.

Excitation in the form of radial and tangential electric dipole situated above the spherical scatterer and the electric field throughout the sphere evaluated via analytic MoM solution of the SVS-EFIE is compared against the exact classical Mie series solution. The two are shown to agree to 12 digits of accuracy upon sufficient number of basis/test functions taken in the MoM solution and the Mie series expansion. The exact solution confirms and validates the rigorous nature of the SVS-EFIE formulation. It also reveals the spectral properties of its individual operators, their products and their linear combination, as well as the spectrum of the MoM impedance matrix. It is shown that upon choosing basis and test functions in Sobolev space $H^{1/2}_{div}(S)$ for SVS-EFIE-J and $L^2(S)$ for SVS-EFIE-M, while performing the testing in the spaces $H^{-1/2}_{div}(S)$ and $L^2(S)$, respectively, S being the surface

of the sphere, the MoM impedance matrix features bounded condition number similar with analogous exact MoM solution of the surface EFIE on perfectly electrically conducting (PEC) sphere and the solution involving MoM of the surface EFIE on perfectly magnetic conductor (PMC). The selection of the proper functional spaces makes proposed SVS-EFIE formulation free of oversampling breakdown. Moreover, both the spectrum of the continuous integral operators of this new magnetic current based SVS-EFIE-M and the spectrum of its MoM impedance matrix are bounded at low frequencies for simply connected smooth dielectric scatterers.

Acknowledgments

Firstly, I would extend my sincerest gratitude to Dr. Vladimir Okhmatovski for all his support, patience and motivation during my Ph.D. program. This work would have not been completed without his guidance and inspiration. I appreciate all his contributions, expertise in the area of electromagnetics. I would like to thank my co-advisor, Dr. Joe LoVetri, for his guidance and confidence in my research work.

I would like to thank my internal examining committee: Dr. BingChen Wang and Dr. Ian Jeffrey for all their valuable time and efforts in evaluating my thesis as well as their constructive comments and feedback.

I would also like to thank my external examiner Dr. Hakan Bagci from King Abdullah University of Science and Technology for evaluation of this work.

I am grateful to all my friends and colleagues whom I have had the pleasure to work with during my studies.

I would like to express my gratitude to Natural Sciences and Engineering Research Council of Canada, University of Manitoba Faculty of Graduate Studies for providing me with sufficient funds and support to complete my research work.

Last but not the least, I would like to express my deepest gratitude to my family, my daughters and my beloved wife for their love and tremendous support and for always being there for me.

To my beloved . . .

Contents

List of Figures

List of Tables

Abbreviations

CEM	**C**omputational **E**lectromagnetic
CFIE	**C**ombined **F**ield **I**ntegral **E**quation
CPU	**C**entral **P**rocessing **U**nit
EFIE	**E**lectric **F**ield **I**ntegral **E**quation
EM	**E**lctro**M**agnetic
FDM	**F**inite **D**ifference **M**ethod
FEM	**F**inite **E**lement **M**ethod
MFIE	**M**agnetic **F**ield **I**ntegral **E**quation
MoM	**M**ethod **o**f **M**oments
PEC	**P**erfect **E**lectric **C**onductor
RWG	**R**ao-**W**ilton-**G**lisson basis functions
SD	**S**kin **D**epth
SE	**S**kin **E**ffect
SIE	**S**urface **I**ntegral **E**quation
SSIE	**S**ingle **S**ource **I**ntegral **E**quation
SVS-EFIE	**S**urface-**V**olume-**S**urface **E**lectric **F**ield **I**ntegral **E**quation
SWG	**S**chaubert-**W**ilton-**G**lisson basis functions
V-EFIE	**V**olume-**E**lectric **F**ield **I**ntegral **E**quation
VIE	**V**olume **I**ntegral **E**quation
2-D	**T**wo **D**imensional
3-D	**T**hree **D**imensional

Symbols

$\hat{\mathbf{x}}$, $\hat{\mathbf{y}}$, $\hat{\mathbf{z}}$	Unit vectors in the x, y and z directions.
$\hat{\mathbf{n}}$	Normal unit vector outward to the boundary.
$\hat{\mathbf{t}}$	Tangential unit vector to the boundary.
$\mathbf{r}$, $\mathbf{r}$	Position vectors in the Cartesian coordinate system.
ϵ_0	Permittivity of free-space.
ϵ_r	Relative complex permittivity of the scatterer.
σ	Conductivity of the scatterer.
μ_0	Permeability of free-space.
μ_r	Relative permeability of the scatterer.
k_0	Wavenumber of free-space.
k_ϵ	Wavenumber inside the scatterer.
ω	Radial frequency.
f	Frequency of operation.
$\mathtt{t}$	Time variable.
λ	Wavelength.
Γ	Gram matrix.
$\boldsymbol{E}(\mathbf{r}, \mathtt{t})$	Time domain electric-field.
$\boldsymbol{H}(\mathbf{r}, \mathtt{t})$	Time domain magnetic-field.
$\boldsymbol{B}(\mathbf{r}, \mathtt{t})$	Time domain magnetic fiux density.
$\boldsymbol{D}(\mathbf{r}, \mathtt{t})$	Time domain electric flux density.
$\boldsymbol{M}(\mathbf{r}, \mathtt{t})$	Time domain impressed magnetic current density.
$\boldsymbol{J}(\mathbf{r}, \mathtt{t})$	Time domain impressed electric current density.

$\mathbf{E}^{\text{inc}}(\mathbf{r})$	Time-harmonic incident electric field.
$\mathbf{H}^{\text{inc}}(\mathbf{r})$	Time-harmonic incident magnetic field.
$\mathbf{E}^{\text{scat}}(\mathbf{r})$	Time-harmonic scattered electric field.
$\mathbf{E}(\mathbf{r})$	Time-harmonic total electric field.
$\mathbf{H}(\mathbf{r})$	Time-harmonic total magnetic field.
$\boldsymbol{j}$	Polarization electric current density.
$\boldsymbol{m}$	Polarization magnetic current density.
$\boldsymbol{\mathcal{J}}$	Fictitious surface electric current density.
$\boldsymbol{\mathcal{M}}$	Fictitious surface magnetic current density.
$\overline{\overline{G}}_{e0}$	Dyadic electric field Green's function of free space.
$\overline{\overline{G}}_{e\epsilon}$	Dyadic electric field Green's function of homogeneous space.
∂S	Boundary contour of the 2D object.
S	Surface of the 2D object.
∂V	Boundary surface of the 3D object.
V	Volume of the 3D object.
Re	Real part.
Im	Imaginary part.
$\boldsymbol{\nabla}$	Gradient operator.
$\boldsymbol{\nabla}\cdot$	Divergence operator.
$\boldsymbol{\nabla}\times$	Curl operator.
$\boldsymbol{\nabla}\times\boldsymbol{\nabla}\times$	Curl curl operator.
$\langle\cdot\,,\cdot\rangle$	Inner product.

Chapter 1

Introduction

Computational electromagnetics (CEM) enables characterization of the physical interactions of the electromagnetic fields with complex media and objects in practically interesting scenarios. Staging corresponding physical experiments is typically the only alternative to revealing details of such interactions. The latter, however, may be expensive, not easy to handle, and in various cases impossible to set up at the current state of measurement instruments development. On the other hand, today's methods of CEM in conjunction with powerful computers enable investigation of the propagation of electromagnetic waves and scattering problems in most cases of interest. Computational scientists are devoted to continuing development of yet more efficient and powerful CEM methodologies bringing unprecedented capabilities for modelling of scattering and radiation phenomena. Such accurate and efficient numerical simulations often eliminate the need for fabrication of physical prototypes and greatly reduce the time and cost of design cycles. One class of such computational frameworks is based on the method of integral equations [51]. The latter can be formulated for scattering and radiation in the presence of complex penetrable, impenetrable, and composite structures. The key advantage offered by the integral equation solutions compared to the direct solution of the differential equations of electromagnetics [1], [2] is their ability to localize the unknown field quantities to the boundaries of the analyzed structures instead of their volumes. Discretization of the boundaries only, instead of volume in the entire space, often leads to substantial reduction of computational effort required to recover the unknown field quantities. In many important practical applications the IE formulations can also include complex environment associated with the model into the pertinent Green's function [53]. Such formulations are typically obtained using the equivalence principle representation of the electromagnetic field in the volumes of the model in terms of its tangential components on their boundaries. These tangential field components can be viewed as the weighting functions for the elementary secondary waves emanating from point sources situated at the boundaries in accord with the Hyugen's principle. Such elementary waves are known as the Green's functions [53]. They correspond to the solution of the Maxwell equations with the Dirac delta-function as a source. When the fields produced by these elementary point sources are known, the fields due to an arbitrary source can readily be obtained using the superposition principle.

For the solution of time-harmonic scattering problems on penetrable objects the following integral equations are commonly formulated. In case of the homogeneous and piecewise homogeneous scatterers, the standard formulations are the electric field integral equation (EFIE) and magnetic field integral equation (MFIE) or their linear combination known as the combined field integral equation (CFIE) [50]. Other linear combinations of the EFIE and MFIE equations and their associated extinction theorem forms are also commonly used to formulate the Muller IEs, volume integral equations for inhomogeneous penetrable scatterers [56] and the Pogglio-Miller-Chu-Harrington-Wu-Tai (PMCHWT) IEs [10], [16]. All of the above IEs feature two unknown surface functions on the boundaries of piece-wise homogeneous regions which are equivalent electric and magnetic surface current densities. Alternative two-source IE formulations include JM-CFIE, N-Mulller, and others etc. [10, 11, 13]. The above formulations have been well studied and used extensively and are the de facto standard in the method of integral equations.

In their original work [40] Maystre and Vincent showed, however, that only one fictitious current source is sufficient to represent both the electric and magnetic field in each region of interest. In such more general form of the internal equivalence principle [9], [45] the field outside a region is left non-zero and unconstrained rather than vanishing as prescribed by the extinction theorem. Similarly, for the external equivalence principle, the integral field representation can be producing a true field outside the object while leaving the field inside of it undefined and non-zero. Such definition of the fields inside the piece-wise regions of the object gave rise to the new class of the IEs suitable for solution of scattering problems on penetrable piece-wise homogeneous objects, which are known as the single-source IEs (SSIE) [45]. The benefit of having only one unknown current in the SSIEs, however, comes at the expense of a large number of integral operator products (18 operator products in the SSIE for 2D scattering problem) or presence of the operator inverses [18]–[23], [47]. Discretization of the operator products is often more involved also. For the above reasons the Single-Source-Integral-Equations (SSIEs) despite significant amount of research work done on them [14]–[17], [40], [41], [44]–[46], remain less popular than their traditional two-source counterparts.

Earlier SSIE formulations were proposed and studied by Marx [41] and Glisson [15]. These SSIEs featured hypersingular kernels and suffered from oversampling breakdown, which manifests itself in the form of increasing condition number of the MoM impedance matrix upon increase of mesh density when physics of the problem of interest (e.g. frequency) remains the same. These earlier formulations also exhibit internal resonance and are susceptible to the low frequency breakdown. Subsequently, various improvements to these formulations were proposed. Among them are the second-kind SSIEs proposed by Colliander and Yla-Oijala [12] that do not suffer from the oversampling breakdown but which are still susceptible to the internal resonances. Recent work by Cools proposed Calderon-projector based formulations of the SSIE which eliminate both the low-frequency and oversampling breakdowns for smooth dielectric objets.

The SSIEs obtained from the classical two-source equivalence principle in which one source is expressed in terms of the other through inverse of an integral operator were proposed in [18] and [47] and further developed in [22]–[24]. In [47] the extinction theorem is used to express the unknown surface magnetic current in terms of the surface electric current acted upon by the electric field operator and the inverse of the magnetic field operator. This relationship termed as the Generalized Impedance Boundary Condition upon substitution into the exterior equivalence principle produces SSIE with respect to only equivalent electric surface current density albeit with the presence of the inverse of the magnetic field operator. Stabilization of such formulation through use of loop-tree basis was also studied with the purpose of eliminating the low-frequency and oversampling breakdowns. Alternative technique for obtaining the SSIE through introduction of a surface admittance operator was developed by De Zutter and Knockaert [18]. The surface admittance operator in this formulation relates a fictitious electric surface current density at each point on the surface of the conductor to the tangential electric field (magnetic surface current density) at every other point on the surface, This operator allows to replace the object with the medium of the exterior space through introduction of the fictitious electric equivalent surface currents. Similarly with [47] this SSIE also features the inverse of an integral operator albeit without the double-layer potential contribution for the external media integral operators [24]. The latter could be handled analytically [19, 26] for conductors of canonical cross-sections or numerically through a dense matrix inverse for arbitrary shapes [22]. Recent extension to this approach was also proposed which demonstrated possibility of obtaining analytically the surface admittance operators for the arbitrary shapes through Fokas transform [27]. Low-frequency and oversampling stabilization of such SSIEs through use of augmented EFIE form of their electric field operators was recently developed by [25].

Another class of single source integral equations which neither features the large number of integral operators and their products nor the presence of the operator inverses was recently developed in our group [28]–[37], [38]–[39]. This formulation obtains the single-source integral equation by combining the ideas of single-source surface integral representation of the electromagnetic field developed in the earlier theory of the single-source integral equations [45] and the traditional volume equivalence principle. Specifically, the integral equation is obtained as a result of constraining the electric current based single-source representation of the electric field with volume integral equation (VIE). As such, it features the integral operators mapping surface functions to the volume functions and vice versa in the process of enforcing VIE on the boundary of the scatterer for tangential components of the total electric field. We termed this equation throughout this thesis as the electric current based Surface-Volume-Surface Electric Field Integral Equation (SVS-EFIE-J).

In [55] it was also hypothesized that another type of SVS-EFIE can be obtained based on magnetic current representation of the electric field in the volume of the scatterer. In this work, we term this new SSIE formulation as SVS-EFIE-M. To prove the correctness of the hypothesis we solve this new SVS-EFIE-M analytically for the case of electric dipole radiation in the vicinity of a dielectric sphere analogously with the recently developed analytic solution of SVS-EFIE-J [35] and solutions of classical surface EFIE and MFIE given in the seminal paper [60]. Besides validating the rigorous nature of the new equation, the obtained analytic solution for it reveals the spectral properties of its operators. The spectra of the SVS-EFIE-M formulation show that unlike its SVS-EFIE-J predecessor the new equation does not suffer from either the low-frequency or the oversampling breakdowns for sufficiently smooth dielectric object [35]. Moreover, we show that the inner products in the Method of Moments (MoM) discretization of the SVS-EFIE-M formulation can be performed in well-familiar and easily tractable L^2 space without jeopardizing the condition number of its matrix. This is opposite to the SVS-EFIE-J formulation as well as traditional surface integral equations containing the electric field operator and requiring the evaluation of the MoM inner products in the Sobolev space $H_{div}^{-1/2}$ [60], [35] in order to ensure that their pertinent MoM matrix condition number remains bounded upon the refinement of the mesh density or when solution is sought at low frequencies. The evaluation of such inner products in $H_{div}^{-1/2}$ space for general 3D scatterers is very difficult and hasn't been demonstrated to date. The evaluation of the inner products in L^2 functional space allowed by the proposed SVS-EFIE-M formulation, however, has been well established in the CEM community and has been routinely done in practical MoM discretizations of various integral equations. This makes the SVS-EFIE-M better suited for numerical solutions and promises to provide significantly lower condition number in the resultant matrix equations compared to either the SVS-EFIE-J formulation [35], or traditional two-source formulations such as PMCHWT, Muller, JM-CFIE [10, 11, 13], or SSIEs utilizing inverses of the integral operators [19], [23], [47].

It is important to point out that the MoM solution of the SVS-EFIE-M equation is analogous to the one implemented for the solution of SVS-EFIE-J formulation in [31] for the practical engineering scattering and radiation problems on simply connected sufficiently smooth dielectric objects and is expected to produce similar spectral properties of the MoM matrix equation as those of the continuous SVS-EFIE-M integral operator presented in this work and be free of the low-frequency and oversampling breakdowns. The theory demonstrating that the spectrum of MoM matrix mimics a sub-set of the eigenvalues of the continuous operator of the integral equation and required conditions for that can be found in [48, 49].

In this work, we compare the analytic solution of SVS-EFIE-M against the Mie series solution for the case of radial and tangential electric dipole radiation in the vicinity of a dielectric sphere. The relative error of the two solutions is shown to be at nearly machine precision level. This demonstrates the rigorous nature of the SVS-EFIE-M equation, the correctness of its analytic MoM solution, and the stability of the formulation at both low frequencies and under conditions of oversampling.

1.1 Research Scope and Contributions

The purpose of this work is twofold. First, an exact solutions of the Surface-Volume-Surface Electric Field Integral Equations (SVS-EFIE-J and SVS-EFIE-M) is presented for the problem of dipole radiation in the vicinity of the homogeneous dielectric sphere. The solution is obtained via Galerkin Method of Moments (MoM) utilizing rotational and irrotational complete sets of orthogonal vector spherical harmonics as basis and test functions according to the Helmholtz decomposition. In the case of radial or tangential electric dipole radiation, the electric field throughout the sphere evaluated via the analytic MoM solution of the SVS-EFIE is compared against the exact classical Mie series solution. The two are shown to agree to 12 digits of accuracy upon a sufficient number of basis/test functions taken in the MoM solution and the Mie series expansion. The exact solution confirms and validates the rigorous nature of both the J- and M-formulations of the SVS-EFIE.

Second, the detailed spectral analysis of SVS-EFIE-J and SVS-EFIE-M formulations is performed. It reveals the spectral properties of its individual operators, their products, and their linear combination, as well as the spectrum of the MoM impedance matrices upon discretization. It is shown that for SVS-EFIE-J upon choosing basis and test functions in Sobolev space $H^{1/2}_{div}(S)$ and performing testing inner products evaluation in the space $H^{-1/2}_{div}(S)$, S being the surface of the sphere, the MoM impedance matrix features bounded condition number with increasing order of discretization. This is similar to analogous exact MoM solution of the surface EFIE on perfectly electrically conducting (PEC) sphere. Similar analytic MoM solution of the SVS-EFIE-M formulation is also performed. It shows that upon choosing basis and test functions in $L^2(S)$ space and evaluating testing inner products in the same space, the MoM impedance matrix features bounded condition number with increasing order of discretization and/or at low frequencies. This makes the proposed SVS-EFIE-M formulation free of oversampling and low-frequency breakdowns giving an advantage both over its SVS-EFIE-J predecessor and classical double-source integral equations such as PMCHWT, Muller, and others suffering from this type of numerical instabilities inherent to their inferior spectral properties.

1.2 Structure of the Thesis

An overview of the fundamental theory in electromagnetics is given in Chapter 2 with a literature review of the primary knowledge required to conduct this research work. The integral equations are formulated through the volume equivalence principle to lay the ground for the derivation of the SVS-EFIE with J-formulation in Chapter 3. It also describes the SVS-EFIE discretization using MoM utilizing rotational and irrotational complete sets of orthogonal vector spherical harmonics as basis and test functions according to the Helmholtz decomposition. Later on, spectral properties of the SVS-EFIE-J operators are demonstrated in Chapter 3 as well. The present analysis shows how performing MoM solution in the proper functional space can in principle eliminate the oversampling and low-frequency breakdown of SVS-EFIE-J formulation. Chapter 3 is a copy of the journal article [35].

In Chapter 4, the exact solution of a new magnetic current based SVS-EFIE-M formulation is presented. The discretization of this integral equation is described in Chapter 4 as well. Later on, spectral properties of this SVS-EFIE-M are investigated. The MoM impedance matrix condition number is shown to remain bounded under the condition of the increasing discretization order n and/or at low frequencies while the SVS-EFIE-M MoM solution is performed in conventional $L^2(S)$ space with easily defined inner products. The MoM solution of the SVS-EFIE-M in $L^2(S)$ space produces an impedance matrix with a condition number that remains constant under conditions of either oversampling or low frequency analysis making it an excellent candidate for the solution of practical scattering and radiation problems. Chapter 4 is a copy of the journal article [36].

Chapter 5 summarizes the thesis and outlines the future work.

Chapter 2

Maxwell's Equations and Equivalence Principle

James Clerk Maxwell [1831-1879] introduced the displacement current into the Ampere's law. In doing so he unified the equation of electricity and magnetism into a set of four equations that became foundational to the theory and applications of electromagnetism. These four equations govern the behavior of the electric field and the magnetic field and describe how they are coupled.

2.1 Maxwell's Equations

Maxwell's equations in time domain can be expressed as follows:

$$\boldsymbol{\nabla} \cdot \boldsymbol{D}(\boldsymbol{r}, \mathtt{t}) = \rho_v(\boldsymbol{r}, \mathtt{t}), \tag{2.1}$$

$$\boldsymbol{\nabla} \cdot \boldsymbol{B}(\boldsymbol{r}, \mathtt{t}) = 0, \tag{2.2}$$

$$\boldsymbol{\nabla} \times \boldsymbol{E}(\boldsymbol{r}, \mathtt{t}) = -\frac{\partial}{\partial \mathtt{t}} \boldsymbol{B}(\boldsymbol{r}, \mathtt{t}), \tag{2.3}$$

$$\boldsymbol{\nabla} \times \boldsymbol{H}(\boldsymbol{r}, \mathtt{t}) = \boldsymbol{J}(\boldsymbol{r}, \mathtt{t}) + \frac{\partial}{\partial \mathtt{t}} \boldsymbol{D}(\boldsymbol{r}, \mathtt{t}), \tag{2.4}$$

where $\boldsymbol{E}$ and $\boldsymbol{H}$ are the electric and magnetic field intensities, $\boldsymbol{D}$ and $\boldsymbol{B}$ are the electric and magnetic flux densities, $\boldsymbol{J}$ is the electric current density, ρ_v is the total electric charge density, $\boldsymbol{r}$ is a position vector and dependence on $\mathtt{t}$ indicates that the quantity is a function of time.

The above can be expressed in spatial domain as a function of space coordinate $\boldsymbol{r}$ and angular frequency ω

$$\boldsymbol{\nabla} \cdot \boldsymbol{D}(\boldsymbol{r}) = \rho_v(\boldsymbol{r}), \tag{2.5}$$

$$\boldsymbol{\nabla} \cdot \boldsymbol{B}(\boldsymbol{r}) = 0, \tag{2.6}$$

$$\boldsymbol{\nabla} \times \boldsymbol{E}(\boldsymbol{r}) = -i\omega \boldsymbol{B}(\boldsymbol{r}), \tag{2.7}$$

$$\boldsymbol{\nabla} \times \boldsymbol{H}(\boldsymbol{r}) = \boldsymbol{J}(\boldsymbol{r}) + i\omega \boldsymbol{D}(\boldsymbol{r}), \tag{2.8}$$

where $\omega = 2\pi f$ and $i = \sqrt{-1}$. Absence of time dependence provides an indication of the complex-valued spectrum and not a real-valued function with respect to time $\mathtt{t}$.

2.2 Electromagnetic Wave Equation

An electromagnetic field satisfies the wave equation which describes the propagation of the electromagnetic wave in a vacuum or source-free space. Ampere's law and Faraday's law can be combined to introduce the wave equation that demonstrates the existence of electromagnetic waves propagating with the speed of light. For an isotropic and homogeneous medium that is characterized by permittivity ϵ and permeability μ, Maxwell's equations can be reduced to

$$\boldsymbol{\nabla} \times \boldsymbol{E} = -\mu \frac{\partial}{\partial \mathtt{t}} \boldsymbol{H}, \tag{2.9}$$

$$\boldsymbol{\nabla} \times \boldsymbol{H} = \epsilon \frac{\partial}{\partial \mathtt{t}} \boldsymbol{E}, \tag{2.10}$$

$$\nabla \cdot \boldsymbol{E} = 0, \tag{2.11}$$

$$\nabla \cdot \boldsymbol{H} = 0. \tag{2.12}$$

These are the general Maxwell's equations specialized to the case with charge and current both set to zero and is known as source-free medium. Combination of these above first-order differential equations yields a second-order differential equation in terms of $\boldsymbol{E}$ or $\boldsymbol{H}$ alone.

Taking the curl of equation (2.9) and using equation (2.10) we obtain

$$\nabla \times \nabla \times \boldsymbol{E} = -\mu \frac{\partial}{\partial \mathtt{t}} (\nabla \times \boldsymbol{H}) = -\mu\epsilon \frac{\partial^2}{\partial \mathtt{t}^2} \boldsymbol{E}. \tag{2.13}$$

Using the following vector identity

$$\nabla \times \nabla \times \boldsymbol{E} = \nabla(\nabla \cdot \boldsymbol{E}) - \nabla^2 \boldsymbol{E}, \tag{2.14}$$

Using (2.11) in source-free region (i.e. where $\nabla \cdot \boldsymbol{D} = \rho_e = 0$), yields

$$\nabla \times \nabla \times \boldsymbol{E} = -\nabla^2 \boldsymbol{E}. \tag{2.15}$$

Equation (2.13) can be rewritten as vector wave equation for the time-domain electric field as

$$\nabla^2 \boldsymbol{E}(\boldsymbol{r}, \mathtt{t}) - \frac{1}{c^2} \frac{\partial^2}{\partial \mathtt{t}^2} \boldsymbol{E}(\boldsymbol{r}, \mathtt{t}) = 0, \tag{2.16}$$

where $c = 1/\sqrt{\mu\epsilon}$ is the speed of light in the medium.

In the spectral domain the above equation reduces to the Helmholtz equation governing the electric field spectrum $\boldsymbol{E}(\boldsymbol{r})$

$$\nabla^2 \boldsymbol{E}(\boldsymbol{r}) + k^2 \boldsymbol{E}(\boldsymbol{r}) = 0, \tag{2.17}$$

where $k = \omega\sqrt{\epsilon\mu}$ is the wave number of the medium.

2.3 Green's Function

To illustrate the Green's function, consider the electrostatic potential at observation point $\boldsymbol{r}$ produced by a point electric charge q placed at location $\boldsymbol{r}'$ in free space

$$\phi = \frac{q}{4\pi\epsilon_0|\boldsymbol{r}-\boldsymbol{r}'|} \ , \tag{2.18}$$

where $|\boldsymbol{r}-\boldsymbol{r}'|$ denotes the distance between observation point $\boldsymbol{r}$ and source point $\boldsymbol{r}'$ and $\epsilon_0 = 8.854 \times 10^{-12}$ Farad/m is a constant called permittivity of free space.

The potential produced by a point source of unit strength is called the Green's function

$$G(\boldsymbol{r},\boldsymbol{r}') = \frac{1}{4\pi\epsilon_0|\boldsymbol{r}-\boldsymbol{r}'|} \ , \tag{2.19}$$

where $G(\boldsymbol{r},\boldsymbol{r}')$ is the scalar electrostatic Green's function.

In electromagnetics, both the source (electric current density) and the response (electric or magnetic field) are vectors. Each component of an electric current density in general produces all three components of the electric or magnetic field. The dyadic Green's function describes the three components of the field produced by each of the three components of the point current source (dipole) in a compact form of a (3×3) matrix containing the nine scalar Green's functions describing each field component to current relationship [53]. For the electric field produced by the electric dipole (vector point source of unit strength) the dyadic Green's function is the following

$$\bar{\bar{G}}_{e0}(\boldsymbol{r},\boldsymbol{r}') = \left(\frac{\boldsymbol{\nabla\nabla}}{k_0^2} + \bar{\bar{I}}\right) G_0(\boldsymbol{r},\boldsymbol{r}'), \tag{2.20}$$

where k_0 is the wave number in the vacuum and $\bar{\bar{I}}$ is idem factor (unit dyad).

The magnetic field dyadic Green's function (magnetic field produced by electric dipole of unit strength) in free space is

$$\bar{\bar{G}}_{m0}(\boldsymbol{r}, \boldsymbol{r}') = \boldsymbol{\nabla} \times \bar{\bar{G}}_{e0}(\boldsymbol{r}, \boldsymbol{r}'). \tag{2.21}$$

2.4 Equivalence Principle: Extinction Theorem

The classical surface integral equations on penetrable objects are derived through the application of the Green's theorem [53] to the volumes inside and outside the scatterer. The integral representation of the field inside the scatterer results in the vanishing field outside of it according to the extinction theorem [52]. Dually, the integral representation of the field outside the scatterer produces zero field inside of it. In both of these traditional integral field representations, the equivalent electric and magnetic surface currents of the scatterer are the tangential components of the magnetic and electric fields, respectively.

Consider the problem in Fig. 2.1 of an object with arbitrary shape situated in a homogeneous medium. The object is excited by incident field $\boldsymbol{E}^{inc}$ and it has complex relative permittivity and relative magnetic permeability ϵ and μ, respectively. The normal vector $\hat{\boldsymbol{n}}$ points outward from volume V and ∂V is the boundary of that volume.

The equivalence principle integral representation of the electric field in region V is demonstrated by application of the second dyadic Green's theorem to the volume V inside the scatterer

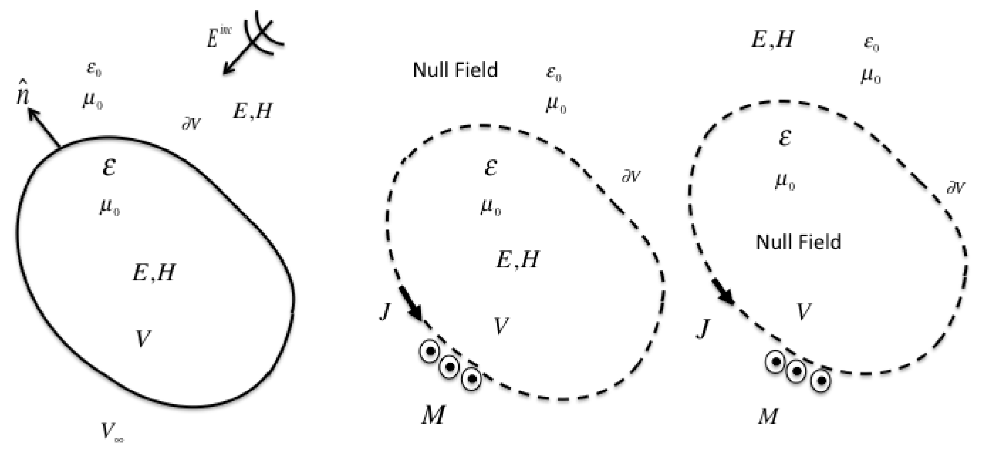

FIGURE 2.1: Scattering problem of an arbitrary non-magnetic dielectric object with incident field $\boldsymbol{E}^{inc}$ (left). The equivalent problem of the interior field (middle). The equivalent problem of the exterior field (right).

$$\begin{aligned} & i\omega\mu \int_{\partial V} \bar{\bar{G}}_{e\epsilon\mu}(\boldsymbol{r},\boldsymbol{r}') \cdot \boldsymbol{J}(\boldsymbol{r}')\, dr' \\ & + \int_{\partial V} \bar{\bar{G}}_{m\epsilon\mu}(\boldsymbol{r},\boldsymbol{r}') \cdot \boldsymbol{M}(\boldsymbol{r}')\, dr' = \begin{cases} \boldsymbol{0}, & \boldsymbol{r} \in V_\infty \setminus \partial V, \\ \boldsymbol{E}(\boldsymbol{r}), & \boldsymbol{r} \in V \setminus \partial V, \end{cases} \end{aligned} \tag{2.22}$$

$$\begin{aligned} & - \int_{\partial V} \bar{\bar{G}}_{m\epsilon\mu}(\boldsymbol{r},\boldsymbol{r}') \cdot \boldsymbol{J}(\boldsymbol{r}')\, dr' \\ & + i\omega\epsilon \int_{\partial V} \bar{\bar{G}}_{e\epsilon\mu}(\boldsymbol{r},\boldsymbol{r}') \cdot \boldsymbol{M}(\boldsymbol{r}')\, dr' = \begin{cases} \boldsymbol{0}, & \boldsymbol{r} \in V_\infty \setminus \partial V, \\ \boldsymbol{H}(\boldsymbol{r}), & \boldsymbol{r} \in V \setminus \partial V, \end{cases} \end{aligned} \tag{2.23}$$

where dyadic Green's functions in region V satisfies inhomogeneous dyadic curl-curl equation:

$$\boldsymbol{\nabla}\times\boldsymbol{\nabla}\times\bar{\bar{G}}_{e\epsilon\mu}(\boldsymbol{r},\boldsymbol{r}')-\omega^2\mu\epsilon\bar{\bar{G}}_{e\epsilon\mu}(\boldsymbol{r},\boldsymbol{r}')=\bar{\bar{I}}\delta(\boldsymbol{r},\boldsymbol{r}'), \tag{2.24}$$

and $\boldsymbol{J},\boldsymbol{M}$ are equivalent sources

$$\boldsymbol{J}=\hat{\mathbf{n}}\times\boldsymbol{H}, \tag{2.25}$$

$$\boldsymbol{M}=-\hat{\mathbf{n}}\times\boldsymbol{E}, \tag{2.26}$$

formed on the volume boundary ∂V. The equivalent surface electric current $\boldsymbol{J}$ is defined as the tangential component of the true magnetic field on ∂V, while the equivalent magnetic current $\boldsymbol{M}$ is defined as the tangential component of the true electric field on ∂V. These currents radiate in a homogeneous medium with ϵ and μ to produce the scattered fields internal to volume V.

The equivalence principle integral representation of the electric field in external region V_∞ is obtained through the application of the second dyadic Green's theorem to the volume V_∞ outside the scatterer

$$\begin{aligned}&\boldsymbol{E}^{inc}(\boldsymbol{r})-i\omega\mu_0\int\limits_{\partial V}\bar{\bar{G}}_{e0}(\boldsymbol{r},\boldsymbol{r}')\cdot\boldsymbol{J}(\boldsymbol{r}')\;dr'\\&-\int\limits_{\partial V}\bar{\bar{G}}_{m0}(\boldsymbol{r},\boldsymbol{r}')\cdot\boldsymbol{M}(\boldsymbol{r}')\;dr'=\begin{cases}\boldsymbol{E}(\boldsymbol{r}), & \boldsymbol{r}\in V_\infty\setminus\partial V,\\ \mathbf{0}, & \boldsymbol{r}\in V\setminus\partial V,\end{cases}\end{aligned} \tag{2.27}$$

$$\begin{aligned}&\boldsymbol{H}^{inc}(\boldsymbol{r})+\int\limits_{\partial V}\bar{\bar{G}}_{m0}(\boldsymbol{r},\boldsymbol{r}')\cdot\boldsymbol{J}(\boldsymbol{r}')\;dr'\\&-i\omega\epsilon_0\int\limits_{\partial V}\bar{\bar{G}}_{e0}(\boldsymbol{r},\boldsymbol{r}')\cdot\boldsymbol{M}(\boldsymbol{r}')\;dr'=\begin{cases}\boldsymbol{H}(\boldsymbol{r}), & \boldsymbol{r}\in V_\infty\setminus\partial V,\\ \mathbf{0}, & \boldsymbol{r}\in V\setminus\partial V,\end{cases}\end{aligned} \tag{2.28}$$

where dyadic Green's functions in region V_∞ satisfies inhomogeneous dyadic wave equation:

$$\boldsymbol{\nabla}\times\boldsymbol{\nabla}\times\bar{\bar{G}}_{e0}(\boldsymbol{r},\boldsymbol{r}')-\omega^2\mu_0\epsilon_0\bar{\bar{G}}_{e0}(\boldsymbol{r},\boldsymbol{r}')=\bar{\bar{I}}\delta(\boldsymbol{r},\boldsymbol{r}'). \tag{2.29}$$

The magnetic field dyadic Green's function in free space with relative permittivity ϵ_0 and permeability μ_0 is $\bar{\bar{G}}_{m0} = \boldsymbol{\nabla} \times \bar{\bar{G}}_{e0}$.

The equivalence principle can be applied to develop two models for this problem, one is the equivalent problem of the interior field and the other model is the equivalent problem of the exterior field [45].

The equivalent problem of the interior field is illustrated in the middle of Fig. 2.1 where the excitation field $\boldsymbol{E^{inc}}$ is provided.

Similarly, the equivalent problem of the exterior field is illustrated at the right of Fig. 2.1. The incident field $\boldsymbol{E^{inc}}$ is provided, and the equivalent sources on the boundary $\boldsymbol{J}, \boldsymbol{M}$ are also formed. Those sources radiate in a homogeneous medium with ϵ_0, μ_0 to produce the scattered fields $\boldsymbol{E}, \boldsymbol{H}$ external to V.

The equivalence principle integral representation of the electric field in region V is demonstrated by application of the second dyadic Green's theorem applied to the volume V inside the scatterer

$$\begin{aligned} & i\omega\mu \int\limits_{\partial V} \bar{\bar{G}}_{e\epsilon\mu}(\boldsymbol{r}, \boldsymbol{r}') \cdot \boldsymbol{J}(\boldsymbol{r}')\ dr' \\ & + \int\limits_{\partial V} \bar{\bar{G}}_{m\epsilon\mu}(\boldsymbol{r}, \boldsymbol{r}') \cdot \boldsymbol{M}(\boldsymbol{r}')\ dr' = \begin{cases} \mathbf{0}, & \boldsymbol{r} \in V_\infty \setminus \partial V, \\ \boldsymbol{E}(\boldsymbol{r}), & \boldsymbol{r} \in V \setminus \partial V, \end{cases} \end{aligned} \tag{2.30}$$

$$\begin{aligned} & - \int\limits_{\partial V} \bar{\bar{G}}_{m\epsilon\mu}(\boldsymbol{r}, \boldsymbol{r}') \cdot \boldsymbol{J}(\boldsymbol{r}')\ dr' \\ & + i\omega\epsilon \int\limits_{\partial V} \bar{\bar{G}}_{e\epsilon\mu}(\boldsymbol{r}, \boldsymbol{r}') \cdot \boldsymbol{M}(\boldsymbol{r}')\ dr' = \begin{cases} \mathbf{0}, & \boldsymbol{r} \in V_\infty \setminus \partial V, \\ \boldsymbol{H}(\boldsymbol{r}), & \boldsymbol{r} \in V \setminus \partial V, \end{cases} \end{aligned} \tag{2.31}$$

where dyadic Green's functions in region V satisfies inhomogeneous dyadic wave equation:

$$\nabla \times \nabla \times \bar{\bar{G}}_{e\epsilon\mu}(\boldsymbol{r}, \boldsymbol{r}') - \omega^2 \mu\epsilon \bar{\bar{G}}_{e\epsilon\mu}(\boldsymbol{r}, \boldsymbol{r}') = \bar{\bar{I}}\delta(\boldsymbol{r}, \boldsymbol{r}'). \tag{2.32}$$

The previous equations state different forms of equivalence principle integral representation. The exterior equivalence principle is applied to volume V_∞ outside the scatterer where the fields vanish through region V as it is illustrated in (2.27) and (2.28). The right-hand side is zero when the observation point is located inside V. Similarly, when the interior equivalence principle is applied to V inside the scatterer, then null fields are produced in the region V_∞ as it is shown in (2.30) and (2.31). The right-hand side is zero when the observation point is located outside V.
Matching the exterior and interior electric field representation yields the electric field integral equation (EFIE) while matching the interior and exterior magnetic field representations gives the magnetic field integral equation (MFIE).
The linear combination of the electric and magnetic integral equation introduces the combined field integral equation (CFIE).

2.4.1 Generalized equivalence principle

A more general form of the equivalence principle is presented in [45]. For the internal equivalence principle, the field outside the scatterer can be left non-zero and unconstrained rather than vanishing as prescribed by the extinction theorem. Similarly, for the external equivalence principle, the integral field representation can be producing a true field outside the object while leaving the field inside of it undefined and non-zero.

The equivalent surface currents on the boundary of the scatterer must be equal to the jump in the tangential components of the field inside and outside of it. Since the field in one of the regions remains unconstrained (arbitrary), the equivalent currents on the boundary become, arbitrary as well in the sense that they are no longer equal to the tangential components of the true field. Indeed, the uniqueness theorem still requires that the field in the regions are to be produced by the tangential components of the true electric and/or magnetic field. Hence, these arbitrary equivalent currents must contain contributions of the tangential components of the true field. However, the ambiguity of the field on one side of the boundary allows us to treat the equivalent currents as arbitrary functions (fictitious currents) unrelated to the tangential components of the true field.

The interior equivalent integral forms in (2.30) and (2.31) force the electric and magnetic fields outside scatterer to vanish, while it can be allowed to be arbitrary. Hence, the following internal equivalent integral representations

$$\begin{aligned} &i\omega\mu \int_{\partial V} \bar{\bar{G}}_{e\epsilon\mu}(\boldsymbol{r}, \boldsymbol{r}') \cdot \boldsymbol{J}(\boldsymbol{r}')\, dr' \\ &+ \int_{\partial V} \bar{\bar{G}}_{m\epsilon\mu}(\boldsymbol{r}, \boldsymbol{r}') \cdot \boldsymbol{M}(\boldsymbol{r}')\, dr' = \begin{cases} \boldsymbol{E}_{out}(\boldsymbol{r}), & \boldsymbol{r} \in V_\infty \setminus \partial V, \\ \boldsymbol{E}(\boldsymbol{r}), & \boldsymbol{r} \in V \setminus \partial V, \end{cases} \end{aligned} \tag{2.33}$$

$$\begin{aligned} &- \int_{\partial V} \bar{\bar{G}}_{m\epsilon\mu}(\boldsymbol{r}, \boldsymbol{r}') \cdot \boldsymbol{J}(\boldsymbol{r}')\, dr' \\ &+ i\omega\epsilon \int_{\partial V} \bar{\bar{G}}_{e\epsilon\mu}(\boldsymbol{r}, \boldsymbol{r}') \cdot \boldsymbol{M}(\boldsymbol{r}')\, dr' = \begin{cases} \boldsymbol{H}_{out}(\boldsymbol{r}), & \boldsymbol{r} \in V_\infty \setminus \partial V, \\ \boldsymbol{H}(\boldsymbol{r}), & \boldsymbol{r} \in V \setminus \partial V, \end{cases} \end{aligned} \tag{2.34}$$

are obtained, where the equivalent surface sources are defined as equivalent currents defined on the boundary to be the difference between the tangential component of the true field $\boldsymbol{H}$ inside the scatterer and the arbitrary Maxwellian magnetic field $\boldsymbol{H}_{out}$ that is specified outside scatterer:

$$\boldsymbol{J} = \hat{\mathbf{n}} \times (\boldsymbol{H} - \boldsymbol{H}_{out}), \tag{2.35}$$

$$\boldsymbol{M} = (\boldsymbol{E} - \boldsymbol{E}_{out}) \times \hat{\mathbf{n}}, \tag{2.36}$$

$\hat{\mathbf{n}}$ being the inward normal to V. Similarly, the external equivalence principle field representations become

$$\begin{aligned} &\boldsymbol{E}^{inc}(\boldsymbol{r}) - i\omega\mu_0 \int\limits_{\partial V} \bar{\bar{G}}_{e0}(\boldsymbol{r},\boldsymbol{r}') \cdot \boldsymbol{J}(\boldsymbol{r}')\ dr' \\ &- \int\limits_{\partial V} \bar{\bar{G}}_{m0}(\boldsymbol{r},\boldsymbol{r}') \cdot \boldsymbol{M}(\boldsymbol{r}')\ dr' = \begin{cases} \boldsymbol{E}(\boldsymbol{r}), & \boldsymbol{r} \in V_\infty \setminus \partial V, \\ \boldsymbol{E}_{in}(\boldsymbol{r}), & \boldsymbol{r} \in V \setminus \partial V, \end{cases} \end{aligned} \tag{2.37}$$

$$\begin{aligned} &\boldsymbol{H}^{inc}(\boldsymbol{r}) + \int\limits_{\partial V} \bar{\bar{G}}_{m0}(\boldsymbol{r},\boldsymbol{r}') \cdot \boldsymbol{J}(\boldsymbol{r}')\ dr' \\ &- i\omega\epsilon_0 \int\limits_{\partial V} \bar{\bar{G}}_{e0}(\boldsymbol{r},\boldsymbol{r}') \cdot \boldsymbol{M}(\boldsymbol{r}')\ dr' = \begin{cases} \boldsymbol{H}(\boldsymbol{r}), & \boldsymbol{r} \in V_\infty \setminus \partial V, \\ \boldsymbol{H}_{in}(\boldsymbol{r}), & \boldsymbol{r} \in V \setminus \partial V. \end{cases} \end{aligned} \tag{2.38}$$

where the fictitious magnetic current $\boldsymbol{M}$ is defined to be the difference between the tangential component of the true field $\boldsymbol{E}$ outside the scatterer and the arbitrary Maxwellian electric field $\boldsymbol{E}_{out}$ that is specified insider the scatterer [45]

$$\boldsymbol{J} = \hat{\mathbf{n}} \times (\boldsymbol{H} - \boldsymbol{H}_{in}), \tag{2.39}$$

$$\boldsymbol{M} = (\boldsymbol{E} - \boldsymbol{E}_{in}) \times \hat{\mathbf{n}}, \tag{2.40}$$

$\hat{\mathbf{n}}$ being the outward normal to V.

2.5 Single-Source Integral Field Representations

A single source integral field representations are formulated with a single unknown current density instead. The ambiguity in the definition of auxiliary fields in (2.37) leads the fictitious equivalent electric current $\boldsymbol{J}$ and the fictitious equivalent magnetic current $\boldsymbol{M}$, which can be related as $\boldsymbol{J} = \mathtt{a}\boldsymbol{J}_0$ and $\boldsymbol{M} = \mathtt{b}\hat{\boldsymbol{n}} \times \boldsymbol{J}_0$, where $\mathtt{a}$ and $\mathtt{b}$ are arbitrary constants.

Substituting the single fictitious current into the general representation of exterior equivalence principle (2.37) and (2.38) yields single-source field representation in region V_∞ that is

$$\begin{aligned} &\boldsymbol{E}^{inc}(\boldsymbol{r}) - i\omega\mu_0 \int_{\partial V} \bar{\bar{G}}_{e0}(\boldsymbol{r},\boldsymbol{r}') \cdot \mathtt{a}\boldsymbol{J}_0(\boldsymbol{r}')\ dr' \\ &- \int_{\partial V} \bar{\bar{G}}_{m0}(\boldsymbol{r},\boldsymbol{r}') \cdot \mathtt{b}\hat{\boldsymbol{n}} \times \boldsymbol{J}_0(\boldsymbol{r}')\ dr' = \begin{cases} \boldsymbol{E}(\boldsymbol{r}), & \boldsymbol{r} \in V_\infty \setminus \partial V, \\ \boldsymbol{E}_{in}(\boldsymbol{r}), & \boldsymbol{r} \in V \setminus \partial V, \end{cases} \end{aligned} \tag{2.41}$$

$$\begin{aligned} &\boldsymbol{H}^{inc}(\boldsymbol{r}) + \int_{\partial V} \bar{\bar{G}}_{m0}(\boldsymbol{r},\boldsymbol{r}') \cdot \mathtt{a}\boldsymbol{J}_0(\boldsymbol{r}')\ dr' \\ &- i\omega\epsilon_0 \int_{\partial V} \bar{\bar{G}}_{e0}(\boldsymbol{r},\boldsymbol{r}') \cdot \mathtt{b}\hat{\boldsymbol{n}} \times \boldsymbol{J}_0(\boldsymbol{r}')\ dr' = \begin{cases} \boldsymbol{H}(\boldsymbol{r}), & \boldsymbol{r} \in V_\infty \setminus \partial V, \\ \boldsymbol{H}_{in}(\boldsymbol{r}), & \boldsymbol{r} \in V \setminus \partial V. \end{cases} \end{aligned} \tag{2.42}$$

In a similar manner, upon substitution into the generalized representation of interior equivalent field (2.33) and (2.34) for $\boldsymbol{J}$ and $\boldsymbol{M}$ in terms of single fictitious current, the single-source field representation in a region V is expressed as follows:

$$\begin{aligned} &i\omega\mu \int_{\partial V} \bar{\bar{G}}_{e\epsilon\mu}(\boldsymbol{r},\boldsymbol{r}') \cdot \mathtt{a}\boldsymbol{J}_0(\boldsymbol{r}')\ dr' \\ &+ \int_{\partial V} \bar{\bar{G}}_{m\epsilon\mu}(\boldsymbol{r},\boldsymbol{r}') \cdot \mathtt{b}\hat{\boldsymbol{n}} \times \boldsymbol{J}_0(\boldsymbol{r}')\ dr' = \begin{cases} \boldsymbol{E}_{out}(\boldsymbol{r}), & \boldsymbol{r} \in V_\infty \setminus \partial V, \\ \boldsymbol{E}(\boldsymbol{r}), & \boldsymbol{r} \in V \setminus \partial V, \end{cases} \end{aligned} \tag{2.43}$$

$$\begin{aligned} &- \int_{\partial V} \bar{\bar{G}}_{m\epsilon\mu}(\boldsymbol{r},\boldsymbol{r}') \cdot \mathtt{a}\boldsymbol{J}_0(\boldsymbol{r}')\ dr' \\ &+ i\omega\epsilon \int_{\partial V} \bar{\bar{G}}_{e\epsilon\mu}(\boldsymbol{r},\boldsymbol{r}') \cdot \mathtt{b}\hat{\boldsymbol{n}} \times \boldsymbol{J}_0(\boldsymbol{r}')\ dr' = \begin{cases} \boldsymbol{H}_{out}(\boldsymbol{r}), & \boldsymbol{r} \in V_\infty \setminus \partial V, \\ \boldsymbol{H}(\boldsymbol{r}), & \boldsymbol{r} \in V \setminus \partial V. \end{cases} \end{aligned} \tag{2.44}$$

2.6 Function Spaces

When the solution of the boundary value problem is required to be unique, the function and the derivative of the function need to be square integrable in a bounded domain, so that the energy in terms of the solution in any bounded domain should be finite. For the interior problem, this solution space is denoted by $H^1(V)$, and for the exterior problems $H^1(V_\infty)$. The superscript "1" denotes the derivatives up to order one were square integrable or in general, $H^m(V)$ sets the function in V whose derivative up to order m were square integrable. Notice that, $H^0(V) = L_2(V)$. These all boundary values functions in $H^1(V)$ or $H^1(V_\infty)$ form a space called Sobolev space, $H^{1/2}(S)$ which is smaller than $L_2(S)$. Hence, not all functions in $L_2(S)$ may be extended from the boundary S to the domain V or V_∞ in such a way that the function itself or its derivatives are square integrable in V or all bounded subdomains of V_∞. This space $H^{1/2}(S)$ is also known as a Hilbert space.

The obvious generalization of $H^{1/2}(S)$ is $H^{m+1/2}(S)$ for nonnegative integer m, by which is meant the set of all functions on S whose tangential derivatives up to mth order are square integrable, and whose mth order tangential derivatives are also in $H^{1/2}(S)$. These inner products and norms in $H^{m+1/2}(S)$ are more difficult to compute than those in L^2 , but it is still possible to do so.

The electromagnetic fields $\boldsymbol{E}_\pm$ and $\boldsymbol{H}_\pm$, whose curls and divergences are locally square integrable, have boundary values at least in $H^{-1/2}(S)$. Since all the components of $\boldsymbol{E}_\pm$ and $\boldsymbol{H}_\pm$ are in $H^{-1/2}(S)$, the tangential divergence of the tangential components are also in this same space. It has shown in [36] in [60]), that if $\boldsymbol{v} \in H(curl, V)$ then $\hat{\boldsymbol{n}} \times \boldsymbol{v} \in H^{1/2}(S)$ and if $\boldsymbol{v} \in H(div, V)$ then $\hat{\boldsymbol{n}} \cdot \boldsymbol{v} \in H^{-1/2}(S)$. In general, this is the fundamental function space for tangential components of electromagnetic fields on smooth surfaces S.

2.7 Approaches to Error Analysis

There are two main categories of error analysis in numerical electromagnetics: First, theoretical method, which can be pursued exclusively by the numerical analysis community, through the investigation of fundamental theorems and operator theory.

This approach has resulted in the asymptotic solution for the error estimation. Second method known as empirical approach which involves comparison of results with existing standard results or measured data as a benchmarks for which an analytical solution is available. In order to predict or improve the accuracy and efficiency of a numerical method, physical behaviour of the fields needs to be analyzed properly.

Asymptotic error estimation relies on the study of Laplace's equation and Sobolev space theory. The goal of this error estimations are to prove the convergence of the numerical solution upon mesh refinement which further dictates the asymptotic convergence rate and required preconditioners that reduces the computational costs and order. This would require estimations of solution error and condition number for the moment matrix.

Physical properties of the scattering problem determine the smoothness of the surface current. The ability of the basis functions to represent functions of the given smoothness class then determines a solution error estimate of the form

$$||\hat{\boldsymbol{J}} - \boldsymbol{J}||_{H^s} \leq ch^{\alpha} \tag{2.45}$$

for 2D problems. The parameter α is the order of convergence of the numerical method

The norm in (2.45) is the Sobolev norm associated with the space of functions of the smoothness class to which the surface current $\boldsymbol{J}$ belongs. The Sobolev norm is an alternative to the scattering amplitude in obtaining a scalar quantity which is finite for singular currents and can be used to quantify numerical error. On the real line, the Sobolev norm can be interpreted in the Fourier domain as a weighted norm, so that

$$||u||_{H^s} = \int_{\infty}^{\infty} dk(1 + |k|)^{2s}|U(k)|^2 \tag{2.46}$$

where $U(k)$ is the Fourier transform of $u(x)$ and $s = \pm 1/2$. The space of functions for which this norm is finite is denoted by H^s. For $s = 1/2$, the space $H^{1/2}$ is smaller than the square integrable function space L^2, and consists of functions smooth enough that the decay of $U(k)$ for large $|k|$ offsets the growth of the weight function. For $s = -1/2$, the weight function acts as a smoothing term, so that functions which are less smooth than L^2 functions belong to the space $H^{1/2}$.

Chapter 3

Analytic Solution of Surface-Volume-Surface Electric Field Integral Equation on Dielectric Sphere and Analysis of Its Spectral Properties

3.1 SVS-EFIE: Introduction

The Surface-Volume-Surface Electric Field Integral Equation (SVS-EFIE) was initially introduces for solution of scalar 2D magneto-quasi-static problems in [28] and 2D scalar full-wave scattering problems in [29]. Its subsequent generalization to the vector full-wave scattering problems in 2D [30] and 3D [31] opened possibilities for solution of practical scattering and radiation problems on general composite dielectric [32], [33] and metal-dielectric objects [34] including those embedded in planar layered medium [37]–[39].

The SVS-EFIE is a single-source integral equation [45], which is formed through constraining of a single-source field representation with the volume equivalence principle [52] enforced on the boundary of the scatterer but only for the tangential component of the total electric field. The single-source representations of the fields are somewhat unusual mathematical constructs as they represent the internal and external fields via fictitious surface current density on the scatterer boundary using either a single-layer ansatz, double-layer ansatz, or both [45], [54]. This is opposed to a more familiar surface equivalence principle expressing such fields in terms of their tangential components on the boundary and making the presence of both the single- and double-layer potentials a must in representation of the fields. The volume equivalence principle and the Volume-EFIE (V-EFIE) it produces, despite their wide use by the electromagnetics practitioners [56], [57] and proofs of validity [58] are not devoid of controversy[1] either as their validity at the boundary of scatterer is questionable unless the permittivity of the scatterer is considered to be a continuous function tending to the permittivity of the external medium (Sec. 2.10, [59]). Naturally, the unorthodox way of forming SVS-EFIE through constraining of a single-source field representation with the V-EFIE enforced at the boundary of the scatterer under condition of the jump in the permittivity at the boundary may cause some degree of skepticism.

In order to validate the rigorous nature of the SVS-EFIE we performed its exact solution for a homogeneous spherical scatterer using Galerkin MoM with a complete set of orthogonal rotational and irrotational spherical functions introduced on the surface of the sphere by analogy with how the exact solution of the traditional surface

[1]Thanks to Dr. S. Skobelev for bringing our attention to these issues.

EFIE (S-EFIE) and MFIE was obtained for PEC sphere in [60]. Using the addition theorem based decomposition of the electric field dyadic Green's function into vector spherical functions [60], [61] and orthogonality of the vector spherical harmonics, the inner products arising from the Galerkin MoM solution of the SVS-EFIE can be evaluated exactly. This produces infinite-dimensional diagonal system of linear algebraic equations (SLAE) with respect to the coefficients in the fictitious current expansion over surface vector spherical functions. Due to diagonal nature of the resultant SLAE each coefficient in the current expansion can be expressed as the ratio of a corresponding spherical harmonic expansion coefficient in the excitation vector element and its corresponding diagonal matrix element which are both available in either closed form or the form of 1D integrals [63]. This provides the formal exact solution for the fictitious current playing the role of the unknown function in the SVS-EFIE in the form of infinite series over rotational and irrotational set of surface vector spherical functions. The expansion is truncated depending on the desired accuracy of the solution. Upon substitution of the fictitious current solution into the single source field representation inside the sphere we can obtain exact expressions for the electric and magnetic field components. The latter are numerically compared to the classical Mie series solution of the radial electric or magnetic dipole radiation problem in the presence of the dielectric sphere [52]. Upon sufficient number of terms retained in the MoM solution of the SVS-EFIE and Mie series the two are shown to agree to 12 digits of accuracy, hence, validating the SVS-EFIE formulation.

Another important benefit of the obtained analytic solution of the SVS-EFIE is that it allows not only to reveal the spectral properties of its integral operators, their products, and their superposition but also to determine the space, in which Galerkin testing must be performed in order to maintain bounded condition number of the resultant MoM impedance matrix. Since SVS-EFIE features $\mathcal{T}$-operator of the classical S-EFIE, it is shown that Galerkin testing should be performed in the same Sobolev space $H_{div}^{-1/2}(S)$, S being the surface of the sphere, as the Galerkin testing of S-EFIE [60]. If such testing is performed in $L^2(S)$ space, for example, the eigenvalues of the impedance matrix resulting from the MoM discretization of the SVS-EFIE are shown to cluster at zero and infinity upon increase of the discretization order, hence, leading to the unbounded growth of the condition number. The latter is known to be responsible for the oversampling and low-frequency instabilities inherent to the S-EFIE.

3.2 Surface-Volume-Surface Electric Field Integral Equation

Consider a homogeneous non-magnetic dielectric object of relative permittivity ϵ situated in free space and occupying volume V bounded by surface S. Under condition of time-harmonic incident field $\boldsymbol{E}^{inc}$ impinging on the object the field inside the object can be defined using the following single-source representation [45]

$$\boldsymbol{E}(\boldsymbol{r}') = i\omega\mu_0 \int_S \bar{\bar{\boldsymbol{G}}}_{e\epsilon}(\boldsymbol{r}', \boldsymbol{r}'') \cdot \mathtt{a}\boldsymbol{J}(r'')ds'' \\ - \int_S \bar{\boldsymbol{G}}_{m\epsilon}(\boldsymbol{r}', \boldsymbol{r}'') \cdot \mathtt{b}\hat{\boldsymbol{n}}'' \times \boldsymbol{J}(\boldsymbol{r}'')ds'', \quad \boldsymbol{r}' \in V, \quad (3.1)$$

where $\boldsymbol{J}$ is the fictitious electric current density, $\mathtt{a}$ and $\mathtt{b}$ are arbitrary constants, ω is the cyclic frequency of the time harmonic field under time convention $e^{i\omega\mathtt{t}}$, which is suppressed here and throughout the paper. In (3.1), $\bar{\boldsymbol{G}}_{e\epsilon}$ and $\bar{\boldsymbol{G}}_{m\epsilon}$ are the electric and magnetic field dyadic Green's functions of homogeneous space with the same permittivity ϵ as the object

$$\bar{\bar{\boldsymbol{G}}}_{e\epsilon}(\boldsymbol{r}', \boldsymbol{r}'') = -\left(\mathbf{I} + \frac{\nabla\nabla}{k_\epsilon^2}\right) G_\epsilon(\boldsymbol{r}', \boldsymbol{r}''), \quad \bar{\bar{\boldsymbol{G}}}_{m\epsilon} = \nabla \times \bar{\bar{\boldsymbol{G}}}_{e\epsilon}, \quad (3.2)$$

where $G_\epsilon(\boldsymbol{r}', \boldsymbol{r}'') = \frac{e^{-ik_\epsilon|\boldsymbol{r}'-\boldsymbol{r}''|}}{4\pi|\boldsymbol{r}'-\boldsymbol{r}''|}$. is the scalar Green's function of homogeneous non-magnetic medium with wavenumber $k_\epsilon = k_0\sqrt{\epsilon}$, $k_0 = \omega\sqrt{\mu_0\epsilon_0}$ being the wave number of vacuum.

Alternative representation of the field, which is valid both inside and outside the object volume V, is given by the volume equivalence principle [52] which produces the following well-known V-EFIE with respect to the unknown electric field inside the scatterer upon localization of the observation point to the volume of the scatterer

$$\boldsymbol{E}(\boldsymbol{r}) + k_0^2(\epsilon - 1) \int_V \bar{\bar{\boldsymbol{G}}}_{e0}(\boldsymbol{r}, \boldsymbol{r}') \cdot \boldsymbol{E}(\boldsymbol{r}')dv', = \boldsymbol{E}^{inc}(\boldsymbol{r}), \quad \boldsymbol{r} \in V. \quad (3.3)$$

The free-space dyadic Green's function $\bar{\bar{\boldsymbol{G}}}_{e0}$ in (3.3) features $1/|\boldsymbol{r}-\boldsymbol{r}'|^3$ singularity, making the volume integral undefined unless it is understood in generalized form $\bar{\bar{\boldsymbol{G}}}_{e0}(\boldsymbol{r},\boldsymbol{r}') = p.v.\bar{\bar{\boldsymbol{G}}}_{e0}(\boldsymbol{r},\boldsymbol{r}') - k_0^{-2}\bar{\mathbf{L}}\delta(\boldsymbol{r}-\boldsymbol{r}')$. Here, $p.v.$ in front of $\bar{\bar{\boldsymbol{G}}}_{e0}$ denotes that the volume integral containing this term is evaluated in the principal value sense through exclusion of small volume V_δ centered at the observation point $\boldsymbol{r}$. The constant dyadic $\bar{\mathbf{L}} = \bar{\mathbf{I}}/3$ in case of small volume V_δ being of spherical or cubic shapes [52].

Volume equivalence principle can be also used to constrain the single-source integral representation of the field (3.1) to produce the integral equation with respect to the fictitious surface current density $\boldsymbol{J}(\boldsymbol{r}'')$. For that purpose we substitute (3.1) with particular case of $\mathtt{a} = 1$ and $\mathtt{b} = 0$ into (3.3) and enforce the latter for the tangential component of the electric field as we tend the observation point $\boldsymbol{r}$ to the boundary S from the inside

$$\begin{aligned} i\omega\mu_0\hat{\boldsymbol{n}} \times \int_S \bar{\bar{\boldsymbol{G}}}_{e\epsilon}(\boldsymbol{r},\boldsymbol{r}'') \cdot \boldsymbol{J}(\boldsymbol{r}'')ds'' + i\omega\mu_0 k_0^2(\epsilon-1) \\ \hat{\boldsymbol{n}} \times \int_V \bar{\bar{\boldsymbol{G}}}_{e0}(\boldsymbol{r},\boldsymbol{r}') \cdot \int_S \bar{\bar{\boldsymbol{G}}}_{e\epsilon}(\boldsymbol{r}',\boldsymbol{r}'') \cdot \boldsymbol{J}(\boldsymbol{r}'')ds''dv' \\ = \hat{\boldsymbol{n}} \times \boldsymbol{E}^{inc}(\boldsymbol{r}), \quad \boldsymbol{r} \in S. \end{aligned} \tag{3.4}$$

It is interesting to note [55] that in the case of vanishing object $\epsilon \to 1$, the above SVS-EFIE reduces to the S-EFIE for PEC object with the negative right-hand-side

$$i\omega\mu_0\hat{\boldsymbol{n}} \times \int_S \bar{\bar{\boldsymbol{G}}}_{e0}(\boldsymbol{r},\boldsymbol{r}'') \cdot \boldsymbol{J}(\boldsymbol{r}'')ds'' = \hat{\boldsymbol{n}} \times \boldsymbol{E}^{inc}(\boldsymbol{r}), \quad \boldsymbol{r} \in S. \tag{3.5}$$

In this case the fictitious current $\boldsymbol{J}$ turns into negative of the conventional equivalent current, i.e. $\boldsymbol{J} = -\hat{\boldsymbol{n}} \times \boldsymbol{H}$. Hence, $\boldsymbol{J}$ produces the incident field $\boldsymbol{E}^{inc}$ inside V. The traditional S-EFIE, on the other hand, produces $-\boldsymbol{E}^{inc}$ inside V in order to cancel incident field inside PEC.

The SVS-EFIE (3.4) can also be represented as the following operator form

$$\mathcal{T}_{e\epsilon}^{S,S} \circ \boldsymbol{J} + \mathcal{T}_{e0}^{S,V} \circ \mathcal{T}_{e\epsilon}^{V,S} \circ \boldsymbol{J} = \hat{\boldsymbol{n}} \times \boldsymbol{E}^{inc}(\boldsymbol{r}), \quad \boldsymbol{r} \in S, \tag{3.6}$$

where the operators are defined, as follows:

$$\mathcal{T}_{e\epsilon}^{S,S} \circ \boldsymbol{J} = i\omega\mu_0 \hat{\boldsymbol{n}} \times \int_S \bar{\bar{\boldsymbol{G}}}_{e\epsilon}(\boldsymbol{r}, \boldsymbol{r}'') \cdot \boldsymbol{J}(\boldsymbol{r}'') ds'', \quad \boldsymbol{r} \in S, \tag{3.7}$$

$$\mathcal{T}_{e\epsilon}^{V,S} \circ \boldsymbol{J} = i\omega\mu_0 \int_S \bar{\bar{\boldsymbol{G}}}_{e\epsilon}(\boldsymbol{r}', \boldsymbol{r}'') \cdot \boldsymbol{J}(\boldsymbol{r}'') ds'', \quad \boldsymbol{r}' \in V, \tag{3.8}$$

$$\mathcal{T}_{e0}^{S,V} \circ \boldsymbol{i} = k_0^2(\epsilon - 1) \hat{\boldsymbol{n}} \times \int_V \bar{\bar{\boldsymbol{G}}}_{e0}(\boldsymbol{r}, \boldsymbol{r}') \cdot \boldsymbol{i}(\boldsymbol{r}') dv', \quad \boldsymbol{r} \in S. \tag{3.9}$$

3.2.1 Function spaces of SVS-EFIE operators for smooth object

In general, fields inside smooth dielectric object of volume V are functions in Sobolev space $H(div, curl, V)$, while their tangential components $\hat{\boldsymbol{n}} \times \boldsymbol{E}$ and $\hat{\boldsymbol{n}} \times \boldsymbol{H}$ are in $H^{-1/2}(S)$ (p. 321 in [60]). However, for SVS-EFIE formed from V-EFIE as

$$\hat{\boldsymbol{n}} \times \boldsymbol{E} - \hat{\boldsymbol{n}} \times \boldsymbol{E}^{scat} = \hat{\boldsymbol{n}} \times \boldsymbol{E}^{inc}, \quad \boldsymbol{r} \in S, \tag{3.10}$$

additional information about the smoothness of the tangential components of the $\hat{\boldsymbol{n}} \times \boldsymbol{E}^{inc}$ on S is available similarly with traditional S-EFIE for PEC object requiring $-\hat{\boldsymbol{n}} \times \boldsymbol{E}^{scat} = \hat{\boldsymbol{n}} \times \boldsymbol{E}^{inc}, \boldsymbol{r} \in S$. Specifically, when object is smooth, the tangential components of incident field $\hat{\boldsymbol{n}} \times \boldsymbol{E}^{inc}$ on S are in $H^{1/2}(S)$ (and not in $H^{-1/2}(S)$) (see last paragraph on p. 321 in [60]). Since $\hat{\boldsymbol{n}} \times \boldsymbol{E}^{inc}$ is in $H^{1/2}(S)$ in SVS-EFIE

(3.10), both the difference $\hat{\boldsymbol{n}} \times \boldsymbol{E} - \hat{\boldsymbol{n}} \times \boldsymbol{E}^{scat}$ as well as $\hat{\boldsymbol{n}} \times \boldsymbol{E}$ and $\hat{\boldsymbol{n}} \times \boldsymbol{E}^{scat}$ must be also in the same Sobolev space $H^{1/2}(S)$ for as long as both the surface S and the incident field remain smooth.

According to (3.6), tangential component $\hat{\boldsymbol{n}} \times \boldsymbol{E}$ is defined as $\mathcal{T}_{e\epsilon}^{S,S} \circ \boldsymbol{J}$, where $\mathcal{T}_{e\epsilon}^{S,S}$ operator is conventional S-EFIE operator for PEC objects. Since for smooth S operator $\mathcal{T}_{e\epsilon}^{S,S}$ maps space $H_{div}^{m-1/2}$ to itself (see (37) in [60]), and $\hat{\boldsymbol{n}} \times \boldsymbol{E}$ is in space $H^{1/2}(S)$ (i.e. $m = 1$), the current $\boldsymbol{J}$ must be in space $H^{1/2}(S)$ also.

Since $\hat{\boldsymbol{n}} \times \boldsymbol{E}$ is in $H^{1/2}(S)$, $\boldsymbol{E}$ in V must be in $H^1(V)$ (see discussion on p. 321 of [60]). Operator $\mathcal{T}_{e\epsilon}^{V,S}$ maps $\boldsymbol{J}$ from S to $\boldsymbol{E}$ in V, i.e. $\boldsymbol{E} = \mathcal{T}_{e\epsilon}^{V,S} \circ \boldsymbol{J}$. Hence, it maps space $H^{1/2}(S)$ to space $H^1(V)$. On the other hand, operator $\mathcal{T}_{e0}^{S,V}$ maps $\boldsymbol{E}$ in V to $\hat{\boldsymbol{n}} \times \boldsymbol{E}^{scat}$ on S. Since, $\hat{\boldsymbol{n}} \times \boldsymbol{E}^{scat}$ is in space $H^{1/2}(S)$, $\mathcal{T}_{e0}^{S,V}$ maps $H^1(V)$ to $H^{1/2}(S)$. As a result, product of the operators $\mathcal{T}_{e0}^{S,V} \circ \mathcal{T}_{e\epsilon}^{V,S}$ maps $H^{1/2}(S)$ to itself just as $\mathcal{T}_{e\epsilon}^{S,S}$ does, and so does overall SVS-EFIE operator $\mathcal{T}_{e\epsilon}^{S,S} + \mathcal{T}_{e0}^{S,V} \circ \mathcal{T}_{e\epsilon}^{V,S}$.

Since the tangential differentiation does not lower the order of smoothness, $\boldsymbol{J}$, $\hat{\boldsymbol{n}} \times \boldsymbol{E}$, $\hat{\boldsymbol{n}} \times \boldsymbol{E}^{scat}$, and $\hat{\boldsymbol{n}} \times \boldsymbol{E}^{inc}$ lie in function space $H_{div}^{1/2}(S)$, which is a sub-space of $H^{1/2}(S)$ (see p. 321 in [60]). For this reason, the test and basis functions in the MoM solution of SVS-EFIE described in the next Section, are members of Sobolev space $H_{div}^{1/2}(S)$.

It is important to point out that the function spaces are different for dielectric objects with non-smooth surfaces S.

3.3 Exact Solution of SVS-EFIE with Galerkin MoM on Sphere

3.3.1 Expansion of current over spherical basis functions

To obtain exact solution $\boldsymbol{J}$ of the SVS-EFIE (3.4) for a dielectric sphere, we perform Helmholtz decomposition of the current $\boldsymbol{J}$ into irrotational and rotational parts as

[60]

$$\boldsymbol{J}(\hat{\boldsymbol{r}}) = \nabla^t \varphi(\hat{\boldsymbol{r}}) + \hat{\boldsymbol{r}} \times \nabla^t \psi(\hat{\boldsymbol{r}}), \tag{3.11}$$

where scalar functions φ and ψ are expanded over complete set[1] of scalar surface spherical harmonics Y_n^m

$$\varphi(\hat{\boldsymbol{r}}) = \sum_{n,m} b_{nm} d_{nm}^{1/2} Y_n^m(\hat{\boldsymbol{r}}), \tag{3.12}$$

$$\psi(\hat{\boldsymbol{r}}) = \sum_{n,m} c_{nm} d_{nm}^{1/2} Y_n^m(\hat{\boldsymbol{r}}), \tag{3.13}$$

and the surface gradient operator ∇^t in the spherical coordinates on the sphere of radius a is defined as

$$\nabla^t = \frac{1}{a}\hat{\boldsymbol{\theta}}\frac{\partial}{\partial\theta} + \frac{1}{a\sin\theta}\hat{\boldsymbol{\phi}}\frac{\partial}{\partial\phi}. \tag{3.14}$$

In (3.12) and (3.13), b and c are the unknown coefficients of expansion, and normalization factors are

$$d_{nm} = \frac{(n-|m|)!(2n+1)}{(n+|m|)!4\pi n(n+1)}. \tag{3.15}$$

The surface spherical harmonics are defined as the product of associated Legendre polynomials P_n^m and azimuthal harmonics

$$Y_n^m(\hat{\boldsymbol{r}}) = Y_n^m(\theta,\phi) = P_n^{|m|}(\cos\theta)e^{im\phi}, \tag{3.16}$$

with θ and ϕ being the angles of the spherical coordinate system. In the sequel the properties $\overline{Y_n^m} = Y_n^{-m}$ is utilized.

The Helmholtz decomposition (3.11) of current $\boldsymbol{J}$ can be viewed as expansion over two sets of vector basis functions $\boldsymbol{u}_{nm}^{(1)}$ and $\boldsymbol{u}_{nm}^{(2)}$ with the unknown coefficients b_{nm} and c_{nm}

$$\boldsymbol{J}(\hat{\boldsymbol{r}}) = \sum_{n,m}\{b_{nm}\boldsymbol{u}_{nm}^{(1)}(\hat{\boldsymbol{r}}) + c_{nm}\boldsymbol{u}_{nm}^{(2)}(\hat{\boldsymbol{r}})\}, \tag{3.17}$$

[1]Here and throughout the paper the double summation $\sum_{n=1}^{\infty}\sum_{m=-n}^{n}$ is denoted as $\sum_{n,m}$

where (see (87)-(88) in [60])

$$\boldsymbol{u}_{nm}^{(1)}(\hat{\boldsymbol{r}}) = d_{nm}^{1/2} \nabla^t Y_n^m(\hat{\boldsymbol{r}}), \tag{3.18}$$

$$\boldsymbol{u}_{nm}^{(2)}(\hat{\boldsymbol{r}}) = d_{nm}^{1/2} \hat{\boldsymbol{r}} \times \nabla^t Y_n^m(\hat{\boldsymbol{r}}). \tag{3.19}$$

Considering definition of the surface gradient (3.14) vector basis functions $\boldsymbol{u}_{nm}^{(1,2)}$ can be written as

$$\boldsymbol{u}_{nm}^{(1)}(\hat{\boldsymbol{r}}) = d_{nm}^{1/2} \left[\hat{\theta} \frac{1}{a} \frac{d}{d\theta} P_n^{|m|}(\cos\theta) e^{im\phi} + \hat{\phi} \frac{1}{a \sin\theta} P_n^{|m|}(\cos\theta) \frac{d}{d\phi} e^{im\phi} \right], \tag{3.20}$$

$$\boldsymbol{u}_{nm}^{(2)}(\hat{\boldsymbol{r}}) = d_{nm}^{1/2} \left[\hat{\phi} \frac{1}{a} \frac{d}{d\theta} P_n^{|m|}(\cos\theta) e^{im\phi} - \hat{\theta} \frac{1}{a \sin\theta} P_n^{|m|}(\cos\theta) \frac{d}{d\phi} e^{im\phi} \right]. \tag{3.21}$$

3.3.2 Expansion of electric field dyadic Green's function over vector spherical functions

The electric field dyadic Green's function of homogenous medium with wavenumber k can be expanded over vector spherical functions $\boldsymbol{p}$ and $\boldsymbol{q}$, as (see [61] or (68) in [60]):

$$\begin{aligned} \bar{\bar{\boldsymbol{G}}}_e(\boldsymbol{r}, \boldsymbol{r}') &= -\left(\mathbf{I} + \frac{\nabla\nabla}{k^2} \right) \frac{e^{-ik|\boldsymbol{r}-\boldsymbol{r}'|}}{4\pi|\boldsymbol{r}-\boldsymbol{r}'|} \\ &= ik \sum_{n,m} d_{nm} \begin{cases} \boldsymbol{q}_{nm}^{(1)}(\boldsymbol{r}) \boldsymbol{q}_{n,-m}^{(2)}(\boldsymbol{r}') + \boldsymbol{p}_{nm}^{(1)}(\boldsymbol{r}) \boldsymbol{p}_{n,-m}^{(2)}(\boldsymbol{r}'), |\boldsymbol{r}| < |\boldsymbol{r}'|, \\ \boldsymbol{q}_{nm}^{(2)}(\boldsymbol{r}) \boldsymbol{q}_{n,-m}^{(1)}(\boldsymbol{r}') + \boldsymbol{p}_{nm}^{(2)}(\boldsymbol{r}) \boldsymbol{p}_{n,-m}^{(1)}(\boldsymbol{r}')\}, |\boldsymbol{r}| > |\boldsymbol{r}'|. \end{cases} \end{aligned} \tag{3.22}$$

When $|\boldsymbol{r}| = |\boldsymbol{r}'|$, the average of the two above representations is taken. In (3.22), the spherical vector functions $\boldsymbol{p}_{nm}^{(j)}$ and $\boldsymbol{q}_{nm}^{(j)}$ are given by the following expressions (see (64)-(65) in [60])

$$\boldsymbol{p}_{nm}^{(j)}(\boldsymbol{r}) = \nabla \times [z_n^{(j)}(kr)Y_n^m(\hat{\boldsymbol{r}})\boldsymbol{r}] = -z_n^{(j)}(kr)\hat{\boldsymbol{r}} \times \nabla^t Y_n^m(\hat{\boldsymbol{r}}), \tag{3.23}$$

$$\boldsymbol{q}_{nm}^{(j)}(\boldsymbol{r}) = \frac{1}{k}\nabla \times \boldsymbol{p}_{nm}^{(j)}(\boldsymbol{r}) = \frac{1}{k}[krz_n^{(j)}(kr)]'\nabla^t Y_n^m(\hat{\boldsymbol{r}}) + \frac{n(n+1)}{kr^2}\boldsymbol{r}z_n^{(j)}(kr)Y_n^m(\hat{\boldsymbol{r}}), \tag{3.24}$$

where $r = |\boldsymbol{r}|$, $\hat{\boldsymbol{r}} = \boldsymbol{r}/|\boldsymbol{r}|$ and $z_n^{(1),(2)}$ are the spherical Bessel and Hankel functions

$$z_n^{(1)}(kr) = j_n(kr), \qquad z_n^{(2)}(kr) = h_n^{(2)}(kr), \tag{3.25}$$

with $'$ denoting differentiation with respect to the entire argument of $z_n^{(j)}$. Note, that since $\boldsymbol{q}^{(j)}$ and $\boldsymbol{p}^{(j)}$ are solutions of the 3D curl-curl equation [52], the following properties hold

$$\nabla \times \boldsymbol{q}_{nm}^{(j)} = k\boldsymbol{p}_{nm}^{(j)}, \quad \nabla \times \boldsymbol{p}_{nm}^{(j)} = k\boldsymbol{q}_{nm}^{(j)}. \tag{3.26}$$

Recalling definition of the surface gradient (3.14) we get explicit formulas for the components of the spherical vector functions

$$\boldsymbol{p}_{nm}^{(j)} = \left(\frac{im}{\sin\theta}P_n^{|m|}(\cos\theta)\hat{\boldsymbol{\theta}} - \frac{d}{d\theta}P_n^{|m|}(\cos\theta)\hat{\boldsymbol{\phi}}\right) z_n^{(j)}(kR)e^{im\phi}, \tag{3.27}$$

$$\begin{aligned}\boldsymbol{q}_{nm}^{(j)} = \Bigg(&\frac{n(n+1)}{kR}z_n^{(j)}(kR)P_n^{|m|}(\cos\theta)\hat{\boldsymbol{r}} \\ &+\frac{1}{kR}\frac{d}{dR}\{kRz_n^{(j)}(kR)\}\frac{d}{d\theta}P_n^{|m|}(\cos\theta)\hat{\boldsymbol{\theta}} \\ &+\frac{im}{kR\sin\theta}\frac{d}{dR}\{kRz_n^{(j)}(kR)\}P_n^{|m|}(\cos\theta)\hat{\boldsymbol{\phi}}\Bigg) e^{im\phi}.\end{aligned} \tag{3.28}$$

We note here that combination of the spherical wave functions $\boldsymbol{p}^{(1)}$ and $\boldsymbol{q}^{(1)}$ form a complete basis $\boldsymbol{v}$

$$\boldsymbol{v}_{nm}^{(j)} = \begin{cases} \boldsymbol{p}_{nm}^{(1)}, & j=1 \\ \boldsymbol{q}_{nm}^{(1)}, & j=2 \end{cases}, \quad 0 \leq n \leq N, |m| \leq n \tag{3.29}$$

for expansion of the electric field inside the sphere over $\boldsymbol{v}^{(1)}$ and $\boldsymbol{v}^{(2)}$ with coefficients β and γ

$$\boldsymbol{E}(\boldsymbol{r}) = \sum_{n,m} \{\beta_{nm}\boldsymbol{v}_{nm}^{(1)}(\boldsymbol{r}) + \gamma_{nm}\boldsymbol{v}_{nm}^{(2)}(\boldsymbol{r})\}, \quad \boldsymbol{r} \in V, \tag{3.30}$$

provided wavenumber k_ϵ is used in the definitions (3.27) and (3.28). For that reason we will use them as the test functions for the range of the operator $\mathcal{T}_{e\epsilon}^{V,S}$ and as basis functions for the domain of the operator $\mathcal{T}_{e0}^{S,V}$ in the MoM solution.

3.3.3 Galerkin testing of SVS-EFIE

The exact MoM solution of the SVS-EFIE (3.4) is performed through its testing with complete set of vector surface spherical functions $\boldsymbol{u}^{(1)}$ and $\boldsymbol{u}^{(2)}$

$$\left\langle \mathcal{T}_{e\epsilon}^{S,S} \circ \boldsymbol{J}, \boldsymbol{u}_{nm}^{(1,2)} \right\rangle + \left\langle \mathcal{T}_{e0}^{S,V} \circ \mathcal{T}_{e\epsilon}^{V,S} \circ \boldsymbol{J}, \boldsymbol{v}_{nm}^{(1,2)} \right\rangle = \left\langle \hat{\boldsymbol{n}} \times \boldsymbol{E}^{inc}(\boldsymbol{r}), \boldsymbol{u}_{nm}^{(1,2)} \right\rangle, \tag{3.31}$$

and expansion of the current $\boldsymbol{J}$ over the same set of functions (3.17). The inner products can be evaluated in different function spaces [60]. However, the $L^2(S)$ space is the most commonly used one. Following [60], we will show that the choice of space may greatly effect the spectrum of the impedance matrix in the MoM matrix equation. Performing testing of the SVS-EFIE in function space $L^2(S)$ produces $O(n^2)$ growth in the matrix condition number with the increase of number of spherical functions n taken in the solution. This is due the presence of S-EFIE operator $\mathcal{T}_{e\epsilon}^{S,S}$ in it, which has the eigenvalues accumulating at zero and infinity. In order to achieve the impedance matrix with bounded condition number the SVS-EFIE must be tested in Sobolev space $H^l_{div}(S)$ the same way as the conventional S-EFIE in the MoM solution of scattering problems on smooth PEC objects [60].

3.3.4 Discretization of the Surface-to-Surface Operator $\mathcal{T}^{S,S}_{e\epsilon}$

The matrix elements $\mathcal{Z}^{S_i,S_j}_{e\epsilon}$ in the Galerkin MoM discretization of the operator $\mathcal{T}^{S,S}_{e\epsilon}$ are obtained through the testing with function $\boldsymbol{u}^{(i)}_{n'm'}$ of the field $\mathcal{T}^{S,S}_{e\epsilon} \circ \boldsymbol{u}^{(j)}_{n''m''}$ produced by basis function $\boldsymbol{u}^{(j)}_{n''m''}$ in the expansion of current $\boldsymbol{J}$ and using electric field dyadic Green's function expansion (3.22)

$$\begin{aligned}\mathcal{Z}^{S_i,S_j}_{e\epsilon\ n'm',n''m''} = &-\left\langle \boldsymbol{u}^{(i)}_{n'm'}, \mathcal{T}^{S,S}_{e\epsilon} \circ \boldsymbol{u}^{(j)}_{n''m''} \right\rangle_{H^l_{div}(S)} \\ &= \omega\mu_0 k_\epsilon \sum_{n,m} \psi^l_n d_{nm} \left(\int_S \boldsymbol{u}^{(i)}_{n'm'}(\boldsymbol{r}) \cdot \hat{\boldsymbol{n}} \times \right. \\ &\boldsymbol{q}^{(1\epsilon)}_{nm}(\boldsymbol{r}) ds \int_S \boldsymbol{q}^{(2\epsilon)}_{n,-m}(\boldsymbol{r}'') \cdot \boldsymbol{u}^{(j)}_{n''m''}(\boldsymbol{r}'') ds'' + \int_S \boldsymbol{u}^{(i)}_{n'm'}(\boldsymbol{r}) \cdot \\ &\left. \hat{\boldsymbol{n}} \times \boldsymbol{p}^{(1\epsilon)}_{nm}(\boldsymbol{r}) ds \int_S \boldsymbol{p}^{(2\epsilon)}_{n,-m}(\boldsymbol{r}'') \cdot \boldsymbol{u}^{(j)}_{n''m''}(\boldsymbol{r}'') ds'' \right). \end{aligned} \tag{3.32}$$

In (4.15), we performed the inner product in Sobolev space $H^l_{div}(S)$, which produces additional factor $\psi^l_n = (1+n^2)^{l+1}$ for $i=1$ and $\psi^l_n = (1+n^2)^l$ for $i=2$ (see (96a) and (96b) in [60]). If the inner product was performed in $L^2(S)$ the factor $\psi^l_n = 1$.

One can show from (3.32) that $\mathcal{Z}^{S_1,S_1}_{e\epsilon\ nm,n''m''}$ vanishes due to orthogonality (see Appendix I)

$$\mathcal{Z}^{S_1,S_1}_{e\epsilon\ n'm',n''m''} = -\left\langle \boldsymbol{u}^{(1)}_{n'm'}, \mathcal{T}^{S,S}_{e\epsilon} \circ \boldsymbol{u}^{(1)}_{n''m''} \right\rangle_{H^l_{div}(S)} = 0. \tag{3.33}$$

Also, due to (3.120), (3.124) and (3.126), $\mathcal{Z}^{S_2,S_2}_{e\epsilon\ nm,n''m''}$ vanishes

$$\mathcal{Z}^{S_2,S_2}_{e\epsilon\ n'm',n''m''} = -\left\langle \boldsymbol{u}^{(2)}_{n'm'}, \mathcal{T}^{S,S}_{e\epsilon} \circ \boldsymbol{u}^{(2)}_{n''m''} \right\rangle_{H^l_{div}(S)} = 0. \tag{3.34}$$

The interactions of basis functions $\boldsymbol{u}^{(2)}_{n'm'}$ with test functions $\boldsymbol{u}^{(1)}_{n'm'}$, however, are non-zero

$$\mathcal{Z}^{S_1,S_2}_{e\epsilon\ n'm',n''m''} = \omega\mu_0 k_\epsilon \sum_{n,m}(1+n^2)^{l+1} d_{nm} \Bigg(\int_S ds \\ \boldsymbol{u}^{(1)}_{n'm'}(\boldsymbol{r}) \cdot \hat{\boldsymbol{n}} \times \boldsymbol{q}^{(1\epsilon)}_{nm}(\boldsymbol{r}) \int_S \boldsymbol{q}^{(2\epsilon)}_{n,-m}(\boldsymbol{r}'') \cdot \boldsymbol{u}^{(2)}_{n''m''}(\boldsymbol{r}'') ds'' + \\ \int_S \boldsymbol{u}^{(1)}_{n'm'}(\boldsymbol{r}) \cdot \hat{\boldsymbol{n}} \times \boldsymbol{p}^{(1\epsilon)}_{nm}(\boldsymbol{r}) ds \int_S \boldsymbol{p}^{(2\epsilon)}_{n,-m}(\boldsymbol{r}'') \cdot \boldsymbol{u}^{(2)}_{n''m''}(\boldsymbol{r}'') ds'' \Bigg)$$

Using [60], we can see that contributions of functions $\boldsymbol{q}$ vanish due to orthogonality and the above expression simplifies to

$$\mathcal{Z}^{S_1,S_2}_{e\epsilon\ n'm',n''m''} = \omega\mu_0\ k_\epsilon \sum_{n,m} d_{nm}(1+n^2)^{l+1} \int_S \boldsymbol{u}^{(1)}_{n'm'}(\boldsymbol{r}) \\ \cdot \hat{\boldsymbol{n}} \times \boldsymbol{p}^{(1\epsilon)}_{nm}(\boldsymbol{r}) ds \int_S \boldsymbol{p}^{(2\epsilon)}_{n,-m}(\boldsymbol{r}'') \cdot \boldsymbol{u}^{(2)}_{n''m''}(\boldsymbol{r}'') ds''. \quad (3.35)$$

With reference to (3.18), (3.19) and (3.27), the expression for $\mathcal{Z}^{S_1,S_2}_{e\epsilon}$ can be further simplified, as follows:

$$\mathcal{Z}^{S_1,S_2}_{e\epsilon\ n'm',n''m''} = \omega\mu_0\ k_\epsilon \sum_{n,m} d^{1/2}_{nm}(1+n^2)^{l+1} \int_S d^{1/2}_{n'm'} \nabla^t Y^{m'}_{n'} \\ \cdot \nabla^t Y^m_n ds(a j_n(k_\epsilon a))(-a h^{(2)}_n(k_\epsilon a))\delta_{nn'}\delta_{mm'} = -\frac{\omega\mu_0}{k_\epsilon} \\ (1+(n')^2)^{l+1} k_\epsilon a j_{n'}(k_\epsilon a) k_\epsilon a h^{(2)}_{n'}(k_\epsilon a)\delta_{n'n''}\delta_{-m'm''}. \quad (3.36)$$

Similarly, we obtain diagonal matrix of interactions of the basis functions $\boldsymbol{u}^{(1)}_{n'm'}$ with the test functions $\boldsymbol{u}^{(2)}_{n'm'}$ via $\mathcal{T}^{S,S}_{e\epsilon}$

$$\begin{aligned}\mathcal{Z}^{S_2,S_1}_{e\epsilon\ n'm',n''m''} = -\left\langle \boldsymbol{u}^{(2)}_{n'm'}, \mathcal{T}^{S,S}_{e\epsilon} \circ \boldsymbol{u}^{(1)}_{n''m''} \right\rangle_{H^l_{div}(S)} = \\ \omega\mu_0 k_\epsilon \sum_{n,m} d_{nm}(1+n^2)^l \left(\int_S \boldsymbol{u}^{(2)}_{n'm'}(\boldsymbol{r}) \cdot \hat{\boldsymbol{n}} \times \right. \\ \boldsymbol{q}^{(1\epsilon)}_{nm}(\boldsymbol{r}) ds \int_S \boldsymbol{q}^{(2\epsilon)}_{n,-m}(\boldsymbol{r}'') \cdot \boldsymbol{u}^{(1)}_{n''m''}(\boldsymbol{r}'') ds'' + \int_S \boldsymbol{u}^{(2)}_{n'm'}(\boldsymbol{r}) \\ \left. \cdot \hat{\boldsymbol{n}} \times \boldsymbol{p}^{(1\epsilon)}_{nm}(\boldsymbol{r}) ds \int_S \boldsymbol{p}^{(2\epsilon)}_{n,-m}(\boldsymbol{r}'') \cdot \boldsymbol{u}^{(1)}_{n''m''}(\boldsymbol{r}'') ds'' \right). \quad (3.37)\end{aligned}$$

Using orthogonality [60], we determine that contributions containing $\boldsymbol{p}$ functions vanish, which produces

$$\begin{aligned}\mathcal{Z}^{S_2,S_1}_{e\epsilon\ n'm',n''m''} = \omega\mu_0 k_\epsilon \sum_{n,m} d_{nm}(1+n^2)^l \int_S d^{1/2}_{n'm'} \hat{\boldsymbol{r}} \times \nabla^t Y^{m'}_{n'}(\hat{\boldsymbol{r}}) \cdot \frac{1}{k_\epsilon}[k_\epsilon a j_n(k_\epsilon a)]' \\ \hat{\boldsymbol{r}} \times \nabla^t Y^m_n(\hat{\boldsymbol{r}}) ds \int_S \boldsymbol{q}^{(2\epsilon)}_{n,-m}(\boldsymbol{r}'') \cdot d^{1/2}_{nm} \nabla^t Y^{m''}_{n''}(\hat{\boldsymbol{r}}'') ds''. \quad (3.38)\end{aligned}$$

Next, using [60], we get close-form expression

$$\begin{aligned}\mathcal{Z}^{S_2,S_1}_{e\epsilon\ n'm',n''m''} &= \frac{\omega\mu_0}{k_\epsilon} \sum_{n,m} (1+n^2)^l [k_\epsilon a j_n(k_\epsilon a)]' (\delta_{nn'}\delta_{m-m'}) [k_\epsilon a h^{(2)}_n(k_\epsilon a)]' \delta_{nn''}\delta_{mm''} \\ &= \frac{\omega\mu_0}{k_\epsilon} (1+(n')^2)^l [k_\epsilon a j_{n'}(k_\epsilon a)]' [k_\epsilon a h^{(2)}_{n'}(k_\epsilon a)]' \delta_{n'n''}\delta_{-m'm''}. \quad (3.39)\end{aligned}$$

Combining (3.33), (3.34), (3.36), and (3.39) we obtain the following hollow matrix representing the MoM discretization of the surface-to-surface operator

$$\boldsymbol{\mathcal{Z}}^{S,S}_{e\epsilon} = \begin{bmatrix} 0 & \boldsymbol{\mathcal{Z}}^{S_1 S_2}_{e\epsilon} \\ \boldsymbol{\mathcal{Z}}^{S_2,S_1}_{e\epsilon} & 0 \end{bmatrix}. \quad (3.40)$$

3.3.5 Discretization of the Surface-to-Volume Operator $\mathcal{T}_{e\epsilon}^{V,S}$

The matrix elements $\mathcal{Z}_{e\epsilon}^{V,S}$ in the MoM discretization of the operator $\mathcal{T}_{e\epsilon}^{V,S}$ are produced by testing of the scattered electric field produced by surface vector basis function $\boldsymbol{u}_{n''m''}^{(j)}$ with volumetric spherical vector functions $\boldsymbol{v}_{n'm'}^{(i)}$ (3.29), as follows:

$$\begin{aligned}\mathcal{Z}_{e\epsilon\ n'm',n''m''}^{V_i,S_j} = \left\langle \boldsymbol{v}_{n'm'}^{(i)}, \mathcal{T}_{e\epsilon}^{V,S} \circ \boldsymbol{u}_{n''m''}^{(j)} \right\rangle_{L^2(V)} = -\omega\mu_0\ k_\epsilon \sum_{n,m} d_{nm} \left(\int_V \boldsymbol{v}_{n'm'}^{(i)}(\boldsymbol{r}) \cdot \right. \\ \boldsymbol{q}_{nm}^{(1\epsilon)}(\boldsymbol{r}) dv \int_S \boldsymbol{q}_{n,-m}^{(2\epsilon)}(\boldsymbol{r}'') \cdot \boldsymbol{u}_{n''m''}^{(j)}(\boldsymbol{r}'') ds'' + \int_V \boldsymbol{v}_{n'm'}^{(i)}(\boldsymbol{r}) \\ \left. \cdot \boldsymbol{p}_{nm}^{(1\epsilon)}(\boldsymbol{r}) dv \int_S \boldsymbol{p}_{n,-m}^{(2\epsilon)}(\boldsymbol{r}'') \cdot \boldsymbol{u}_{n''m''}^{(j)}(\boldsymbol{r}'') ds'' \right). \quad (3.41)\end{aligned}$$

Here for simplicity we take the inner product in function space $L^2(V)$ when testing the range of the $\mathcal{T}_{e\epsilon}^{V,S}$ operator. The reason is that the choice of space for this inner product has no impact on the overall spectrum of the MoM impedance matrix. It is negated by the factor coming from the inverse of the Gram matrix for which the inner product are defined in the same space.

Let's first consider the case of $\mathcal{Z}_{e\epsilon\ n'm',n''m''}^{V_1,S_1}$. Here we have

$$\begin{aligned}\mathcal{Z}_{e\epsilon\ n'm',n''m''}^{V_1,S_1} = -\omega\mu_0\ k_\epsilon \sum_{n,m} d_{nm} \left(\int_V \boldsymbol{v}_{n'm'}^{(1)}(\boldsymbol{r}) \cdot \right. \\ \boldsymbol{q}_{nm}^{(1\epsilon)}(\boldsymbol{r}) dv \int_S \boldsymbol{q}_{n,-m}^{(2\epsilon)}(\boldsymbol{r}'') \cdot \boldsymbol{u}_{n''m''}^{(1)}(\boldsymbol{r}'') ds'' + \int_V \boldsymbol{v}_{n'm'}^{(1)}(\boldsymbol{r}) \cdot \\ \left. \boldsymbol{p}_{nm}^{(1\epsilon)}(\boldsymbol{r}) dv \int_S \boldsymbol{p}_{n,-m}^{(2\epsilon)}(\boldsymbol{r}'') \cdot \boldsymbol{u}_{n''m''}^{(1)}(\boldsymbol{r}'') ds'' \right). \quad (3.42)\end{aligned}$$

Employing definition (3.29) and orthogonality relations (3.121) and (3.125) we obtain vanishing result for $\mathcal{Z}_{e\epsilon\ n'm',n''m''}^{V_1,S_1}$

$$\mathcal{Z}_{e\epsilon\ n'm',n''m''}^{V_1,S_1} = 0. \quad (3.43)$$

Next, let's consider the case $\mathcal{Z}^{V_1,S_2}_{e\epsilon\ n'm',n''m''}$

$$\mathcal{Z}^{V_1,S_2}_{e\epsilon\ n'm',n''m''} = -\omega\mu_0\ k_\epsilon \sum_{n,m} d_{nm} \Bigg(\int_V \boldsymbol{v}^{(1)}_{n'm'}(\boldsymbol{r})\cdot$$
$$\boldsymbol{q}^{(1\epsilon)}_{nm}(\boldsymbol{r})dv \int_S \boldsymbol{q}^{(2\epsilon)}_{n,-m}(\boldsymbol{r}'') \cdot \boldsymbol{u}^{(2)}_{n''m''}(\boldsymbol{r}'')ds'' + \int_V \boldsymbol{v}^{(1)}_{n'm'}(\boldsymbol{r})\cdot$$
$$\boldsymbol{p}^{(1\epsilon)}_{nm}(\boldsymbol{r})dv \int_S \boldsymbol{p}^{(2\epsilon)}_{n,-m}(\boldsymbol{r}'') \cdot \boldsymbol{u}^{(2)}_{n''m''}(\boldsymbol{r}'')ds'' \Bigg). \quad (3.44)$$

In the case of elements $\mathcal{Z}^{V_2,S_1}_{e\epsilon\ n'm',n''m''}$ we have

$$\mathcal{Z}^{V_2,S_1}_{e\epsilon\ n'm',n''m''} = -\omega\mu_0\ k_\epsilon \sum_{n,m} d_{nm} \Bigg(\int_V \boldsymbol{v}^{(2)}_{n'm'}(\boldsymbol{r})\cdot$$
$$\boldsymbol{q}^{(1\epsilon)}_{nm}(\boldsymbol{r})dv \int_S \boldsymbol{q}^{(2\epsilon)}_{n,-m}(\boldsymbol{r}'') \cdot \boldsymbol{u}^{(1)}_{n''m''}(\boldsymbol{r}'')ds'' + \int_V \boldsymbol{v}^{(2)}_{n'm'}(\boldsymbol{r})$$
$$\cdot\boldsymbol{p}^{(1\epsilon)}_{nm}(\boldsymbol{r})dv \int_S \boldsymbol{p}^{(2\epsilon)}_{n,-m}(\boldsymbol{r}'') \cdot \boldsymbol{u}^{(1)}_{n''m''}(\boldsymbol{r}'')ds'' \Bigg). \quad (3.45)$$

The test function definition (3.29) and orthogonality relations (3.121) and (3.123) produce

$$
\begin{aligned}
\mathcal{Z}^{V_2,S_1}_{\epsilon\epsilon\ n'm',n''m''} &= -\omega\mu_0\ k_\epsilon \sum_{n,m} d_{nm} \left(\int_V \boldsymbol{q}^{(1\epsilon)}_{n'm'}(\boldsymbol{r}) \cdot \boldsymbol{q}^{(1\epsilon)}_{nm}(\boldsymbol{r}) dv \int_S \boldsymbol{q}^{(2\epsilon)}_{n,-m}(\boldsymbol{r}'') \cdot \right. \\
& \left. d^{1/2}_{n''m''} \nabla^t Y^{m''}_{n''}(\hat{\boldsymbol{r}}'') ds'' + \int_V \boldsymbol{q}^{(1\epsilon)}_{n'm'}(\boldsymbol{r}) \cdot \boldsymbol{p}^{(1\epsilon)}_{nm}(\boldsymbol{r}) dv \int_S \boldsymbol{p}^{(2\epsilon)}_{n,-m}(\boldsymbol{r}'') \cdot d^{1/2}_{n''m''} \nabla^t Y^{m''}_{n''}(\hat{\boldsymbol{r}}'') ds'' \right) \\
&= -\omega\mu_0\ k_\epsilon \sum_{n,m} d_{nm} \left(\int_V \boldsymbol{q}^{(1\epsilon)}_{n'm'}(\boldsymbol{r}) \right. \\
& \left. \cdot \boldsymbol{q}^{(1\epsilon)}_{nm}(\boldsymbol{r}) dv \right) \cdot \left(\frac{1}{k_\epsilon} [k_\epsilon a h^{(2)}_n(k_\epsilon a)]' d^{-1}_{nm} \delta_{nn''} \delta_{mm''} d^{1/2}_{n''m''} \right) \\
&= -\omega\mu_0\ k_\epsilon \sum_{n,m} d_{nm} \left(\frac{n(n+1)}{k^2_\epsilon} \int_0^a j_n(k_\epsilon r) \right. \\
& \left. j_{n'}(k_\epsilon r) dr \cdot a^2 + \frac{1}{k^2_\epsilon} \int_0^a [k_\epsilon r j_n(k_\epsilon r)]' [k_\epsilon r j_{n'}(k_\epsilon r)]' dr \right) \\
& (\delta_{nn'} \delta_{m-m'}) d^{-1/2}_{nm} d^{-1/2}_{n'm'} \cdot \frac{1}{k_\epsilon} [k_\epsilon a h^{(2)}_n(k_\epsilon a)]' \\
& d^{-1}_{nm} \delta_{nn''} \delta_{mm''} d^{1/2}_{n''m''} = -\omega\mu_0\ k_\epsilon d^{-1/2}_{n'm'} \\
& \left(\frac{n'(n'+1)}{k^2_\epsilon} \int_0^a j_{n'}(k_\epsilon r) j_{n''}(k_\epsilon r) dr \cdot a^2 \right. \\
& \left. + \frac{1}{k^2_\epsilon} \int_0^a [k_\epsilon r j_{n'}(k_\epsilon r)]' [k_\epsilon r j_{n''}(k_\epsilon r)]' dr \right) \\
& \frac{1}{k_\epsilon} [k_\epsilon a h^{(2)}_{n'}(k_\epsilon a)]' \delta_{n'n''} \delta_{-m'm''}. \qquad (3.46)
\end{aligned}
$$

Performing analogous derivations using definition of test function (3.29) and integral relations (3.122) and (3.125) we obtain

$$
\mathcal{Z}^{V_1,S_2}_{\epsilon\epsilon\ n'm',n''m''} \ = \ \omega\mu_0\ k_\epsilon \int_0^a j_{n'}(k_\epsilon r) j_{n'}(k_\epsilon r) r^2 dr d^{-1/2}_{n'm'} a h^{(2)}_{n'}(k_\epsilon a) \delta_{n'n''} \delta_{-m'm''}. \qquad (3.47)
$$

Finally, for the elements $\mathcal{Z}^{V_2,S_2}_{e\epsilon\ n'm',n''m''}$

$$\mathcal{Z}^{V_2,S_2}_{e\epsilon\ n'm',n''m''} = -\omega\mu_0\ k_\epsilon \sum_{n,m} d_{nm} \left(\int_V \boldsymbol{v}^{(2)}_{n'm'}(\boldsymbol{r}) \cdot \boldsymbol{q}^{(1\epsilon)}_{nm}(\boldsymbol{r}) dv \int_S \boldsymbol{q}^{(2\epsilon)}_{n,-m}(\boldsymbol{r}'') \cdot \boldsymbol{u}^{(2)}_{n''m''}(\boldsymbol{r}'') ds'' + \int_V \boldsymbol{v}^{(2)}_{n'm'}(\boldsymbol{r}) \cdot \boldsymbol{p}^{(1\epsilon)}_{nm}(\boldsymbol{r}) dv \int_S \boldsymbol{p}^{(2\epsilon)}_{n,-m}(\boldsymbol{r}'') \cdot \boldsymbol{u}^{(2)}_{n''m''}(\boldsymbol{r}'') ds'' \right), \quad (3.48)$$

we get vanishing result due to orthogonality relations (3.124) and (3.125)

$$\mathcal{Z}^{V_2,S_2}_{e\epsilon\ n'm',n''m''} = 0. \quad (3.49)$$

Considering (3.43), (3.47), (3.46), and (3.49) we can express the MoM matrix pertinent to the surface-to-volume operator in the following hollow matrix form:

$$\boldsymbol{\mathcal{Z}}^{V,S}_{e\epsilon} = \begin{bmatrix} 0 & \boldsymbol{\mathcal{Z}}^{V_1,S_2}_{e\epsilon} \\ \boldsymbol{\mathcal{Z}}^{V_2,S_1}_{e\epsilon} & 0 \end{bmatrix}. \quad (3.50)$$

3.3.6 Discretization of the Volume-to-Surface Operator $\mathcal{T}^{S,V}_{e0}$

The matrix elements $\mathcal{Z}^{S_i,V_j}_{e0}$ in the MoM discretization of the operator $\mathcal{T}^{S,V}_{e0}$ are obtained through testing of the scattered field $\mathcal{T}^{S,V}_{e0} \circ \boldsymbol{v}^{(j)}_{n''m''}$ produced by the vector spherical function $\boldsymbol{v}^{(j)}_{n''m''}$ which represents polarization current density in the volume V with the surface vector spherical functions $\boldsymbol{u}^{(i)}_{n'm'}$. Here, we take the inner product in the Sobolev space $H^l_{div}(S)$ similarly with the testing of the surface-to-surface operator

$$\mathcal{Z}_{e0\ n'm',n''m''}^{S_i,V_j} = \left\langle \boldsymbol{u}_{n'm'}^{(i)}, \mathcal{T}_{e0}^{S,V} \circ \boldsymbol{v}_{n''m''}^{(j)} \right\rangle_{H^l_{div}(S)} =$$
$$k_0^2(\epsilon-1)ik_0 \sum_{n,m} d_{nm}\psi_n^l \left(\int_S \boldsymbol{u}_{n'm'}^{(i)}(\boldsymbol{r}) \cdot \hat{\boldsymbol{n}} \times \boldsymbol{q}_{nm}^{(20)}(\boldsymbol{r}) ds \right.$$
$$\int_V \boldsymbol{q}_{n,-m}^{(10)}(\boldsymbol{r}'') \cdot \boldsymbol{v}_{n''m''}^{(j)}(\boldsymbol{r}'') dv'' + \int_S \boldsymbol{u}_{n'm'}^{(i)}(\boldsymbol{r})$$
$$\left. \cdot\, \hat{\boldsymbol{n}} \times \boldsymbol{p}_{nm}^{(20)}(\boldsymbol{r}) ds \int_V \boldsymbol{p}_{n,-m}^{(10)}(\boldsymbol{r}'') \cdot \boldsymbol{v}_{n''m''}^{(j)}(\boldsymbol{r}'') dv'' \right). \quad (3.51)$$

For elements $\mathcal{Z}_{e0}^{S_1,V_1}$ orthogonality relation [(72) or (75) in [60]] makes terms containing functions $\boldsymbol{q}$ vanish

$$\mathcal{Z}_{e0\ n'm',n''m''}^{S_1,V_1} = k_0^2(\epsilon-1)ik_0 \sum_{n,m} d_{nm}(1+n^2)^{l+1} \left(\int_S \right.$$
$$\left. \boldsymbol{u}_{n'm'}^{(1)}(\boldsymbol{r}) \cdot \hat{\boldsymbol{n}} \times \boldsymbol{p}_{nm}^{(20)}(\boldsymbol{r}) ds \int_V \boldsymbol{p}_{n,-m}^{(10)}(\boldsymbol{r}'') \cdot \boldsymbol{p}_{n''m''}^{(1\epsilon)}(\boldsymbol{r}'') dv'' \right)$$
$$= k_0^2(\epsilon-1)ik_0 \sum_{n,m} d_{nm}(1+n^2)^{l+1} \left(a h_n^{(2)}(k_0 a) \int_S d_{nm}^{1/2} \right.$$
$$\left. \nabla^t Y_n^m(\boldsymbol{r}) \cdot \nabla^t Y_{n'}^{m'}(\boldsymbol{r}) ds \int_V \boldsymbol{p}_{n,-m}^{(10)}(\boldsymbol{r}'') \cdot \boldsymbol{p}_{n''m''}^{(1\epsilon)}(\boldsymbol{r}'') dv'' \right). \quad (3.52)$$

Furthermore, using orthogonality relationship of [(47) in [60]] and (3.129), the above equation is reduces to the close-form expression.

$$\mathcal{Z}_{e0\ n'm',n''m''}^{S_1,V_1} = k_0^2(\epsilon-1)ik_0(1+(n')^2)^{l+1} a h_{n'}^{(2)}(k_0 a) d_{n'm'}^{-1/2}$$
$$\int_0^a j_{n'}(k_0 r) j_{n''}(k_\epsilon r) r^2 dr\, \delta_{n'n''} \delta_{-m'm''}. \quad (3.53)$$

For $\mathcal{Z}_{e0}^{S_1,V_2}$ elements basis functions definition (3.29) and orthogonality relations (3.123) and (3.125) produce zero result

$$\mathcal{Z}_{e0\ n'm',n''m''}^{S_1,V_2} = \left\langle \boldsymbol{u}_{n'm'}^{(1)}, \mathcal{T}_{e0}^{S,V} \circ \boldsymbol{v}_{n''m''}^{(2)} \right\rangle_{H_{div}^{l}(S)} = 0. \tag{3.54}$$

Similarly, elements $\mathcal{Z}_{e0}^{S_2,V_1}$ vanish according to (3.120), (3.125), and (3.126),

$$\mathcal{Z}_{e0\ n'm',n''m''}^{S_2,V_1} = \left\langle \boldsymbol{u}_{n'm'}^{(2)}, \mathcal{T}_{e0}^{S,V} \circ \boldsymbol{v}_{n''m''}^{(1)} \right\rangle_{H_{div}^{l}(S)} = 0. \tag{3.55}$$

Finally, for elements $\mathcal{Z}_{e0\ n'm',n''m''}^{S_2,V_2}$

$$\begin{aligned}
\mathcal{Z}_{e0\ n'm',n''m''}^{S_2,V_2} = k_0^2(\epsilon-1)ik_0 \sum_{n,m} d_{nm}(1+n^2)^l \Bigg(\int_S d_{n'm'}^{1/2} \\
\hat{\boldsymbol{r}} \times \nabla^t Y_{n'}^{m'}(\hat{\boldsymbol{r}}) \cdot \frac{1}{k_0}[k_0 a h_n^{(2)}(k_0 a)]' \hat{\boldsymbol{r}} \times \nabla^t Y_n^m(\hat{\boldsymbol{r}}) ds \\
\int_V \boldsymbol{q}_{n,-m}^{(10)}(\boldsymbol{r}'') \cdot \boldsymbol{q}_{n''m''}^{(1\epsilon)}(\boldsymbol{r}'') dv'' \Bigg) = k_0^2(\epsilon-1)ik_0 \\
\sum_{n,m} d_{nm}(1+n^2)^l \left(d_{nm}^{-1/2} \cdot \frac{1}{k_0}[k_0 a h_n^{(2)}(k_0 a)]' \right) \\
(\delta_{nn'}\delta_{m-m'}) \cdot \Bigg(\frac{n(n+1)}{k_0 k_\epsilon} \int_0^a j_n(k_0 r) j_{n''}(k_\epsilon r) dr \cdot a^2 + \\
\frac{1}{k_0 k_\epsilon} \int_0^a [k_0 r j_n(k_0 r)]' [k_\epsilon r j_{n''}(k_\epsilon r)]' dr \Bigg) \\
\delta_{nn''}\delta_{mm''} d_{nm}^{-1/2} d_{n''m''}^{-1/2} = k_0^2(\epsilon-1)ik_0 \\
(1+(n')^2)^l \left(d_{n''m''}^{-1/2} \cdot \frac{1}{k_0}[k_0 a h_{n'}^{(2)}(k_0 a)]' \right) \cdot \\
\Bigg(\frac{n'(n'+1)}{k_0 k_\epsilon} \int_0^a j_{n'}(k_0 r) j_{n''}(k_\epsilon r) dr \cdot a^2 + \\
\frac{1}{k_0 k_\epsilon} \int_0^a [k_0 r j_{n'}(k_0 r)]' [k_\epsilon r j_{n''}(k_\epsilon r)]' dr \Bigg) \delta_{n'n''}\delta_{-m'm''}.
\end{aligned} \tag{3.56}$$

Unfortunately, close-form expressions for the integrals in (3.56) over r are not available [63].

Combining (3.53), (3.54), (3.55), and (3.56) we get the following block diagonal matrix representation for the MoM impedance matrix corresponding to discretization of the volume-to-surface operator $\mathcal{T}_{e0}^{S,V}$

$$\boldsymbol{\mathcal{Z}}_{e0}^{S,V} = \begin{bmatrix} \boldsymbol{\mathcal{Z}}_{e0}^{S_1,V_1} & 0 \\ 0 & \boldsymbol{\mathcal{Z}}_{e0}^{S_2,V_2} \end{bmatrix}. \tag{3.57}$$

3.4 MoM Matrix Assembly

As a result of the MoM discretization of the integral operators $\mathcal{T}_{e\epsilon}^{S,S}$, $\mathcal{T}_{e\epsilon}^{V,S}$, $\mathcal{T}_{e0}^{S,V}$ and the incident field, the SVS-EFIE (3.6) is reduced to the system of linear algebraic equations with respect to the vector of unknown coefficients b_{nm} and c_{nm} in the expansion of the auxiliary single source surface current density $\boldsymbol{J}$ (3.17) that has the following a compact representation

$$\boldsymbol{\mathcal{Z}}_{SVS} \cdot \mathbf{I} = \mathbf{E}, \tag{3.58}$$

where $\mathbf{I} = [\mathbf{b}, \mathbf{c}]^t$ is vector of unknown coefficients b and c in the current expansion (3.17), $\mathbf{E}$ is the vector of excitation

$$\mathbf{E} = \begin{bmatrix} \mathbf{E}_1 \\ \mathbf{E}_2 \end{bmatrix} = \begin{bmatrix} \left\langle \hat{\boldsymbol{n}} \times \boldsymbol{E}^{inc}, \boldsymbol{u}_{nm}^{(1)} \right\rangle_{H_{div}^l(S)} \\ \left\langle \hat{\boldsymbol{n}} \times \boldsymbol{E}^{inc}, \boldsymbol{u}_{nm}^{(2)} \right\rangle_{H_{div}^l(S)} \end{bmatrix}, \tag{3.59}$$

and $\boldsymbol{\mathcal{Z}}_{\mathrm{SVS}}$ is the hollow matrix defined as

$$\begin{gathered} \boldsymbol{\mathcal{Z}}_{\mathrm{SVS}} = \begin{bmatrix} 0 & \boldsymbol{\mathcal{Z}}_{\mathrm{SVS}}^1 \\ \boldsymbol{\mathcal{Z}}_{\mathrm{SVS}}^2 & 0 \end{bmatrix} = - \begin{bmatrix} 0 & \boldsymbol{\mathcal{Z}}_{e\epsilon}^{S_1,S_2} \\ \boldsymbol{\mathcal{Z}}_{e\epsilon}^{S_2,S_1} & 0 \end{bmatrix} + \\ \begin{bmatrix} \boldsymbol{\mathcal{Z}}_{e0}^{S_1,V_1} & 0 \\ 0 & \boldsymbol{\mathcal{Z}}_{e0}^{S_2,V_2} \end{bmatrix} \cdot \begin{bmatrix} \boldsymbol{\Gamma}_1 & 0 \\ 0 & \boldsymbol{\Gamma}_2 \end{bmatrix}^{-1} \cdot \begin{bmatrix} 0 & \boldsymbol{\mathcal{Z}}_{e\epsilon}^{V_1,S_2} \\ \boldsymbol{\mathcal{Z}}_{e\epsilon}^{V_2,S_1} & 0 \end{bmatrix}, \end{gathered} \tag{3.60}$$

and the Gram matrix blocks $\mathbf{\Gamma}_j$ are defined as

$$\mathbf{\Gamma}_j = \left\langle \boldsymbol{v}^{(j\epsilon)}_{n'm'}, \boldsymbol{v}^{(j\epsilon)}_{n''m''} \right\rangle_{L^2(V)} = \int_V \boldsymbol{v}^{(j\epsilon)}_{n'm'} \cdot \boldsymbol{v}^{(j\epsilon)}_{n''m''} dv. \tag{3.61}$$

Multiplication and addition of the matrices in (3.60) produces multiplication of the block $\boldsymbol{\mathcal{Z}}^1_{\text{SVS}}$ with vector of unknown coefficients $\mathbf{c}$ in the following form according to (3.36), (3.56), (3.46), and (3.61)

$$\begin{gathered}
\boldsymbol{\mathcal{Z}}^1_{\text{SVS}} \cdot \mathbf{c} = [-\boldsymbol{\mathcal{Z}}^{S_1,S_2}_{e\epsilon} + \boldsymbol{\mathcal{Z}}^{S_1,V_1}_{e0} \cdot \mathbf{\Gamma}^{-1}_1 \cdot \boldsymbol{\mathcal{Z}}^{V_1,S_2}_{e\epsilon}] \cdot \mathbf{c} = \\
\frac{\omega\mu_0}{k_\epsilon} \sum_{n'',m''} (1+(n'')^2)^{l+1} c_{n''m''} (k_\epsilon a)^2 j_{n'}(k_\epsilon a) h^{(2)}_{n'}(k_\epsilon a) \delta_{n'n''} \delta_{-m'm''} + \\
i\omega\mu_0 (ik_0)^2 (\epsilon - 1) \sum_{n'',m''} (1+(n'')^2)^{l+1} c_{n''m''} \\
k_0 a h^{(2)}_{n'}(k_0 a) \int_0^a j_{n'}(k_0 r) j_{n''}(k_\epsilon r) r^2 dr \delta_{n'n''} \delta_{-m'm''} \\
\left(\int_0^a j_{n'}(k_\epsilon r) j_{n''}(k_\epsilon r) r^2 dr \right)^{-1} (-1) k_\epsilon a h^{(2)}_{n'}(k_\epsilon a) \int_0^a j_{n'}(k_\epsilon r) j_{n''}(k_\epsilon r) r^2 dr.
\end{gathered} \tag{3.62}$$

Due to diagonal structure of the block $\boldsymbol{\mathcal{Z}}^1_{\text{SVS}}$ we can explicitly evaluate unknown coefficients c_{nm} in the the following close form

$$c_{nm} = \frac{E_{1,n-m}}{(1+n^2)^{(l+1)} \Lambda^{(2)}_n}, \tag{3.63}$$

where

$$\Lambda^{(2)}_n = \Lambda^{S,S}_{2,e\epsilon,n} + \Lambda^{S,V}_{2,e0,n} \hat{\Gamma}^{-1}_{1,n} \Lambda^{V,S}_{2,e\epsilon,n}, \tag{3.64}$$

$\Lambda^{S,S}_{2,e\epsilon,n}$, $\Lambda^{S,V}_{2,e0,n}$, and $\Lambda^{V,S}_{2,e\epsilon,n}$ are defined in close-form [63] as

$$\Lambda^{S,S}_{2,e\epsilon,n} = \frac{\omega\mu_0}{k_\epsilon} (k_\epsilon a)^2 j_n(k_\epsilon a) h^{(2)}_n(k_\epsilon a), \tag{3.65}$$

$$\Lambda^{S,V}_{2,e0,n} = k_0 a h_n^{(2)}(k_0 a) k_0^2(\epsilon - 1) \int_0^a j_n(k_0 r) j_n(k_\epsilon r) r^2 dr$$
$$= a^2 k_0^2(\epsilon - 1) \frac{k_0 a h_n^{(2)}(k_0 a)}{k_0^2 - k_\epsilon^2} [k_\epsilon j_{n-1}(k_\epsilon a) j_n(k_0 a) - k_0 j_{n-1}(k_0 a) j_n(k_\epsilon a)], \quad (3.66)$$

$$\Lambda^{V,S}_{2,e\epsilon,n} = i\omega\mu_0 (k_\epsilon a) h_n^{(2)}(k_\epsilon a) \int_0^a j_n(k_\epsilon r) j_n(k_\epsilon r) r^2 dr =$$
$$i\omega\mu_0 (k_\epsilon a) h_n^{(2)}(k_\epsilon a) \frac{a^3}{2} [j_n(k_\epsilon a)^2 - j_{n-1}(k_\epsilon a) j_{n+1}(k_\epsilon a)], \quad (3.67)$$

and the elements of the Gram matrix are

$$\hat{\Gamma}_{1,n} = \int_0^a j_n(k_\epsilon r) j_n(k_\epsilon r) r^2 dr = \frac{a^3}{2} [j_n(k_\epsilon a)^2 - j_{n-1}(k_\epsilon a) j_{n+1}(k_\epsilon a)]. \quad (3.68)$$

Similarly, multiplication and addition of the matrices in (3.60) produces multiplication of the block $\boldsymbol{\mathcal{Z}}^2_{\mathrm{SVS}}$ with vector of unknown coefficients $\mathbf{b}$ in the following form according to (3.36), (3.56), (3.46), and (3.61)

$$\begin{aligned}\boldsymbol{\mathcal{Z}}^2_{\mathrm{SVS}}\cdot\mathbf{b} = [-\boldsymbol{\mathcal{Z}}^{S_2,S_1}_{e\epsilon} + \boldsymbol{\mathcal{Z}}^{S_2,V_2}_{e0}\cdot\boldsymbol{\Gamma}_2^{-1}\cdot\boldsymbol{\mathcal{Z}}^{V_2,S_1}_{e\epsilon}]\cdot\mathbf{b} \\ = -\frac{\omega\mu_0}{k_\epsilon}\sum_{n'',m''}(1+(n'')^2)^l b_{n''m''}\ [k_\epsilon a j_{n'}(k_\epsilon a)]' \\ [k_\epsilon a h^{(2)}_{n'}(k_\epsilon a)]'\delta_{n'n''}\delta_{m'-m''} + i\omega\mu_0(ik_0)^2(\epsilon-1) \\ \sum_{n'',m''}(1+(n'')^2)^l b_{n''m''}[k_0 a h^{(2)}_{n'}(k_0 a)]'\cdot \\ \Big(\frac{n'(n'+1)}{k_0k_\epsilon}\int_0^a j_{n'}(k_0r)j_{n''}(k_\epsilon r)dr+ \\ \frac{1}{k_0k_\epsilon}\int_0^a[k_0rj_{n'}(k_0r)]'[k_\epsilon r j_{n''}(k_\epsilon r)]'dr\Big)\delta_{n'n''}\delta_{-m'm''}\cdot \\ \left(\frac{n'(n'+1)}{k_\epsilon k_\epsilon}\int_0^a j_{n'}(k_\epsilon r)j_{n''}(k_\epsilon r)dr\right. \\ \left.+\frac{1}{k_\epsilon k_\epsilon}\int_0^a[k_\epsilon rj_{n'}(k_\epsilon r)]'[k_\epsilon r j_{n''}(k_\epsilon r)]'dr\right)^{-1} \\ [k_\epsilon a h^{(2)}_{n}(k_\epsilon a)]'\left(\frac{n'(n'+1)}{k_\epsilon k_\epsilon}\int_0^a j_{n'}(k_\epsilon r)\right. \\ \left. j_{n''}(k_\epsilon r)dr + \frac{1}{k_\epsilon k_\epsilon}\int_0^a[k_\epsilon rj_{n'}(k_\epsilon r)]'[k_\epsilon r j_{n''}(k_\epsilon r)]'dr\right).\end{aligned} \tag{3.69}$$

The diagonal structure of $\boldsymbol{\mathcal{Z}}^2_{\mathrm{SVS}}$ allows explicit evaluate of unknown coefficients b_{nm} in the following closed form

$$b_{nm} = \frac{E_{2,n-m}}{(1+n^2)^l\Lambda^{(1)}_n}, \tag{3.70}$$

where

$$\Lambda^{(1)}_n = \Lambda^{S,S}_{1,e\epsilon,n} + \Lambda^{S,V}_{1,e0,n}\hat{\Gamma}^{-1}_{2,n}\Lambda^{V,S}_{1,e\epsilon,n}, \tag{3.71}$$

the eigenvalues $\Lambda^{S,S}_{1,e\epsilon,n}$, $\Lambda^{S,V}_{1,e0,n}$, and $\Lambda^{V,S}_{1,e\epsilon,n}$ are

$$\Lambda^{S,S}_{1,e\epsilon,n} = -\frac{\omega\mu_0}{k_\epsilon}[(k_\epsilon a)j_n(k_\epsilon a)]'[(k_\epsilon a)h^{(2)}_n(k_\epsilon a)]', \tag{3.72}$$

$$\Lambda^{S,V}_{1,e0,n} = -k_0^2(\epsilon - 1)[(k_0a)h_n^{(2)}(k_0a)]' \left(\frac{n(n+1)}{k_0k_\epsilon}a^2 \int_0^a j_n(k_0r)j_n(k_\epsilon r)dr + \frac{1}{k_0k_\epsilon}\int_0^a [k_0rj_n(k_0r)]'[k_\epsilon rj_n(k_\epsilon r)]'dr\right), \quad (3.73)$$

$$\Lambda^{V,S}_{1,e\epsilon,n} = i\omega\mu_0[(k_\epsilon a)h_n^{(2)}(k_\epsilon a)]' \left(\frac{n(n+1)}{k_\epsilon^2}a^2 \int_0^a j_n(k_\epsilon r) j_n(k_\epsilon r)dr + \frac{1}{k_\epsilon^2}\int_0^a [(k_\epsilon r)j_n(k_\epsilon r)]'[(k_\epsilon r)j_n(k_\epsilon r)]'dr\right), \quad (3.74)$$

and the Gram matrix elements are given by

$$\hat{\Gamma}_{2,n} = \left(\frac{n(n+1)}{k_\epsilon^2}a^2 \int_0^a j_n(k_\epsilon r)j_n(k_\epsilon r)dr + \frac{1}{k_\epsilon^2}\int_0^a [(k_\epsilon r)j_n(k_\epsilon r)]'[(k_\epsilon r)j_n(k_\epsilon r)]'dr\right). \quad (3.75)$$

Note, we could not find a close-form expressions for the integrals in (3.73)-(3.75) and neither could the authors of [63]. We compute them numerically to 10 digits of accuracy in Mathcad.

3.5 Spectral Analysis of SVS-EFIE and its Galerkin MoM Matrix

3.5.1 Spectra of SVS-EFIE operators

It can be shown that $\Lambda^{S,S}_{2,e\epsilon,n}$ are the eigenvalues of the operator $\mathcal{T}^{S,S}_{e\epsilon}$ since

$$\mathcal{T}^{S,S}_{e\epsilon} \circ (\hat{\boldsymbol{r}} \times \nabla^t Y_n^m) = \Lambda^{S,S}_{2,e\epsilon,n}\nabla^t Y_n^m, \quad (3.76)$$

and the product $\Lambda^{S,V}_{2,e0,n}\hat{\Gamma}^{-1}_{1,n}\Lambda^{V,S}_{2,e\epsilon,n}$ forms the eigenvalues of the product of the operators $\mathcal{T}^{S,V}_{e0} \circ \mathcal{T}^{V,S}_{e\epsilon}$ according to

$$\mathcal{T}^{S,V}_{e0} \circ \mathcal{T}^{V,S}_{e\epsilon} \circ (\hat{\boldsymbol{r}} \times \nabla^t Y^m_n) = \Lambda^{S,V}_{2,e0,n}\hat{\Gamma}^{-1}_{1,n}\Lambda^{V,S}_{2,e\epsilon,n}\nabla^t Y^m_n, \tag{3.77}$$

making $\Lambda^{(2)}_n = \Lambda^{S,S}_{2,e\epsilon,n} + \Lambda^{S,V}_{2,e0,n}\hat{\Gamma}^{-1}_{1,n}\Lambda^{V,S}_{2,e\epsilon,n}$ the eigenvalues of the total SVS-EFIE operator $\mathcal{T}_{SVS} = \mathcal{T}^{S,S}_{e\epsilon} + \mathcal{T}^{S,V}_{e0} \circ \mathcal{T}^{V,S}_{e\epsilon}$

$$\mathcal{T}^{S,S}_{e\epsilon} \circ (\hat{\boldsymbol{r}} \times \nabla^t Y^m_n) + \mathcal{T}^{S,V}_{e0} \circ \mathcal{T}^{V,S}_{e\epsilon} \circ (\hat{\boldsymbol{r}} \times \nabla^t Y^m_n) = \Lambda^{(2)}_n \nabla^t Y^m_n. \tag{3.78}$$

Similarly, $\Lambda^{S,S}_{1,e\epsilon,n}$ are the eigenvalues of the operator $\mathcal{T}^{S,S}_{e\epsilon}$ (see Appendix II), since

$$\mathcal{T}^{S,S}_{e\epsilon} \circ (\nabla^t Y^m_n) = \Lambda^{S,S}_{1,e\epsilon,n}\hat{\boldsymbol{r}} \times \nabla^t Y^m_n, \tag{3.79}$$

and the product $\Lambda^{S,V}_{1,e0,n}\hat{\Gamma}^{-1}_{2,n}\Lambda^{V,S}_{1,e\epsilon,n}$ forms the eigenvalues of the product of the operators $\mathcal{T}^{S,V}_{e0} \circ \mathcal{T}^{V,S}_{e\epsilon}$ according to

$$\mathcal{T}^{S,V}_{e0} \circ \mathcal{T}^{V,S}_{e\epsilon} \circ (\nabla^t Y^m_n) = \Lambda^{S,V}_{1,e0,n}\hat{\Gamma}^{-1}_{2,n}\Lambda^{V,S}_{1,e\epsilon,n}(\hat{\boldsymbol{r}} \times \nabla^t Y^m_n), \tag{3.80}$$

making $\Lambda^{(1)}_n = \Lambda^{S,S}_{1,e\epsilon,n} + \Lambda^{S,V}_{1,e0,n}\hat{\Gamma}^{-1}_{2,n}\Lambda^{V,S}_{1,e\epsilon,n}$ the eigenvalues of the total SVS-EFIE operator $\mathcal{T}^{S,S}_{e\epsilon} + \mathcal{T}^{S,V}_{e0} \circ \mathcal{T}^{V,S}_{e\epsilon}$

$$\mathcal{T}^{S,S}_{e\epsilon} \circ (\nabla^t Y^m_n) + \mathcal{T}^{S,V}_{e0} \circ \mathcal{T}^{V,S}_{e\epsilon} \circ (\nabla^t Y^m_n) = \Lambda^{(1)}_n \hat{\boldsymbol{r}} \times \nabla^t Y^m_n. \tag{3.81}$$

3.5.2 Spectrum of Galerkin MoM matrix

In order to investigate the spectral property of the Galerkin MoM matrix by analogy with (96a) and (97b) in [60] we can state the close-form expressions (3.63) for coefficients c_{nm} and (3.70) for coefficients b_{nm} in the form of the following diagonal matrix equation

$$\left\langle \mathcal{T}_{SVS} \circ \boldsymbol{J}, \boldsymbol{u}^{(1)}_{n'm'} \right\rangle_{H^l_{div}(S)} = \sum_{n,m} c_{nm} \Lambda^{(2)}_n (1+n^2)^{l+1} \delta_{nn'} \delta_{mm'} = \left\langle \hat{\boldsymbol{n}} \times \boldsymbol{E}^{inc}, \boldsymbol{u}^{(1)}_{n'm'} \right\rangle_{H^l_{div}(S)}, \tag{3.82}$$

$$\left\langle \mathcal{T}_{SVS} \circ \boldsymbol{J}, \boldsymbol{u}^{(2)}_{n'm'} \right\rangle_{H^l_{div}(S)} = \sum_{n,m} b_{nm} \Lambda^{(1)}_n (1+n^2)^{l} \delta_{nn'} \delta_{mm'} = \left\langle \hat{\boldsymbol{n}} \times \boldsymbol{E}^{inc}, \boldsymbol{u}^{(2)}_{n'm'} \right\rangle_{H^l_{div}(S)}. \tag{3.83}$$

3.5.3 Oversampling breakdown

The asymptotic behaviour of the eigenvalues of the operators forming the SVS-EFIE at large n is the following

$$\Lambda^{S,S}_{1,e\epsilon,n} \sim n, \qquad \Lambda^{S,V}_{1,e0,n} \hat{\Gamma}^{-1}_{2,n} \Lambda^{V,S}_{1,e\epsilon,n} \sim n, \tag{3.84}$$

$$\Lambda^{S,S}_{2,e\epsilon,n} \sim n^{-1}, \quad \Lambda^{S,V}_{2,e0,n} \hat{\Gamma}^{-1}_{1,n} \Lambda^{V,S}_{2,e\epsilon,n} \sim n^{-4}, \tag{3.85}$$

which makes the eigenvalues of the SVS-EFIE operator $\mathcal{T}_{SVS}$ to asymptotically behave according to the asymptotic behaviour of the S-EFIE operator $\mathcal{T}^{S,S}_{e\epsilon}$ eigenvalues, i.e.

$$\Lambda^{(1)}_n = \Lambda^{S,S}_{1,e\epsilon,n} + \Lambda^{S,V}_{1,e0,n} \hat{\Gamma}^{-1}_{2,n} \Lambda^{V,S}_{1,e\epsilon,n} \sim n, \tag{3.86}$$

$$\Lambda^{(2)}_n = \Lambda^{S,S}_{2,e\epsilon,n} + \Lambda^{S,V}_{2,e0,n} \hat{\Gamma}^{-1}_{1,n} \Lambda^{V,S}_{2,e\epsilon,n} \sim \frac{1}{n}. \tag{3.87}$$

From (3.86) and (3.87) we can see that for the eigenvalues $\hat{\Lambda}^{(1)}$ and $\hat{\Lambda}^{(2)}$ of the Galerkin MoM impedance matrix to tend to a constant

$$\hat{\Lambda}_n^{(1)} = \Lambda_n^{(1)}(1+n^2)^l \sim O(1), \tag{3.88}$$

$$\hat{\Lambda}_n^{(2)} = \Lambda_n^{(2)}(1+n^2)^{l+1} \sim O(1), \tag{3.89}$$

and ensure constant condition number upon increased order of discretization n, the Galerkin MoM solution of the SVS-EFIE must be sought in Sobolev space $H^l_{div}(S)$ with $l = -1/2$ the same as S-EFIE [60]. If the Galerkin testing is performed in functional space $L^2(S)$ as most commonly done in practice the condition number of the MoM impedance matrix grows as $O(n^2)$ due to accumulation of the spectrum at zero (eigenvalues $\Lambda^{(2)}$) and infinity (eigenvalues $\Lambda^{(1)}$).

3.5.4 Internal resonances breakdown

At certain discrete frequencies $\omega = \omega_n^{(1)}$ when

$$\Lambda^{S,S}_{1,e\epsilon,n} = -\Lambda^{S,V}_{1,e0,n}\hat{\Gamma}^{-1}_{2,n}\Lambda^{V,S}_{1,e\epsilon,n}, \tag{3.90}$$

nth eigenvalue $\Lambda_n^{(1)}$ becomes zero. Similarly, nth eigenvalue $\Lambda_n^{(2)}$ becomes zero at frequencies $\omega = \omega_n^{(2)}$, when

$$\Lambda^{S,S}_{2,e\epsilon,n} = -\Lambda^{S,V}_{2,e0,n}\hat{\Gamma}^{-1}_{1,n}\Lambda^{V,S}_{2,e\epsilon,n}. \tag{3.91}$$

Frequencies $\omega_n^{(1)}$ and $\omega_n^{(2)}$ are not equal to each other. At each such frequency $\omega_n^{(1)}$ or $\omega_n^{(2)}$ solution of the SVS-EFIE loses its uniqueness and experiences what is commonly known as internal resonance breakdown. Note, that frequencies $\omega_n^{(1)}$ and $\omega_n^{(2)}$ are different from those, at which eigenvalues of the surface-to-surface operators $\Lambda^{S,S}_{1,e\epsilon,n}$ or $\Lambda^{S,S}_{2,e\epsilon,n}$ become zero. Physically, these spurious resonances occur when nth rotational or irrotational mode of the total and scattered electric field tangential components exactly cancel on sphere's surface.

3.5.5 Low frequency breakdown

As frequency tends to zero, eigenvalues can be shown to behave as

$$\Lambda_n^{(1)} \sim \frac{1}{\omega}, \quad \Lambda_n^{(2)} \sim \omega, \tag{3.92}$$

which results in low frequency breakdown of the SVS-EFIE.

It's important to point out that MoM testing of SVS-EFIE in Sobolev space $H_{div}^{-1/2}(S)$ multiplies the eigenvalues by frequency independent factors $(1+n^2)^{\pm 1/2}$ and, hence, does not eliminate either the internal resonances or low frequency breakdown. Other remedies have to be sought for these breakdowns as will be addressed in the future publicaitons.

3.6 Sphere Excitation by Electric Dipole

The electric field due to a general current distribution $\boldsymbol{i}$ can be defined in free space using the definition of the dyadic Green's function of the electric field (3.22), as follows:

$$\begin{aligned}\boldsymbol{E}^{inc}(\boldsymbol{r}) = i\omega\mu_0 \int_V \bar{\boldsymbol{G}}_{e0}(\boldsymbol{r},\boldsymbol{r}') \cdot \boldsymbol{i}(\boldsymbol{r}')dv' = \\ i\omega\mu_0 \int_V (ik_0) \sum_{n,m} d_{nm} \{\boldsymbol{q}_{nm}^{(1)}(\boldsymbol{r})\boldsymbol{q}_{n,-m}^{(2)}(\boldsymbol{r}') \\ + \boldsymbol{p}_{nm}^{(1)}(\boldsymbol{r})\boldsymbol{p}_{n,-m}^{(2)}(\boldsymbol{r}')\} \cdot \boldsymbol{i}(\boldsymbol{r}')dv'.\end{aligned} \tag{3.93}$$

In the case an electric dipole having length l, current I, dipole moment Il and situated at location $\boldsymbol{r}_0$, current $\boldsymbol{i}$ is defined as $\boldsymbol{i}(\boldsymbol{r}) = Il\hat{\boldsymbol{l}}\delta(\boldsymbol{r}-\boldsymbol{r}_0)$, which assumes the following form in the spherical coordinates

$$\boldsymbol{i}(\boldsymbol{r}) = \frac{Il\hat{\boldsymbol{l}}}{r_0^2 \sin\theta_0} \delta(r - r_0)\delta(\theta - \theta_0)\delta(\phi - \phi_0), \tag{3.94}$$

where $\hat{\boldsymbol{l}}$ is the unit vector of the dipole orientation and r_0, θ_0, and ϕ_0 are the position coordinates of the dipole in the spherical system.

3.6.1 Incident electric field due to radial electric dipole

Let's consider the incident field in case of a radial electric dipole with the dipole moment $Il = 1[A{\cdot}m]$. The dipole will be placed on z axis ($\boldsymbol{r}_0 = \hat{\boldsymbol{z}}r_0 = \hat{\boldsymbol{r}}r_0 + \hat{\boldsymbol{\theta}}0 + \hat{\boldsymbol{\phi}}0$) in order to produce solution independent on azimuthal angle ϕ. In this case $\hat{\boldsymbol{l}} = \hat{\boldsymbol{r}} = \hat{\boldsymbol{z}}$ and the incident field will be represented in terms of spherical wave functions for the Green's function, as follows:

$$\boldsymbol{E}^{inc}(\boldsymbol{r}) = -\omega\mu k_0 \sum_{n,m} d_{nm} \{\boldsymbol{q}_{nm}^{(1)}(\boldsymbol{r})\boldsymbol{q}_{n,-m}^{(2)}(\hat{\boldsymbol{z}}r_0) \cdot \hat{\boldsymbol{z}} + \boldsymbol{p}_{nm}^{(1)}(\boldsymbol{r})\boldsymbol{p}_{n,-m}^{(2)}(\hat{\boldsymbol{z}}r_0) \cdot \hat{\boldsymbol{z}}\}. \tag{3.95}$$

From the definition of spherical vector wave function $\boldsymbol{p}$ in (3.27), $\boldsymbol{p}$ has only $\hat{\theta}$ and $\hat{\phi}$ components. This results in vanishing second term of (3.95)

$$\boldsymbol{E}^{inc}(\boldsymbol{r}) = -\omega\mu_0 k_0 \sum_{n,m} d_{nm} \boldsymbol{q}_{nm}^{(1)}(\boldsymbol{r})\boldsymbol{q}_{n,-m}^{(2)}(\hat{\boldsymbol{z}}r_0) \cdot \hat{\boldsymbol{z}}. \tag{3.96}$$

Taking the inner product of $\hat{\boldsymbol{n}} \times \boldsymbol{E}^{inc}$ with $\boldsymbol{u}_{n'm'}^{(1)}$ and considering orthogonality relations [60], we get vanishing $\boldsymbol{E}_1$ part of the excitation vector

$$E_{1,n'm'} = \left\langle \hat{\boldsymbol{n}} \times \boldsymbol{E}^{inc}, \boldsymbol{u}^{(1)}_{n'm'} \right\rangle_{H^l_{div}(S)} =$$
$$-\omega\mu_0 k_0 \sum_{n,m} d_{nm}(1+n^2)^{l+1} d^{1/2}_{n'm'} \boldsymbol{q}^{(2)}_{n,-m}(\hat{\boldsymbol{z}} r_0)\cdot\hat{\boldsymbol{z}} \int_S \hat{\boldsymbol{n}} \times \boldsymbol{q}^{(1)}_{nm}(\boldsymbol{r}) \cdot \nabla^t Y^{m'}_{n'}(\hat{\boldsymbol{r}}) ds = 0. \tag{3.97}$$

Similarly, taking the inner product of $\hat{\boldsymbol{n}} \times \boldsymbol{E}^{inc}$ with $\boldsymbol{u}^{(2)}_{n'm'}$ we get

$$\begin{aligned} E_{2,n'm'} = \left\langle \hat{\boldsymbol{n}} \times \boldsymbol{E}^{inc}, \boldsymbol{u}^{(2)}_{n'm'} \right\rangle_{H^l_{div}(S)} &= -\omega\mu_0 k_0 \\ &\sum_{n,m} d_{nm} \boldsymbol{q}^{(2)}_{n,-m}(\hat{\boldsymbol{z}} r_0)\cdot\hat{\boldsymbol{z}} \left\langle \hat{\boldsymbol{n}} \times \boldsymbol{q}^{(1)}_{nm}(\boldsymbol{r}), \boldsymbol{u}^{(2)}_{n'm'} \right\rangle_{H^l_{div}(S)} \\ &= -\omega\mu_0 k_0 \sum_{n,m} d_{nm}(1+n^2)^l \boldsymbol{q}^{(2)}_{n,-m}(\hat{\boldsymbol{z}} r_0)\cdot\hat{\boldsymbol{z}} \\ &\qquad d^{1/2}_{n'm'} \int_S \hat{\boldsymbol{n}} \times \boldsymbol{q}^{(1)}_{nm}(\boldsymbol{r}) \cdot [\hat{\boldsymbol{r}} \times \nabla^t Y^{m'}_{n'}(\hat{\boldsymbol{r}})] ds. \end{aligned} \tag{3.98}$$

According to the definition of $\boldsymbol{q}$ in (3.28) for radial dipole located on z-axis we have $\theta_0 = 0$, $\phi_0 = 0$ yielding

$$\begin{aligned} \boldsymbol{q}^{(2)}_{n,-m}(\hat{\boldsymbol{z}} r_0)\cdot\hat{\boldsymbol{z}} &= \frac{n(n+1)}{k_0 r_0} h^{(2)}_n(k_0 r_0) e^{-im\phi_0} P^{|m|}_n(\cos\theta_0) \\ &= \frac{n(n+1)}{k_0 r_0} h^{(2)}_n(k_0 r_0)\delta_{m0}. \end{aligned} \tag{3.99}$$

Substituting (3.99) into (3.98) and taking into consideration orthogonality relation [(47) in [60]] we obtain

$$\begin{aligned} E_{2,n'm'} = \left\langle \hat{\boldsymbol{n}} \times \boldsymbol{E}^{inc}, \boldsymbol{u}^{(2)}_{n'm'} \right\rangle_{H^l_{div}(S)} &= -(1+(n')^2)^l \delta_{m'0} \\ &\omega\mu_0 d^{1/2}_{0n'} [k_0 a j_{n'}(k_0 a)]' \frac{n'(n'+1)}{k_0 r_0} h^{(2)}_{n'}(k_0 r_0). \end{aligned} \tag{3.100}$$

Substituting (3.97) into (3.63) and (3.100) into (3.70) we get closed form expressions for the coefficients $\mathbf{b}$ and $\mathbf{c}$ in the expansion (3.17) of the unknown current $\boldsymbol{J}$. Note that since the part of the excitation vector $\mathbf{E}_1$ is zero, coefficients $\mathbf{c}$ vanish and only functions $\boldsymbol{u}^{(1)}$ are present in the solution. The physical meaning of vanishing contribution of functions $\boldsymbol{u}^{(2)}$ from the solution is that radial electric dipole excites only the TM_r-waves with respect to the radial coordinate r (i.e. waves with $H_r = 0$) [52]. These waves are produced by the irrotational part of the fictitious current $\boldsymbol{J}$ represented by functions $\boldsymbol{u}^{(1)}$.

3.6.2 Incident electric field due to tangential electric dipole

Next, we consider excitation by the tangential electric dipole situated on z-axis at the location defined in spherical coordinates as ($\boldsymbol{r}_0 = \hat{\boldsymbol{z}} r_0 = \hat{\boldsymbol{r}} r_0 + \hat{\boldsymbol{\theta}} 0 + \hat{\boldsymbol{\phi}} 0$) and directed along θ-coordinate, i.e. $\hat{\boldsymbol{l}} = \hat{\boldsymbol{\theta}} = \hat{\boldsymbol{x}}$. Thus, the dipole current is defined as $\boldsymbol{j}(\boldsymbol{r}) = Il\hat{\boldsymbol{\theta}}\delta(\boldsymbol{r} - \boldsymbol{r}_0)$. Substituting the expression for current into the incident field expression (3.93) we obtain

$$\boldsymbol{E}^{inc}(\boldsymbol{r}) = -\omega\mu_0 k_0 \sum_{n,m} d_{nm} \Big(\hat{\boldsymbol{n}} \times \boldsymbol{q}^{(1)}_{nm}(\boldsymbol{r}) \boldsymbol{q}^{(2)}_{n,-m}(\boldsymbol{r}_0) \cdot \hat{\boldsymbol{\theta}}(\boldsymbol{r}_0) \\ + \hat{\boldsymbol{n}} \times \boldsymbol{p}^{(1)}_{nm}(\boldsymbol{r}) \boldsymbol{p}^{(2)}_{n,-m}(\boldsymbol{r}_0) \cdot \hat{\boldsymbol{\theta}}(\boldsymbol{r}_0) \Big). \quad (3.101)$$

Testing the incident field with functions $\boldsymbol{u}^{(1)}$ and performing the inner product in Sobolev space $H^l_{div}(S)$ we obtain

$$E_{1,n'm'} = \left\langle \hat{\boldsymbol{n}} \times \boldsymbol{E}^{inc}, \boldsymbol{u}^{(1)}_{n'm'} \right\rangle_{H^l_{div}(S)} = -\omega\mu_0 k_0 \sum_{n,m} d_{nm} \\ (1+n^2)^{l+1} \Big(\boldsymbol{q}^{(2)}_{n,-m}(\boldsymbol{r}_0) \cdot \hat{\boldsymbol{\theta}}(\boldsymbol{r}_0) \int_S \hat{\boldsymbol{n}} \times \boldsymbol{q}^{(1)}_{nm}(\boldsymbol{r}) \cdot \boldsymbol{u}^{(1)}_{n'm'}(\boldsymbol{r}) ds \\ + \boldsymbol{p}^{(2)}_{n,-m}(\boldsymbol{r}_0) \cdot \hat{\boldsymbol{\theta}}(\boldsymbol{r}_0) \int_S \hat{\boldsymbol{n}} \times \boldsymbol{p}^{(1)}_{nm}(\boldsymbol{r}) \cdot \boldsymbol{u}^{(1)}_{n'm'}(\boldsymbol{r}) ds \Big). \quad (3.102)$$

By virtue of the orthogonality relations of the volume spherical harmonics $\boldsymbol{q}^{(1)}$ with surface spherical functions $\boldsymbol{u}^{(1)}$ the above expression simplifies to

$$\begin{aligned} E_{1,n'm'} = \left\langle \hat{\boldsymbol{n}} \times \boldsymbol{E}^{inc}, \boldsymbol{u}^{(1)}_{n'm'} \right\rangle_{H^l_{div}(S)} &= -\omega\mu_0 k_0 \sum_{n,m} d_{nm} \\ (1+n^2)^{l+1} \boldsymbol{p}^{(2)}_{n,-m}(\boldsymbol{r}_0) \cdot \hat{\boldsymbol{\theta}}(\boldsymbol{r}_0) \int_S & \hat{\boldsymbol{n}} \times \boldsymbol{p}^{(1)}_{nm}(\boldsymbol{r}) \cdot \boldsymbol{u}^{(1)}_{n'm'}(\boldsymbol{r}) ds = \\ -\omega\mu_0 k_0 d^{1/2}_{n'm'}(1+(n')^2)^{l+1} a j_{n'}(k_0 a) & \boldsymbol{p}^{(2)}_{n',-m'}(\boldsymbol{r}_0) \cdot \hat{\boldsymbol{\theta}}(\boldsymbol{r}_0). \end{aligned} \quad (3.103)$$

Taking $\hat{\boldsymbol{\theta}}$-component of $\boldsymbol{p}^{(2)}_{n',-m'}$ at $\boldsymbol{r}_0$ we get

$$\begin{aligned} E_{1,n'm'} = \left\langle \hat{\boldsymbol{n}} \times \boldsymbol{E}^{inc}, \boldsymbol{u}^{(1)}_{n'm'} \right\rangle_{H^l_{div}(S)} &= -\omega\mu_0 k_0 \\ a j_{n'}(k_0 a) d^{1/2}_{n'm'}(1+(n')^2)^{l+1}(-im') h^{(2)}_{n'}(kr_0) & \lim_{\theta_0 \to 0} \frac{P^{|m'|}_{n'}(\cos\theta_0)}{\sin\theta_0}. \end{aligned} \quad (3.104)$$

Since the limit is non-zero only when $|m'| \neq 1$ and equals to $\lim_{\theta_0 \to 0} \frac{P^{|m'|}_{n'}(\cos\theta_0)}{\sin\theta_0} = \frac{n'(n'+1)}{2}\delta_{|m'|,1}$ we obtain the sought close-form expression for the elements of the excitation vector $\mathbf{E}_1$

$$\begin{aligned} E_{1,n'm'} = \left\langle \hat{\boldsymbol{n}} \times \boldsymbol{E}^{inc}, \boldsymbol{u}^{(1)}_{n'm'} \right\rangle_{H^l_{div}(S)} &= -\frac{n'(n'+1)}{2} \\ \omega\mu_0 k_0 \delta_{|m'|,1} d^{1/2}_{n'm'}(-im') a j_{n'}(k_0 a) & (1+(n')^2)^{l+1} h^{(2)}_{n}(kr_0). \end{aligned} \quad (3.105)$$

Similarly, we obtain the values for $\mathbf{E}_2$ part of the excitation vector through testing of the incident field with functions $\boldsymbol{u}^{(2)}$ in Sobolev space $H^l_{div}(S)$

$$\begin{aligned} E_{2,n'm'} = \left\langle \hat{\boldsymbol{n}} \times \boldsymbol{E}^{inc}, \boldsymbol{u}^{(2)}_{n'm'} \right\rangle_{H^l_{div}(S)} &= -\omega\mu_0 \frac{n'(n'+1)}{2} \\ \delta_{|m'|,1} d^{1/2}_{n'm'}(1+(n')^2)^{l} [k_0 a j_{n'}(k_0 a)]' & \frac{1}{kr_0} [k_0 r_0 h^{(2)}_{n'}(kr_0)]'. \end{aligned} \quad (3.106)$$

Substitution of (3.105) into (3.63) and (3.106) into (3.70) provides close-form expressions for the coefficients $\mathbf{b}$ and $\mathbf{c}$ in the expansion of the unknown fictitious current $\boldsymbol{J}$ and formalizes the exact solution of the SVS-EFIE (3.4) for the case of the tangential electric dipole radiation near dielectric sphere.

3.7 Evaluation of Electric Field Inside the Sphere

After determining coefficients b_{nm} and c_{nm} in the MoM expansion (3.17) of the fictitious currrent $\boldsymbol{J}$ on S over complete set of basis functions $\boldsymbol{u}^{(1)}$ and $\boldsymbol{u}^{(2)}$, the electric field $\boldsymbol{E}$ in the scatterer volume V can be evaluated using the single-source representation (4.2) under condition $\mathtt{a} = 1$ and $\mathtt{b} = 0$, i.e.

$$\boldsymbol{E}(\boldsymbol{r}) = i\omega\mu_0 \int_S \bar{\boldsymbol{G}}_{e\epsilon}(\boldsymbol{r}, \boldsymbol{r}') \cdot \boldsymbol{J}(\boldsymbol{r'}) dv' \quad r \in V. \tag{3.107}$$

To evaluate the field inside the sphere according (3.107), we substitute expression (3.22) for $\bar{\boldsymbol{G}}_{e\epsilon}$ into (3.107)

$$\begin{aligned}\boldsymbol{E}(\boldsymbol{r}) = i\omega\mu_0(ik_\epsilon) \sum_{n,m} d_{nm} \Bigg(\boldsymbol{q}^{(1\epsilon)}_{nm}(\boldsymbol{r}) \int_S \boldsymbol{q}^{(2\epsilon)}_{n,-m}(\boldsymbol{r}') \cdot \\ \boldsymbol{J}(\boldsymbol{r'}) dr' + \boldsymbol{p}^{(1\epsilon)}_{nm}(\boldsymbol{r}) \int_S \boldsymbol{p}^{(2\epsilon)}_{n,-m}(\boldsymbol{r}') \cdot \boldsymbol{J}(\boldsymbol{r'}) dr' \Bigg), \quad r \in V.\end{aligned} \tag{3.108}$$

Plugging current expansion (3.17) into field definition (3.108) we get

$$\begin{aligned}\boldsymbol{E}(\boldsymbol{r}) = -\omega\mu_0 k_\epsilon \sum_{n,m} d_{nm} \Big(\boldsymbol{q}^{(1\epsilon)}_{nm}(\boldsymbol{r}) \sum_{n'',m''} b_{n''m''} \int_S \boldsymbol{q}^{(2\epsilon)}_{n,-m}(\boldsymbol{r}') \cdot \boldsymbol{u}^{(1)}_{n''m''}(\boldsymbol{r}') dr' + \\ \boldsymbol{q}^{(1\epsilon)}_{nm}(\boldsymbol{r}) \sum_{n'',m''} c_{n''m''} \int_S \boldsymbol{q}^{(2\epsilon)}_{n,-m}(\boldsymbol{r}') \cdot \boldsymbol{u}^{(2)}_{n''m''}(\boldsymbol{r}') dr' + \\ \boldsymbol{p}^{(1\epsilon)}_{nm}(\boldsymbol{r}) \sum_{n'',m''} b_{n''m''} \int_S \boldsymbol{p}^{(2\epsilon)}_{n,-m}(\boldsymbol{r}') \cdot \boldsymbol{u}^{(1)}_{n''m''}(\boldsymbol{r}') dr' + \\ \boldsymbol{p}^{(1\epsilon)}_{nm}(\boldsymbol{r}) \sum_{n'',m''} c_{n''m''} \int_S \boldsymbol{p}^{(2\epsilon)}_{n,-m}(\boldsymbol{r}') \cdot \boldsymbol{u}^{(2)}_{n''m''}(\boldsymbol{r}') dr' \Big).\end{aligned} \tag{3.109}$$

3.7.1 Electric field inside sphere due to radial electric dipole

In case of the radial electric dipole excitation coefficients c_{nm} are zero. Considering orthogonality relationships [60], we simplify (3.109) to the following

$$\boldsymbol{E}(\boldsymbol{r}) = -\omega\mu_0 \sum_{n=1}^{\infty} d_{0n}^{1/2} b_{n0} \Big(\boldsymbol{q}_{0n}^{(1\epsilon)}(\boldsymbol{r}) [k_\epsilon a h_n^{(2)}(k_\epsilon a)]' \Big). \tag{3.110}$$

Using definitions of the function $\boldsymbol{q}$ we get components of the field inside the sphere

$$E_r = -\omega\mu_0 \sum_{n=1}^{\infty} d_{0n}^{1/2} b_{n0} \frac{n(n+1)}{k_\epsilon r} j_n(k_\epsilon r) P_n(\cos\theta) [k_\epsilon a h_n^{(2)}(k_\epsilon a)]', \tag{3.111}$$

$$E_\theta = -\omega\mu_0 \sum_{n=1}^{\infty} d_{0n}^{1/2} b_{n0} \frac{1}{k_\epsilon r} [k_\epsilon r j_n(k_\epsilon r)]' \frac{d}{d\theta} P_n(\cos\theta) [(k_\epsilon a) h_n^{(2)}(k_\epsilon a)]', \tag{3.112}$$

$$E_\phi = 0. \tag{3.113}$$

3.7.2 Electric field inside sphere due to tangential electric dipole

In case of tangential dipole excitation both coefficients b_{nm} and c_{nm} in (3.109) are non-zero producing the following expressions for the components of the field inside the sphere considering definitions of spherical functions and orthogonality relations [60],

$$E_r = -\omega\mu_0 k_\epsilon \sum_{n=1}^{\infty} \sum_{m=-1,1} d_{nm}^{1/2} b_{nm} \left(\frac{n(n+1)}{k_\epsilon r} j_n(k_\epsilon r) P_n^{|m|}(\cos\theta) e^{im\phi} \right) \left(\frac{1}{k_\epsilon} [k_\epsilon a h_n^{(2)}(k_\epsilon a)]' \right), \tag{3.114}$$

$$
\begin{aligned}
E_\theta = -\omega\mu_0 k_\epsilon \sum_{n=1}^{\infty} \sum_{m=-1,1} d_{nm}^{1/2} \Big[b_{nm} & \left(\frac{1}{k_\epsilon r} [k_\epsilon r j_n(k_\epsilon r)]' \right. \\
& \left. \frac{d}{d\theta} P_n^{|m|}(\cos\theta) e^{im\phi} \right) \left(\frac{1}{k_\epsilon} [(k_\epsilon a) h_n^{(2)}(k_\epsilon a)]' \right) \\
& + c_{nm} \left(\frac{im}{\sin\theta} P_n^{|m|}(\cos\theta) j_n(k_\epsilon r) e^{im\phi} \right) \left(-a h_n^{(2)}(k_\epsilon a) \right) \Big], \quad (3.115)
\end{aligned}
$$

$$
\begin{aligned}
E_\phi = -\omega\mu_0 k_\epsilon \sum_{n=1}^{\infty} \sum_{m=-1,1} d_{nm}^{1/2} \Big[b_{nm} & \left(\frac{im}{k_\epsilon r \sin\theta} \right. \\
& \left. [k_\epsilon r j_n(k_\epsilon r)]' P_n^{|m|}(\cos\theta) e^{im\phi} \right) \left(\frac{1}{k_\epsilon} [(k_\epsilon a) h_n^{(2)}(k_\epsilon a)]' \right) \\
& + c_{nm} \left(\frac{d}{d\theta} P_n^{|m|}(\cos\theta) j_n(k_\epsilon r) e^{im\phi} \right) \left(a h_n^{(2)}(k_\epsilon a) \right) \Big]. \quad (3.116)
\end{aligned}
$$

3.8 Numerical Results

To validate analytic solution of the SVS-EFIE, we consider the problems of electric dipole radiation in the presence of dielectric sphere. Alternative analytic solution for such problems is available in the form of the classical Mie series [52] and can be used as a reference. We conducted various numerical experiments and compared field components obtained using presented exact Galerkin MoM solution of the SVS-EFIE and Mie series solution.

In the first experiment we consider the excitation of $a = 1$m radius homogeneous dielectric sphere having relative permittivity $\epsilon = 10$ by the radial electric dipole situated on the z-axis at location $\boldsymbol{r}_0 = \hat{\boldsymbol{z}}10$m and having dipole moment $Il = 1[A \cdot m]$. The frequency of analysis is 599.584916MHz. The magnitude of E_r and E_θ components of the electric field inside the dielectric sphere are demonstrated on the surface of the sphere as functions of angle θ in Fig. 3.1 and as function of radial

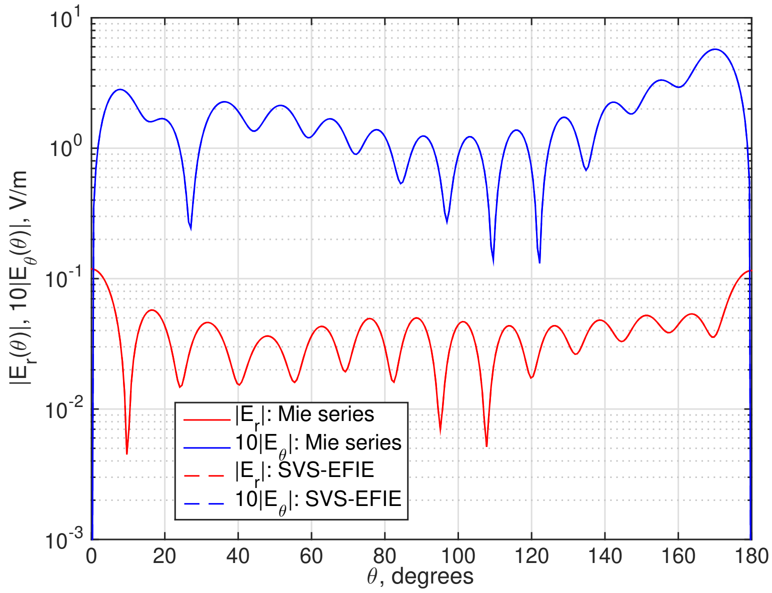

FIGURE 3.1: Electric field components on the surface of the sphere versus angle θ in the case of radial dipole excitation. Mie series results are shown by solid lines and SVS-EFIE solution is shown by dashed lines.

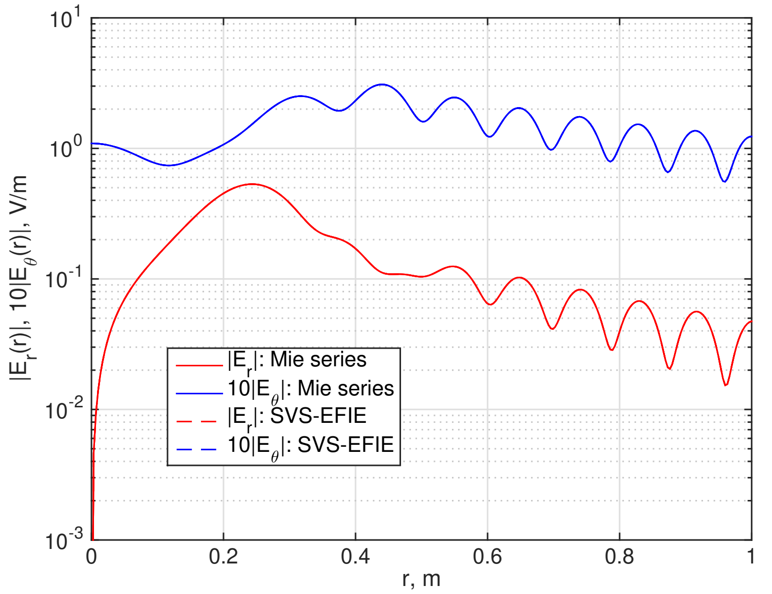

FIGURE 3.2: Electric field components inside the sphere versus radial coordinate r at $\theta = \pi/2$ in the case of radial dipole excitation. Mie series results are shown by solid lines and SVS-EFIE solution is shown by dashed lines.

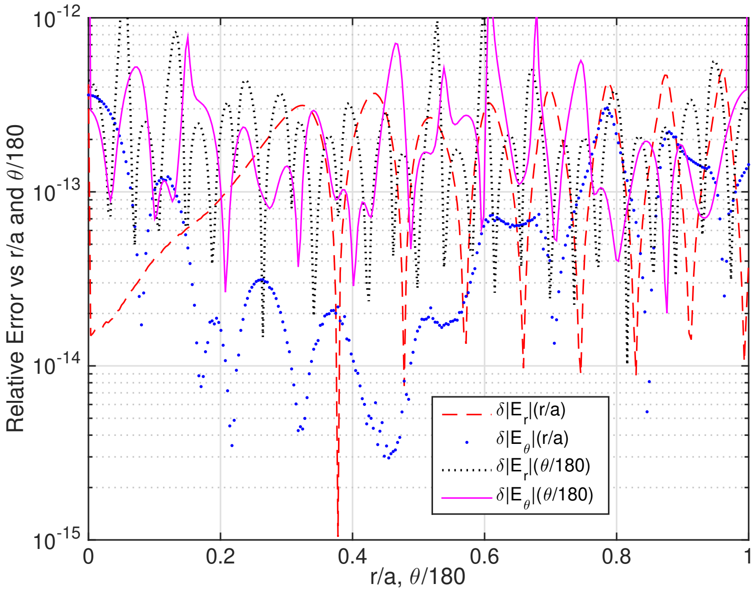

FIGURE 3.3: Relative error δE in the electric field components obtained by SVS-EFIE (compared to Mie series) on the surface of the sphere versus normalized angle $\theta/180$ corresponding to the curves in Fig. 3.1 (dashed lines) and relative error in the electric inside the sphere versus radial normalized coordinate r/a at $\theta = \pi/2$ corresponding to the curves in Fig. 3.2 (solid lines).

coordinate r in Fig. 3.2. In the case of radial dipole excitation only TM_r-waves are excited and the field is independent on the azimuthal angle ϕ. In Fig. 4.1 and Fig. 3.2 both the field components evaluated using the Galerkin MoM solution of the SVS-EFIE and those evaluated using Mie series are shown. The maximum and average value of relative errors between the SVS-EFIE and Mie series solutions evaluated with 50 terms are in the range of 10^{-12} to 10^{-13} respectively, The standard deviation for the E_r and E_θ components of the radial electric field was found to be 1.3×10^{-13} and 8×10^{-14} respectively.

In the second example we consider the same $1m$ radius sphere with relative permittivity of $\epsilon = 10$ but excited with the tangential θ-directed electric dipole. Under such excitation both the TE_r- and TM_r-waves are excited, the field has all components, and they depend on all three spherical coordinates. Once again we place the dipole on z-axis at the distance $r_0 = 10$m. The frequency of analysis is 599.584916MHz.

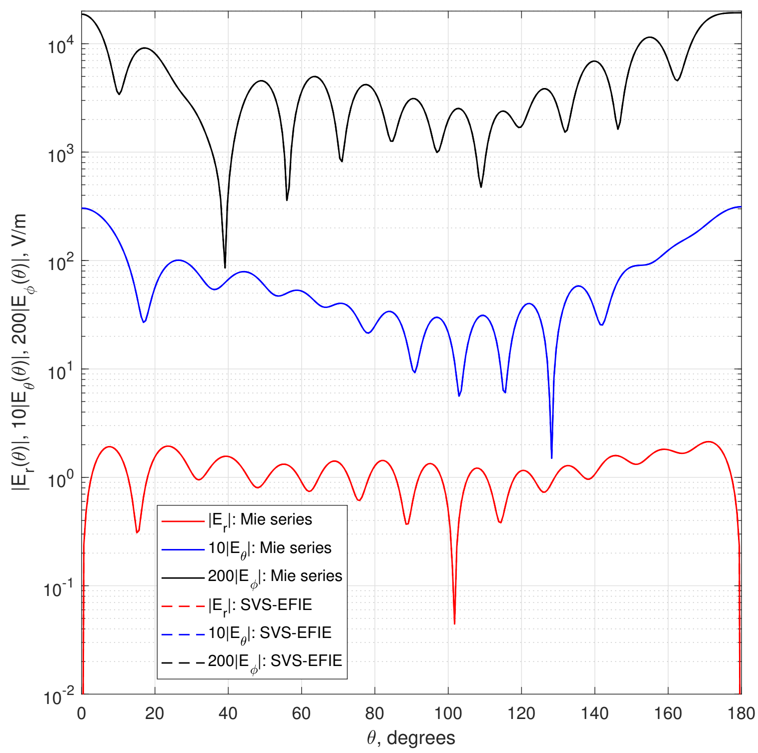

FIGURE 3.4: Electric field components on the surface of the sphere versus angle θ at $\phi = 0.4\pi$ in the case of tangential θ-directed dipole excitation. Mie series results are shown by solid lines and SVS-EFIE solution is shown by dashed lines.

In Fig. 3.3, the magnitude of E_r, E_θ, and E_ϕ components of the electric field as function of elevation angle θ are shown for both MoM solution of the SVS-EFIE and Mie series. In Fig. 3.4, the magnitude of the electric field component are shown as function of the radial coordinate r for both MoM solution of the SVS-EFIE and Mie series.

The maximum and average value of relative errors between the SVS-EFIE and Mie series solutions evaluated with 50 terms and are in the range of 10^{-12} to 10^{-13} respectively. The standard deviation for the E_r, E_θ and E_ϕ components of the electric field with respect to θ was found to be 7.3×10^{-12}, 6.2×10^{-12} and 8.6×10^{-12} respectively.

All the computations were performed in MathCAD 15 software with integrals in (3.73) computed numerically to 10^{-10} tolerance. The Legendre polynomials were

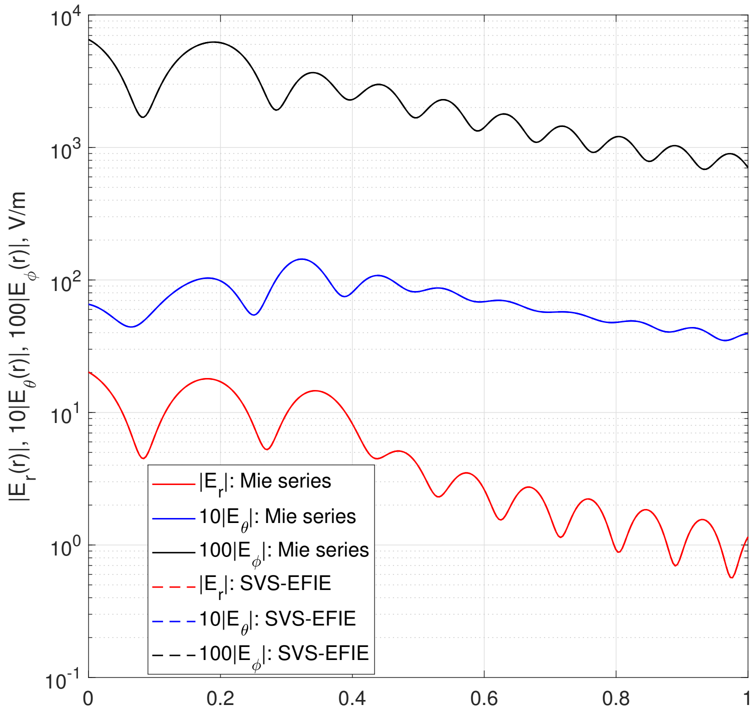

FIGURE 3.5: Electric field components inside the sphere versus radial coordinate r at $\theta = 0.4\pi$ at $\phi = 0.4\pi$ in the case of tangential θ-directed dipole excitation. Mie series results are shown by solid lines and SVS-EFIE solution is shown by dashed lines.

defined in terms of the integrals and computed to the same 10^{-10} tolerance. This tolerance is seen to be forcing the maximum level of relative error between the analytic Galerkin MoM solution of the SVS-EFIE and Mie series to be in the range of 10^{-12} and below. The achieved level of relative error between the SVS-EFIE solution and Mie series undoubtedly validates both the rigorous nature of the SVS-EFIE and exactness of its MoM solution.

Next, we demonstrate the spectral properties of the SVS-EFIE and the impact of the functional space choice in MoM testing on the condition number of the impedance matrix. In Fig. 3.7 and Fig. 3.8, the eigenvalues $\Lambda_{1,2}^{S,S}$ the product of the eigenvalues $\Lambda_{1,2}^{S,V}\Gamma_{2,1}^{-1}\Lambda_{1,2}^{V,S}$ and their weighted sum are shown under condition of the Galerkin MoM testing performed in Sobolev space $H_{div}^{-1/2}(S)$ (Figs. 3.7-3.8) and in $L^2(S)$ space (Figs. 3.9-3.10). One can see that while testing performe d in $H_{div}^{-1/2}(S)$ space

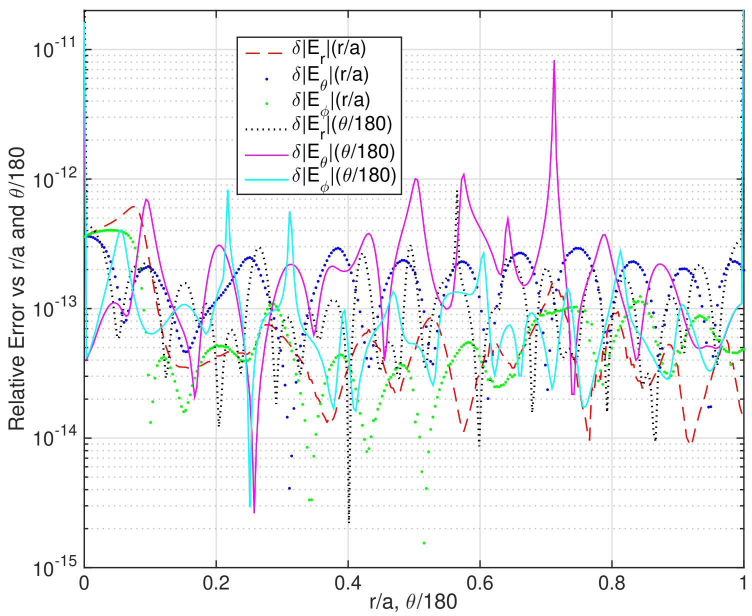

FIGURE 3.6: Relative error δE in the electric field components obtained by SVS-EFIE (compared to Mie series) on the surface of the sphere versus normalized angle $\theta/180$ at $\phi = 0.4\pi$ corresponding to the curves in Fig. 3.1 (dashed lines) and relative error in the electric inside the sphere versus radial normalized coordinate r/a at $\theta = 0.4\pi$ at $\phi = 0.4\pi$ corresponding to the curves in Fig. 3.2 (solid lines).

results in bounded eigenvalues of the impedance matrix, MoM testing of the SVS-EFIE performed in $L^2(S)$ space results in its unbounded spectrum. The eigenvalues depicted in Fig. 3.7-3.10 correspond to the solution of the tangential dipole radiation problem in Figs. 3.3 and 3.4.

3.9 Conclusions

The paper presents analytic solution of the Surface-Volume-Surface Electric Field Integral Equations (SVS-EFIE) with Galerkin Method of Moments (MoM) for the problem of homogenous dielectric sphere excitation. The expansion of the unknown fictitious current in the single source SVS-EFIE is performed over the eigenfunctions

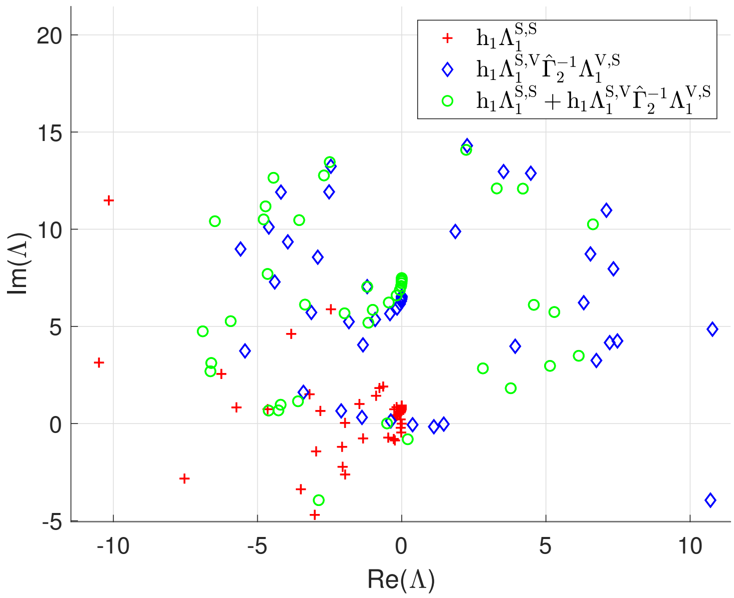

FIGURE 3.7: Eigenvalues $\Lambda^{S,S}_{1,e\epsilon,n}$ of the surface-to-surface operator multiplied by factor $h_1 = (1+n^2)^{-1/2}$ and eigenvalues $\Lambda^{S,V}_{1,e0,n}\hat{\Gamma}^{-1}_{2,n}\Lambda^{V,S}_{1,e\epsilon,n}$ corresponding to the product of the surface-to-volume and volume-to-surface operators multiplied by the same factor h_1. One can observe the MoM impedance matrix eigenvalues $\hat{\Lambda}^{(1)}_n = h_1\Lambda^{S,S}_{1,e\epsilon,n} + h_1\Lambda^{S,V}_{1,e0,n}\hat{\Gamma}^{-1}_{2,n}\Lambda^{V,S}_{1,e\epsilon,n}$ clustering at a constant value with the increased index n according to (3.89). This $O(1)$ boundedness of the eigenvalues $\hat{\Lambda}^{(1)}_n$ in conjunction of the $O(1)$ boundedness of the eigenvalues $\hat{\Lambda}^{(2)}_n$ in Fig. 3.8 produces $O(1)$ boundedness in the MoM matrix condition number when testing of SVS-EFIE is performed in Sobolev space $H^{-1/2}_{div}(S)$.

of its integral operator. Spectral analysis of the integral operators forming the SVS-EFIE is conducted. The Galerkin testing of the SVS-EFIE is performed in different functional spaces and spectral properties of the resultant MoM impedance matrix are analyzed. It is shown that in order for the MoM impedance matrix condition number to remain bounded under condition of the increasing discretization order the SVS-EFIE must be tested in Sobolev space $H^{-1/2}_{div}(S)$. Testing in conventional functional space $L^2(S)$ results in $O(n^2)$ growing of the MoM matrix condition number with the discretization order n. The analytic MoM solution of the SVS-EFIE is compared against Mie series and is shown to match the latter to 12 significant digits, hence, proving the rigorous nature of the SVS-EFIE formulation and exactness of its MoM solution. Although these present analysis shows how performing MoM solution in the

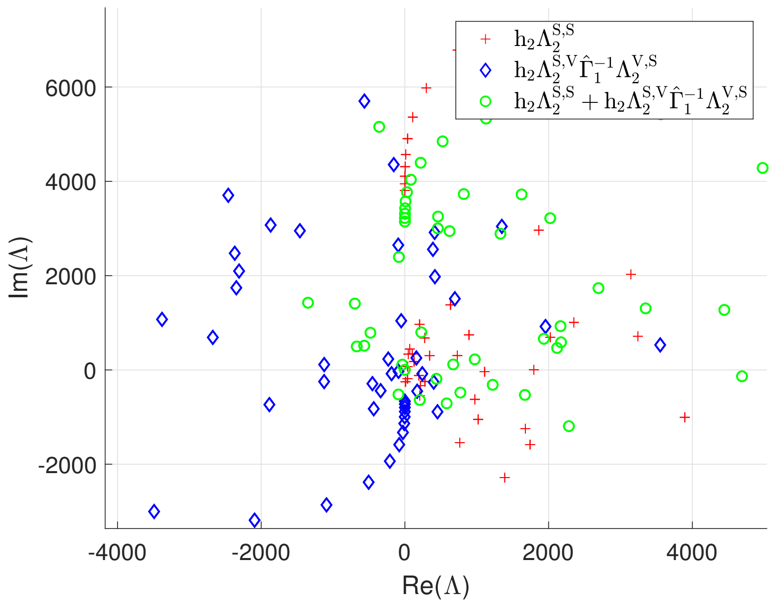

FIGURE 3.8: Eigenvalues $\Lambda^{S,S}_{2,e\epsilon,n}$ of the surface-to-surface operator multiplied by factor $h_2 = (1+n^2)^{1/2}$ and eigenvalues $\Lambda^{S,V}_{2,e0,n}\hat{\Gamma}^{-1}_{1,n}\Lambda^{V,S}_{2,e\epsilon,n}$ corresponding to the product of the surface-to-volume and volume-to-surface operators multiplied by the same factor h_2. One can observe the eigenvalues $\hat{\Lambda}^{(2)}_n = h_2\Lambda^{S,S}_{2,e\epsilon,n} + h_2\Lambda^{S,V}_{2,e0,n}\hat{\Gamma}^{-1}_{1,n}\Lambda^{V,S}_{2,e\epsilon,n}$ clustering at a constant value with the increased index n according to (3.89). This $O(1)$ boundedness of the eigenvalues $\hat{\Lambda}^{(2)}_n$ in conjunction of the $O(1)$ boundedness of the eigenvalues $\hat{\Lambda}^{(1)}_n$ in Fig. 3.7 produces $O(1)$ boundedness in the MoM matrix condition number when testing of SVS-EFIE is performed in Sobolev space $H^{-1/2}_{div}(S)$.

proper functional space can in principle eliminate the oversampling breakdown, the low frequency breakdown and internal resonances of SVS-EFIE remain uneffected by it. Remedies for the remaining breakdowns require further investigation.

3.10 Appendix I: Orthogonality Relations

The following orthogonality relations (see (46)-(48) in [60]) are utilized in this work for surface spherical harmonics

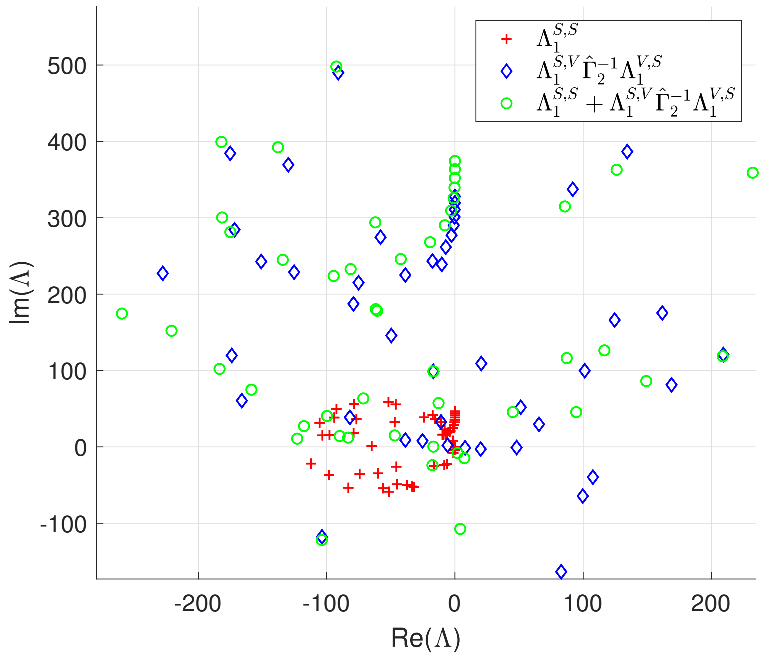

FIGURE 3.9: Eigenvalues $\Lambda^{S,S}_{1,e\epsilon,n}$ of the surface-to-surface operator and eigenvalues $\Lambda^{S,V}_{1,e0,n}\hat{\Gamma}^{-1}_{2,n}\Lambda^{V,S}_{1,e\epsilon,n}$ corresponding to the product of the surface-to-volume and volume-to-surface operators. One can observe the eigenvalues $\Lambda^{(1)}_n = \Lambda^{S,S}_{1,e\epsilon,n} + \Lambda^{S,V}_{1,e0,n}\hat{\Gamma}^{-1}_{2,n}\Lambda^{V,S}_{1,e\epsilon,n}$ tending to infinity with the increased index n according to (3.86). This $O(n)$ growth of the eigenvalues $\Lambda^{(1)}_n$ in conjunction of the $O(n^{-1})$ decrease of the eigenvalues $\Lambda^{(2)}_n$ in Fig. 3.10 produces $O(n^2)$ growth in the MoM matrix condition number when testing of SVS-EFIE is performed in $L^2(S)$ space.

$$\int_S d^{1/2}_{mn} d^{1/2}_{m'n'} \overline{Y}^m_n(\hat{\boldsymbol{r}}) Y^{m'}_{n'}(\hat{\boldsymbol{r}}) ds = a^2 \frac{\delta_{nn'}\delta_{mm'}}{n(n+1)}, \tag{3.117}$$

$$\int_S d^{1/2}_{mn} d^{1/2}_{m'n'} \nabla^t \overline{Y}^m_n(\hat{\boldsymbol{r}}) \cdot \nabla^t Y^{m'}_{n'}(\hat{\boldsymbol{r}}) ds = \delta_{nn'}\delta_{mm'}, \tag{3.118}$$

$$\int_S d^{1/2}_{mn} d^{1/2}_{m'n'} \hat{\boldsymbol{r}} \times \nabla^t \overline{Y}^m_n(\hat{\boldsymbol{r}}) \cdot \hat{\boldsymbol{r}} \times \nabla^t Y^{m'}_{n'}(\hat{\boldsymbol{r}}) ds = \delta_{nn'}\delta_{mm'}, \tag{3.119}$$

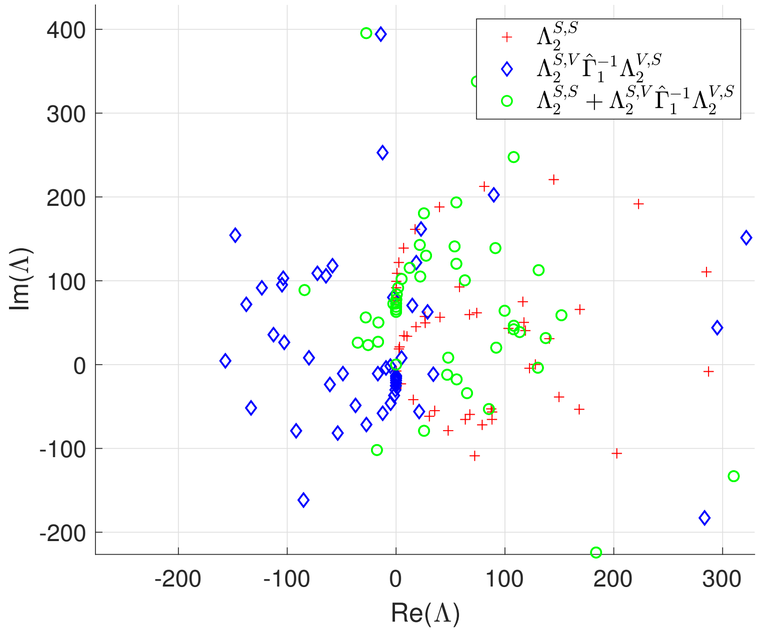

FIGURE 3.10: Eigenvalues $\Lambda^{S,S}_{2,e\epsilon,n}$ of the surface-to-surface operator and eigenvalues $\Lambda^{S,V}_{2,e0,n}\hat{\Gamma}^{-1}_{1,n}\Lambda^{V,S}_{2,e\epsilon,n}$ corresponding to the product of the surface-to-volume and volume-to-surface operators. One can observe the eigenvalues $\Lambda^{(2)}_n = \Lambda^{S,S}_{2,e\epsilon,n} + \Lambda^{S,V}_{2,e0,n}\hat{\Gamma}^{-1}_{1,n}\Lambda^{V,S}_{1,e\epsilon,n}$ tending to zero with the increased index n according to (3.87). This $O(1/n)$ decrease of the eigenvalues $\Lambda^{(2)}_n$ in conjunction of the $O(n)$ growth of the eigenvalues $\Lambda^{(1)}_n$ in Fig. 3.9 produces $O(n^2)$ growth in the MoM matrix condition number when testing of SVS-EFIE is performed in $L^2(S)$ space.

$$\int_S \nabla^t Y_n^m(\hat{\boldsymbol{r}}) \cdot \hat{\boldsymbol{r}} \times \nabla^t \overline{Y}_{n'}^{m'}(\hat{\boldsymbol{r}}) ds = 0. \tag{3.120}$$

From above relations (3.117), (3.118), (3.119) and (3.120), we get for for $\boldsymbol{r} \in S$

$$\int_S \boldsymbol{p}^{(j)}_{nm}(\boldsymbol{r}) \cdot \nabla^t Y_{n'}^{m'}(\hat{\boldsymbol{r}}) ds = 0, \tag{3.121}$$

$$d_{nm} \int_S \boldsymbol{p}^{(j)}_{n,m}(\boldsymbol{r}) \cdot \hat{\boldsymbol{r}}_y \times \nabla^t Y_{n'}^{m'}(\hat{\boldsymbol{r}}) ds = -a z_n^{(j)}(ka)\delta_{nn'}\delta_{m,-m'}, \tag{3.122}$$

$$d_{nm} \int_S \boldsymbol{q}^{(j)}_{n,m}(\boldsymbol{r}) \cdot \nabla^t Y_{n'}^{m'}(\hat{\boldsymbol{r}}) ds = \frac{1}{k}[ka z_n^{(j)}(ka)]'\delta_{nn'}\delta_{m,-m'}, \tag{3.123}$$

$$\int_S \boldsymbol{q}^{(j)}_{nm}(\boldsymbol{r}) \cdot \hat{\boldsymbol{r}} \times \nabla^t Y_{n'}^{m'}(\hat{\boldsymbol{r}}) ds = 0. \tag{3.124}$$

Spherical wave functions $\boldsymbol{p}_{nm}^{(j)}$ and $\boldsymbol{q}_{nm}^{(j)}$ are orthogonal to each other, which leads to

$$\int_V \boldsymbol{p}_{nm}^{(j)}(\boldsymbol{r}) \cdot \boldsymbol{q}_{nm}^{(j)}(\boldsymbol{r}) dv = 0. \tag{3.125}$$

We also have for $\boldsymbol{r} \in S$

$$\hat{\boldsymbol{n}} \times \boldsymbol{p}_{n,-m}^{(j)}(\boldsymbol{r}) = a z_n^{(j)}(ka) \nabla^t Y_n^{-m}(\hat{\boldsymbol{r}}), \tag{3.126}$$

$$\hat{\boldsymbol{n}} \times \boldsymbol{q}_{n,-m}^{(j)}(\boldsymbol{r}) = \frac{1}{k}[ka z_n^{(j)}(ka)]' \hat{\boldsymbol{r}} \times \nabla^t Y_n^{-m}(\hat{\boldsymbol{r}}). \tag{3.127}$$

We can find the following

$$\int_S \boldsymbol{u}_{n'm'}^{(1)}(\boldsymbol{r}) \cdot \hat{\boldsymbol{n}} \times \boldsymbol{p}_{n,-m}^{(1\epsilon)}(\boldsymbol{r}) ds = -a j_n(k_\epsilon a) \delta_{nn'} \delta_{mm'} d_{nm}^{-1/2}, \tag{3.128}$$

$$\int_V \boldsymbol{p}_{n,-m}^{(10)}(\boldsymbol{r}) \boldsymbol{p}_{n''m''}^{(1\epsilon)}(\boldsymbol{r}) dv = \delta_{nn''} \delta_{mm''} d_{nm}^{-1/2} d_{n''m''}^{-1/2} \int_0^a j_n(k_0 r) j_n(k_\epsilon r) r^2 dr, \tag{3.129}$$

$$\begin{aligned} \int_V \boldsymbol{q}_{n,-m}^{(10)}(\boldsymbol{r}) \boldsymbol{q}_{n''m''}^{(1\epsilon)}(\boldsymbol{r}) dv = {} & \delta_{nn''} \delta_{mm''} d_{nm}^{-1/2} d_{n''m''}^{-1/2} \\ & \left(\frac{n''(n''+1)}{k_0 k_\epsilon} \int_0^a j_n(k_0 r) j_{n''}(k_\epsilon r) dr \cdot a^2 + \right. \\ & \left. \frac{1}{k_0 k_\epsilon} \int_0^a [k_0 r j_n(k_0 r)]' [k_\epsilon r j_{n''}(k_\epsilon r)]' dr \right). \end{aligned} \tag{3.130}$$

3.11 Appendix II: Eigenvalues of SVS-EFIE Operators

In this Appendix we prove the following eigenvalue relations for the SVS-EFIE operator $\mathcal{T}_{SVS}$

$$\mathcal{T}_{SVS} \circ (\nabla^t Y_n^m) = \Lambda_n^{(1)} (\hat{\boldsymbol{r}} \times \nabla^t Y_n^m), \tag{3.131}$$

and

$$\mathcal{T}_{SVS} \circ (\hat{\boldsymbol{r}} \times \nabla^t Y_n^m) = \Lambda_n^{(2)}(\nabla^t Y_n^m), \tag{3.132}$$

where

$$\mathcal{T}_{SVS} \circ \nabla^t Y_n^m = \mathcal{T}_{e\epsilon}^{S,S} \circ \nabla^t Y_n^m + \mathcal{T}_{e0}^{S,V} \circ \mathcal{T}_{e\epsilon}^{V,S} \circ \nabla^t Y_n^m. \tag{3.133}$$

We start with the surface-surface operator

$$\mathcal{T}_{e\epsilon}^{S,S} \circ \nabla^t Y_n^m = i\omega\mu_0 \hat{\boldsymbol{n}} \times \int_S \bar{\bar{\boldsymbol{G}}}_{e\epsilon}(\boldsymbol{r}, \boldsymbol{r}'') \cdot \nabla^t Y_n^m(\boldsymbol{r}'') ds'', \quad \boldsymbol{r} \in S. \tag{3.134}$$

Recalling (3.22) and substituting it here for $|\boldsymbol{r}| < |\boldsymbol{r}''|$ we get

$$\begin{aligned}\mathcal{T}_{e\epsilon}^{S,S} \circ \nabla^t Y_{n''}^{m''} = i\omega\mu_0 \; (ik_\epsilon) \sum_{n,m} d_{nm} \, (\hat{\boldsymbol{n}} \times \\ \boldsymbol{q}_{nm}^{(1\epsilon)}(\boldsymbol{r}) \int_S \boldsymbol{q}_{n,-m}^{(2\epsilon)}(\boldsymbol{r}'') \cdot \nabla^t Y_{n''}^{m''}(\hat{\boldsymbol{r}}'') ds'' + \\ \hat{\boldsymbol{n}} \times \boldsymbol{p}_{nm}^{(1\epsilon)}(\boldsymbol{r}) \int_S \boldsymbol{p}_{n,-m}^{(2\epsilon)}(\boldsymbol{r}'') \cdot \nabla^t Y_{n''}^{m''}(\hat{\boldsymbol{r}}'') ds'' \Big) .\end{aligned} \tag{3.135}$$

By virtue of [(72) and (74) in [60]], we obtain

$$\begin{aligned}\mathcal{T}_{e\epsilon}^{S,S} \circ \nabla^t Y_{n''}^{m''} &= i\omega\mu_0 \; (ik_\epsilon) \sum_{n,m} d_{nm} \, (\hat{\boldsymbol{n}} \times \\ &\quad \boldsymbol{q}_{nm}^{(1\epsilon)}(\boldsymbol{r}) \int_S \boldsymbol{q}_{n,-m}^{(2\epsilon)}(\boldsymbol{r}'') \cdot \nabla^t Y_{n''}^{m''}(\hat{\boldsymbol{r}}'') ds'' \Big) \\ &= -\omega\mu_0 k_\epsilon \sum_{n,m} d_{nm} \left(\frac{1}{k_\epsilon} [k_\epsilon a j_n(k_\epsilon a)]' \hat{\boldsymbol{r}} \times \nabla^t Y_{n''}^{m''}(\hat{\boldsymbol{r}}) \right. \\ &\quad \left. d_{nm}^{-1} \frac{1}{k_\epsilon} [k_\epsilon a h_n^{(2)}(k_\epsilon a)]' \delta_{nn''} \delta_{mm''} \right) = -\frac{\omega\mu_0}{k_\epsilon} \\ &\quad \left([k_\epsilon a j_{n''}(k_\epsilon a)]' [k_\epsilon a h_{n''}^{(2)}(k_\epsilon a)]' \hat{\boldsymbol{r}} \times \nabla^t Y_{n''}^{m''}(\hat{\boldsymbol{r}}) \right) .\end{aligned} \tag{3.136}$$

Recalling (3.72), it follows from the above that

$$\mathcal{T}_{e\epsilon}^{S,S} \circ \nabla^t Y_n^m = \Lambda_{1,e\epsilon,n}^{S,S} \hat{\boldsymbol{r}} \times \nabla^t Y_n^m(\hat{\boldsymbol{r}}). \tag{3.137}$$

Next, we consider the surface-volume-surface operator (3.133). Using definition of integral operators (3.9), (3.8) we have

$$\begin{aligned}
\mathcal{T}_{e0}^{S,V} \circ \mathcal{T}_{e\epsilon}^{V,S} \circ \nabla^t Y_{n''}^{m''} = k_0^2(\epsilon - 1)& \\
ik_0 \sum_{n,m} d_{nm} \quad \hat{\boldsymbol{n}} \times \int_V dv' \Big(& \boldsymbol{q}_{nm}^{(20)}(\boldsymbol{r}) \boldsymbol{q}_{n,-m}^{(10)}(\boldsymbol{r}') + \boldsymbol{p}_{nm}^{(20)}(\boldsymbol{r}) \\
\boldsymbol{p}_{n,-m}^{(10)}(\boldsymbol{r}') \Big) (i\omega\mu_0) ik_\epsilon \sum_{n',m'} d_{n'm'} \int_S \Big(& \boldsymbol{q}_{n'm'}^{(1\epsilon)}(\boldsymbol{r}') \boldsymbol{q}_{n',-m'}^{(2\epsilon)}(\boldsymbol{r}'') \\
&+ \boldsymbol{p}_{n'm'}^{(1\epsilon)}(\boldsymbol{r}') \boldsymbol{p}_{n',-m'}^{(2\epsilon)}(\boldsymbol{r}'') \Big) \nabla^t Y_{n''}^{m''}(\hat{\boldsymbol{r}}'') ds'' \\
= k_0^2(\epsilon - 1) ik_0 \sum_{n,m} d_{nm} (i\omega\mu_0) ik_\epsilon \sum_{n',m'} d_{n'm'} \Big(& \hat{\boldsymbol{n}} \times \boldsymbol{q}_{nm}^{(20)}(\boldsymbol{r}) \\
\int_V \boldsymbol{q}_{n,-m}^{(10)}(\boldsymbol{r}') \cdot \boldsymbol{q}_{n'm'}^{(1\epsilon)}(\boldsymbol{r}') dv' \int_S & \boldsymbol{q}_{n',-m'}^{(2\epsilon)}(\boldsymbol{r}'') \cdot \nabla^t Y_{n''}^{m''}(\hat{\boldsymbol{r}}'') ds'' \\
+ \hat{\boldsymbol{n}} \times \boldsymbol{p}_{nm}^{(20)}(\boldsymbol{r}) \int_V & \boldsymbol{p}_{n,-m}^{(10)}(\boldsymbol{r}') \cdot \boldsymbol{p}_{n'm'}^{(1\epsilon)}(\boldsymbol{r}') dv' \\
& \int_S \boldsymbol{p}_{n',-m'}^{(2\epsilon)}(\boldsymbol{r}'') \cdot \nabla^t Y_{n''}^{m''}(\hat{\boldsymbol{r}}'') ds'' \Big).
\end{aligned} \tag{3.138}$$

After using [(72) in [60]], we can simplify the above to

$$\begin{aligned}
\mathcal{T}_{e0}^{S,V} \circ \mathcal{T}_{e\epsilon}^{V,S} \circ \nabla^t Y_{n''}^{m''} = k_0^2(\epsilon - 1) ik_0 \sum_{n,m} d_{nm} (i\omega\mu_0) ik_\epsilon & \\
\sum_{n',m'} d_{n'm'} \hat{\boldsymbol{n}} \times \boldsymbol{q}_{nm}^{(20)}(\boldsymbol{r}) \int_V \boldsymbol{q}_{n',-m'}^{(10)}(\boldsymbol{r}') \cdot \boldsymbol{q}_{n'm'}^{(1\epsilon)}(\boldsymbol{r}') dv' & \\
\int_S \boldsymbol{q}_{n',-m'}^{(2\epsilon)}(\boldsymbol{r}'') \cdot \nabla^t Y_{n''}^{m''}(\hat{\boldsymbol{r}}'') ds''. &
\end{aligned} \tag{3.139}$$

With reference to [(74) in [60]] and (3.130), the above equation can be reorganized, as follows:

$$\begin{aligned}\mathcal{T}_{e0}^{S,V} \circ \mathcal{T}_{e\epsilon}^{V,S} \circ \nabla^t Y_n^m = -i\omega\mu_0 k_0^2(\epsilon-1)[k_0 a h_n^{(2)}(k_0 a)]'& \\ \hat{\boldsymbol{r}} \times \nabla^t Y_n^m(\hat{\boldsymbol{r}})\Big(\frac{n(n+1)}{k_0 k_\epsilon} a^2 \int_0^a j_n(k_0 r) j_n(k_\epsilon r) dr& \\ + \frac{1}{k_0 k_\epsilon}\int_0^a [k_0 r j_n(k_0 r)]'[k_\epsilon r j_n(k_\epsilon r)]' dr\Big)[k_\epsilon a h_n^{(2)}(k_\epsilon a)]'& \\ = \Lambda_{1,e0,n}^{S,V} \hat{\Gamma}_{2,n}^{-1} \Lambda_{1,e\epsilon,n}^{V,S} \hat{\boldsymbol{r}} \times \nabla^t Y_n^m.& \end{aligned} \tag{3.140}$$

Derived relation (3.140) is stated in abbreviated form as eigenvalue relation (3.80). Eigenvalue relation (3.77) can be proven in a similar manner.

Chapter 4

Exact Solution of New Magnetic Current Based Surface-Volume-Surface EFIE and Analysis of Its Spectral Properties

4.1 Introduction

Integral equations of electromagnetics have provided a theoretical foundation for the construction of efficient numerical schemes enabling the analysis of electromagnetic fields in the presence of complex 3D objects. Such schemes have been essential in design cycles of novel devices of microelectronics and photonics [3], [4], antennas for 5G systems [5], environmental studies [6], and many other areas [7], [8].

For penetrable objects, integral equations can be largely classified as two-source equations, which include widely used formulations such as EFIE, MFIE, CFIE, PMCHWT, Muller, JM-CFIE, etc. [10, 11, 13], and single-source equations [14]–[17], [40], [41], [44]–[46] [18]–[23]. The Single-Source-Integral-Equations (SSIEs) are less popular as they involve a large number of integral operators and their products [45] or feature inverses of the integral operators [47], [21], [22]. Either the large number of integral operators and their products or the presence of their inverses greatly diminish the advantages of SSIEs compared to their traditional two-source counterparts coming from the reduction of the unknown functions from two to one.

In our recent work [28]–[39] we proposed and studied a new kind of SSIE, which neither featured a large number of integral operators nor required evaluation of their inverses. It was obtained as a result of constraining the electric current based single-source representation of the electric field with volume integral equation (VIE). As such, it features the integral operators mapping surface functions to the volume functions and vice versa in the process of enforcing of VIE on the boundary of the scatterer for tangential components of the total electric field. We term this equation throughout as the electric current based Surface-Volume-Surface Electric Field Integral Equation (SVS-EFIE-J).

It was hypothesized in [55], however, that another type of SVS-EFIE can also be obtained, namely the one utilizing a magnetic current single-source representation of an electric field inside a non-magnetic penetrable scatterer. In this work we term this new SSIE formulation as SVS-EFIE-M. To prove the correctness of the hypothesis we solve this new SVS-EFIE-M analytically for the case of electric dipole radiation in the vicinity of a dielectric sphere analogously with the recently developed analytic solution of SVS-EFIE-J [35] and solutions of classical surface EFIE and MFIE given in the seminal paper [60]. Besides validating the rigorous nature of the new equation, the obtained analytic solution for it reveals the spectral properties of its operators. The spectra of the SVS-EFIE-M formulation shows that unlike its SVS-EFIE-J predecessor the new equation does not suffer from either the low frequency or the oversampling breakdowns [35]. Moreover, we show that the inner products in the Method of Moments (MoM) solutions of the SVS-EFIE-M formulation can be performed in well-familiar and easily tractable L^2 space without jeopardizing the condition number of its matrix. This is opposite to the SVS-EFIE-J formulation as well as traditional surface integral equations containing the EFIE operator and requiring the evaluation of the MoM inner products in the Sobolev space $H_{div}^{-1/2}$ [60], [35] to ensure that their pertinent MoM matrix condition number remains bounded upon the refinement of the mesh density. The evaluation of such inner products in $H_{div}^{-1/2}$ space for general 3D scatterers is very difficult and hasn't been demonstrated to date. The evaluation of the inner products in L^2 functional space allowed by the proposed SVS-EFIE-M formulation, however, has been well established in the computational electromagnetics community and has been routinely done in practical MoM discretizations of various integral equations. This makes the SVS-EFIE-M better suited for numerical solutions and promises to provide much low condition numbers in the resultant matrix equations compared to either the SVS-EFIE-J formulation, or traditional two-source formulations such as PMCHWT, Muller, JM-CFIE [10, 11, 13], or SSIEs utilizing inverses of the integral operators [19], [23],[47].

It is important to point out that the MoM solution of the SVS-EFIE-M equation analogous to the one implemented for the solution of SVS-EFIE-J formulation in [31] for the practical engineering scattering and radiation problems on simply connected sufficiently smooth dielectric objects is expected to produce similar spectral properties of the MoM matrix equation as those of the continuous SVS-EFIE-M integral operator presented in this work and be free of the low-frequency and oversampling breakdowns. The theory demonstrating that the spectrum of MoM matrix mimics a sub-set of the eigenvalues of the continuous operator of the integral equation and required conditions for that can be found in [48, 49].

In this work we compare the analytic solution of SVS-EFIE-M against the Mie series solution for the case of radial and tangential electric dipole radiation in the vicinity of a dielectric sphere. The relative error of the two solutions is shown to be at nearly machine precision level. This demonstrates the rigorous nature of the SVS-EFIE-M equation, the correctness of its analytic MoM solution, and the stability of the formulation at both low frequencies and under conditions of oversampling.

4.2 Surface-Volume-Surface Electric Field Integral Equation

Consider the volume equivalence principle [52] stated in the time-harmonic regime with the cyclic frequency ω for the electric field $\boldsymbol{E}$ in case of a homogeneous, non-magnetic dielectric object of volume V with complex relative permittivity ϵ

$$\boldsymbol{E}(\boldsymbol{r}) = \boldsymbol{E}^{inc}(\boldsymbol{r}) + k_0^2(\epsilon - 1)\int_V \bar{\bar{\boldsymbol{G}}}_{e0}(\boldsymbol{r},\boldsymbol{r'})\cdot\boldsymbol{E}(\boldsymbol{r'})dv', \quad \forall \;\; \boldsymbol{r} \tag{4.1}$$

where $\boldsymbol{r}$ is an arbitrary field location in space, and $\boldsymbol{r'}$ is the position-vector of the total electric field inside the scatterer satisfying the homogeneous wave equation.

The electric field inside a homogeneous, non-magnetic dielectric scatterer situated in free space and occupying volume V bounded by surface S can alternatively be expressed using the following single-source integral representation [16], [17],[45].

$$\begin{aligned}\boldsymbol{E}(\boldsymbol{r}) = -i\omega\mu_0\int_S \bar{\bar{\boldsymbol{G}}}_{e\epsilon}(\boldsymbol{r},\boldsymbol{r}')\cdot \mathsf{a}\boldsymbol{J}(r')ds' \\ + \int_S \bar{\bar{\boldsymbol{G}}}_{m\epsilon}(\boldsymbol{r},\boldsymbol{r}')\cdot \mathsf{b}\hat{\boldsymbol{n}}'\times\boldsymbol{J}(\boldsymbol{r}')ds', \quad \boldsymbol{r}\in V,\end{aligned} \tag{4.2}$$

where $\boldsymbol{J}$ is the fictitious electric current density and $\hat{\boldsymbol{n}}\times\boldsymbol{J}$ is the rotated fictitious electric current density, which plays a role of the surface magnetic current density.

$\bar{\bar{\boldsymbol{G}}}_{e\epsilon}$ and $\bar{\bar{\boldsymbol{G}}}_{m\epsilon}$ are the electric and magnetic field dyadic Green's functions of homogeneous space [35].

Since the volume equivalence principle is valid everywhere in space for fully 3D vector representation of the electric field, it can be also used to constrain the single-source integral representation of the field (4.2) to produce the integral equation with respect to the fictitious surface current density $\boldsymbol{J}(\boldsymbol{r}')$. For that purpose we substitute (4.2) into (4.1) and enforce the volume equivalence principle for the tangential component of the electric field only as we tend the observation point $\boldsymbol{r}$ to the boundary S from the inside the object

$$\begin{aligned}
&-i\omega\mu_0\hat{\boldsymbol{n}}\times\int_S \bar{\bar{\boldsymbol{G}}}_{e\epsilon}(\boldsymbol{r},\boldsymbol{r}'')\cdot \mathtt{a}\boldsymbol{J}(\boldsymbol{r}'')ds''+\hat{\boldsymbol{n}}\times\int_S \bar{\bar{\boldsymbol{G}}}_{m\epsilon}(\boldsymbol{r},\boldsymbol{r}'')\cdot\\
&\qquad \mathtt{b}\hat{\boldsymbol{n}}''\times\boldsymbol{J}(\boldsymbol{r}'')ds''-k_0^2(\epsilon-1)\hat{\boldsymbol{n}}\times\int_V \bar{\bar{\boldsymbol{G}}}_{e0}(\boldsymbol{r},\boldsymbol{r}')\cdot\\
&\qquad \{-i\omega\mu_0\int_S \bar{\bar{\boldsymbol{G}}}_{e\epsilon}(\boldsymbol{r}',\boldsymbol{r}'')\cdot \mathtt{a}\boldsymbol{J}(\boldsymbol{r}'')ds''+\int_S \bar{\bar{\boldsymbol{G}}}_{m\epsilon}(\boldsymbol{r}',\boldsymbol{r}'')\cdot\\
&\qquad \mathtt{b}\hat{\boldsymbol{n}}''\times\boldsymbol{J}(\boldsymbol{r}'')ds''\}dv'=\hat{\boldsymbol{n}}\times\boldsymbol{E}^{inc}(\boldsymbol{r}),\quad \boldsymbol{r}\in V,\quad \boldsymbol{r}\to S. \quad (4.3)
\end{aligned}$$

The above integral equation is the combined-source SVS-EFIE (CS-SVS-EFIE) with respect to the unknown current $\boldsymbol{J}$. In its complete form (4.3) it was hypothesized in [55]. However, in [55] and all prior publications only the particular case of CS-SVS-EFIE for $\mathtt{a}=1$ and $\mathtt{b}=0$ was considered. In this work, it is shown that the SVS-EFIE can also be formulated with respect to the fictitious magnetic current density $\boldsymbol{M}=\hat{\boldsymbol{n}}\times\boldsymbol{J}$ by considering (4.3) for $\mathtt{a}=0$ and $\mathtt{b}=1$, as follows:

$$\begin{aligned}
&\hat{\boldsymbol{n}}\times\int_S \bar{\bar{\boldsymbol{G}}}_{m\epsilon}(\boldsymbol{r},\boldsymbol{r}'')\cdot\hat{\boldsymbol{n}}''\times\boldsymbol{J}(\boldsymbol{r}'')dS''-k_0^2(\epsilon-1)\hat{\boldsymbol{n}}\times\\
&\qquad \int_V \bar{\bar{\boldsymbol{G}}}_{e0}(\boldsymbol{r},\boldsymbol{r}')\cdot\int_S \bar{\bar{\boldsymbol{G}}}_{m\epsilon}(\boldsymbol{r}',\boldsymbol{r}'')\cdot\hat{\boldsymbol{n}}''\times\boldsymbol{J}(\boldsymbol{r}'')ds''dv'\\
&\qquad\qquad =\hat{\boldsymbol{n}}\times\boldsymbol{E}^{inc}(\boldsymbol{r}),\quad \boldsymbol{r}\in S. \quad (4.4)
\end{aligned}$$

The above equation is termed SVS-EFIE-M formulation throughout the paper.

It is interesting to note [55] that in the case of a vanishing object $\epsilon \to 1$, the above SVS-EFIE-M reduces to the traditional surface EFIE (S-EFIE) for PMC object

$$\hat{\boldsymbol{n}} \times \int_S \bar{\bar{\boldsymbol{G}}}_{m\epsilon}(\boldsymbol{r}, \boldsymbol{r}'') \cdot \hat{\boldsymbol{n}}'' \times \boldsymbol{J}(\boldsymbol{r}'') ds'' = \hat{\boldsymbol{n}} \times \boldsymbol{E}^{inc}(\boldsymbol{r}), \quad \boldsymbol{r} \in S. \tag{4.5}$$

Conveniently, the SVS-EFIE-M (4.4) can also be represented in the following concise operator form

$$\mathcal{T}_{m\epsilon}^{S,S} \circ \boldsymbol{M} - \mathcal{T}_{e0}^{S,V} \circ \mathcal{T}_{m\epsilon}^{V,S} \circ \boldsymbol{M} = \hat{\boldsymbol{n}} \times \boldsymbol{E}^{inc}(\boldsymbol{r}), \quad \boldsymbol{r} \in S. \tag{4.6}$$

Here the integral operators are defined, as follows:

$$\mathcal{T}_{m\epsilon}^{S,S} \circ \boldsymbol{M} = \hat{\boldsymbol{n}} \times \int_S \bar{\bar{\boldsymbol{G}}}_{m\epsilon}(\boldsymbol{r}, \boldsymbol{r}'') \cdot \boldsymbol{M}(\boldsymbol{r}'') ds'', \quad \boldsymbol{r} \in S, \tag{4.7}$$

$$\mathcal{T}_{m\epsilon}^{V,S} \circ \boldsymbol{M} = \int_S \bar{\bar{\boldsymbol{G}}}_{m\epsilon}(\boldsymbol{r}', \boldsymbol{r}'') \cdot \boldsymbol{M}(\boldsymbol{r}'') ds'', \quad \boldsymbol{r}' \in V, \tag{4.8}$$

$$\mathcal{T}_{e0}^{S,V} \circ \boldsymbol{i} = k_0^2(\epsilon - 1)\hat{\boldsymbol{n}} \times \int_V \bar{\bar{\boldsymbol{G}}}_{e0}(\boldsymbol{r}, \boldsymbol{r}') \cdot \boldsymbol{i}(\boldsymbol{r}') dv', \quad \boldsymbol{r} \in S. \tag{4.9}$$

4.3 Exact Solution of SVS-EFIE-M with Galerkin MoM on Sphere

4.3.1 Expansion of magnetic current over spherical basis functions

To obtain the exact solution $\hat{\boldsymbol{n}} \times \boldsymbol{J}$ of the SVS-EFIE-M (4.4) for a dielectric sphere, we perform surface Helmholtz decomposition of the fictitious electric current $\boldsymbol{J}$ into irrotational and rotational components as [60]

$$\boldsymbol{J}(\hat{\boldsymbol{r}}) = \nabla^t \varphi(\hat{\boldsymbol{r}}) + \hat{\boldsymbol{r}} \times \nabla^t \psi(\hat{\boldsymbol{r}}). \tag{4.10}$$

The surface Helmholtz decomposition of the current $\hat{\boldsymbol{n}} \times \boldsymbol{J}$ can be expanded over two sets of vector basis functions $\hat{\boldsymbol{n}} \times \boldsymbol{u}_{nm}^{(1)}$ and $\hat{\boldsymbol{n}} \times \boldsymbol{u}_{nm}^{(2)}$ with the unknown coefficients b_{nm} and c_{nm}, respectively

$$\hat{\boldsymbol{n}} \times \boldsymbol{J}(\hat{\boldsymbol{r}}) = \sum_{n,m} \{ b_{nm} \hat{\boldsymbol{n}} \times \boldsymbol{u}_{nm}^{(1)}(\hat{\boldsymbol{r}}) + c_{nm} \hat{\boldsymbol{n}} \times \boldsymbol{u}_{nm}^{(2)}(\hat{\boldsymbol{r}}) \}, \tag{4.11}$$

where $\sum_{n,m}$ is an abbreviated notation for the double sum $\sum_{n=1}^{\infty} \sum_{m=-n}^{n}$. Taking $\boldsymbol{u}_{nm}^{(1)}$ and $\boldsymbol{u}_{nm}^{(2)}$ as complete set of surface spherical harmonics yields

$$\boldsymbol{M}(\hat{\boldsymbol{r}}) = \hat{\boldsymbol{n}} \times \boldsymbol{J}(\hat{\boldsymbol{r}}) = \sum_{n,m} d_{nm}^{1/2} \{ b_{nm} \hat{\boldsymbol{r}} \times \nabla^t Y_n^m(\hat{\boldsymbol{r}}) - c_{nm} \nabla^t Y_n^m(\hat{\boldsymbol{r}}) \}. \tag{4.12}$$

Detailed definition of coefficients d_{nm} and surface spherical harmonics Y_n^m can be found in [35, 60].

4.3.2 Expansion of magnetic field dyadic Green's function over vector spherical functions

The magnetic field dyadic Green's function of homogeneous medium with wavenumber k can be expanded over vector spherical functions $\boldsymbol{p}$ and $\boldsymbol{q}$, as (see [61] or (68) in [60])[1]:

$$\bar{\bar{\boldsymbol{G}}}_{m\epsilon}(\boldsymbol{r},\boldsymbol{r}') = \nabla \times \bar{\bar{\boldsymbol{G}}}_{e\epsilon} = -ik^2 \sum_{n,m} d_{nm} \begin{cases} \boldsymbol{p}^{(1)}_{nm}(\boldsymbol{r})\boldsymbol{q}^{(2)}_{n,-m}(\boldsymbol{r}') + \boldsymbol{q}^{(1)}_{nm}(\boldsymbol{r})\boldsymbol{p}^{(2)}_{n,-m}(\boldsymbol{r}'), |\boldsymbol{r}| < |\boldsymbol{r}'|, \\ \boldsymbol{p}^{(2)}_{nm}(\boldsymbol{r})\boldsymbol{q}^{(1)}_{n,-m}(\boldsymbol{r}') + \boldsymbol{q}^{(2)}_{nm}(\boldsymbol{r})\boldsymbol{p}^{(1)}_{n,-m}(\boldsymbol{r}')\}, |\boldsymbol{r}| > |\boldsymbol{r}'|. \end{cases} \tag{4.13}$$

When $|\boldsymbol{r}| = |\boldsymbol{r}'|$, the average of the two above representations is taken.

Expansion of the electric field throughout volume V of the sphere over volumetric spherical functions $\boldsymbol{p}^{(j)}_{nm}$ and $\boldsymbol{q}^{(j)}_{nm}$ will be also used in the MoM solution. Details of this expansion can be found in the previous work (see (24)-(26) in [35]).

4.3.3 Galerkin testing of SVS-EFIE-M

In order to solve the SVS-EFIE-M (4.4) with MoM, we perform its testing with the complete set of vector surface spherical functions $\boldsymbol{u}^{(1)}$ and $\boldsymbol{u}^{(2)}$

$$\left\langle \mathcal{T}^{S,S}_{m\epsilon} \circ \boldsymbol{M}, \boldsymbol{u}^{(1,2)}_{nm} \right\rangle - \left\langle \mathcal{T}^{S,V}_{e0} \circ \mathcal{T}^{V,S}_{m\epsilon} \circ \boldsymbol{M}, \boldsymbol{u}^{(1,2)}_{nm} \right\rangle = \left\langle \hat{\boldsymbol{n}} \times \boldsymbol{E}^{inc}(\boldsymbol{r}), \boldsymbol{u}^{(1,2)}_{nm} \right\rangle, \tag{4.14}$$

and expand the current $\boldsymbol{M} = \hat{\boldsymbol{n}} \times \boldsymbol{J}$ over the same set of functions as shown in (4.12).

It is known [35, 60] that the choice of space in which the inner products are performed may greatly effect the spectrum of the impedance matrix in the MoM matrix

[1] Note, here and throughout the paper definition of the Green's function is taken with minus sign with respect to its definition adopted in [35].

equation [35]. The inner products [1] in the above Galerkin MoM solution of SVS-EFIE-M should be carried out in $L^2(S)$ space as in the case of the surface MFIE (S-MFIE) solution for PEC [60] due to the presence of the S-MFIE operator [60] $\mathcal{T}_{m\epsilon}^{S,S}$ in it. The latter is in the form of a sum of constant and compact operators having eigenvalues accumulation points at a constant and zero, respectively, provided surface S is smooth. Performing testing of the SVS-EFIE-M in function space $L^2(S)$, we will achieve the impedance matrix with bounded condition number behaviour analogous to that in MoM solution of conventional S-MFIE for smooth PEC objects demonstrated in [60].

4.3.4 Discretization of the Surface-to-Surface Operator $\mathcal{T}_{m\epsilon}^{S,S}$

The MoM discretization of the integral operator $\mathcal{T}_{m\epsilon}^{S,S}$ is obtained by testing with the functions $\boldsymbol{u}_{n'm'}^{(i)}$ the electric field $\mathcal{T}_{m\epsilon}^{S,S} \circ \hat{\boldsymbol{n}} \times \boldsymbol{u}_{n''m''}^{(j)}$ produced by the basis functions $\boldsymbol{u}_{n''m''}^{(j)}$ in the expansion of current $\hat{\boldsymbol{n}} \times \boldsymbol{J}$. The following matrix elements $\mathcal{Z}_{m\epsilon}^{S_i,S_j}$ are formed using the expansion of magnetic dyadic Green's function (4.13)

$$
\begin{aligned}
\mathcal{Z}_{m\epsilon\ n'm',n''m''}^{S_i,S_j} &= \left\langle \mathcal{T}_{m\epsilon}^{S,S} \circ \hat{\boldsymbol{n}} \times \boldsymbol{u}_{n''m''}^{(j)}, \boldsymbol{u}_{n'm'}^{(i)} \right\rangle_{L^2(S)} \\
&= (-ik_\epsilon^2) \sum_{n,m} d_{nm} \left(\int_S \overline{\boldsymbol{u}}_{n'm'}^{(i)}(\boldsymbol{r}) \cdot \hat{\boldsymbol{n}} \times \boldsymbol{p}_{nm}^{(1\epsilon)}(\boldsymbol{r}) ds \right. \\
&\int_S \boldsymbol{q}_{n,-m}^{(2\epsilon)}(\boldsymbol{r}'') \cdot \hat{\boldsymbol{n}}'' \times \boldsymbol{u}_{n''m''}^{(j)}(\boldsymbol{r}'') ds'' + \int_S \overline{\boldsymbol{u}}_{n'm'}^{(i)}(\boldsymbol{r}) \cdot \\
&\qquad \left. \hat{\boldsymbol{n}} \times \boldsymbol{q}_{nm}^{(1\epsilon)}(\boldsymbol{r}) ds \int_S \boldsymbol{p}_{n,-m}^{(2\epsilon)}(\boldsymbol{r}'') \cdot \hat{\boldsymbol{n}}'' \times \boldsymbol{u}_{n''m''}^{(j)}(\boldsymbol{r}'') ds'' \right). \qquad (4.15)
\end{aligned}
$$

One can show from (4.15) that $\mathcal{Z}_{m\epsilon\ n'm',n''m''}^{S_1,S_1}$ and $\mathcal{Z}_{m\epsilon\ n'm',n''m''}^{S_2,S_2}$ vanish due to orthogonality [60] (also in Appendix I of [35]), i.e.

[1]Throughout the paper the inner product is defined as $\langle a, b\rangle = \langle a, b\rangle_{L^2(\Omega)} = \int_\Omega a \cdot \bar{b} d\Omega$, where bar indicates complex conjugation and Ω is domain of integration

$$\mathcal{Z}^{S_1,S_1}_{m\epsilon\ n'm',n''m''} = \left\langle \mathcal{T}^{S,S}_{m\epsilon} \circ \hat{\boldsymbol{n}} \times \boldsymbol{u}^{(1)}_{n''m''}, \boldsymbol{u}^{(1)}_{n'm'} \right\rangle_{L^2(S)} = 0, \tag{4.16}$$

$$\mathcal{Z}^{S_2,S_2}_{m\epsilon\ n'm',n''m''} = \left\langle \mathcal{T}^{S,S}_{m\epsilon} \circ \hat{\boldsymbol{n}} \times \boldsymbol{u}^{(2)}_{n''m''}, \boldsymbol{u}^{(2)}_{n'm'} \right\rangle_{L^2(S)} = 0. \tag{4.17}$$

However,

$$\mathcal{Z}^{S_i,S_j}_{m\epsilon\ n'm',n''m''} \neq 0, \quad i \neq j. \tag{4.18}$$

For the case $i = 1$ and $j = 2$, we have

$$\begin{aligned}
\mathcal{Z}^{S_1,S_2}_{m\epsilon\ n'm',n''m''} &= \left\langle \mathcal{T}^{S,S}_{m\epsilon} \circ \hat{\boldsymbol{n}} \times \boldsymbol{u}^{(2)}_{n''m''}, \boldsymbol{u}^{(1)}_{n'm'} \right\rangle_{L^2(S)} \\
&= -ik_\epsilon^2 \sum_{n,m} d_{nm} \left(\int_S \overline{\boldsymbol{u}}^{(1)}_{n'm'}(\boldsymbol{r}) \cdot \hat{\boldsymbol{n}} \times \boldsymbol{p}^{(1\epsilon)}_{nm}(\boldsymbol{r}) ds \right. \\
&\quad \int_S \boldsymbol{q}^{(2\epsilon)}_{n,-m}(\boldsymbol{r}'') \cdot \hat{\boldsymbol{n}}'' \times \boldsymbol{u}^{(2)}_{n''m''}(\boldsymbol{r}'') ds'' + \int_S \overline{\boldsymbol{u}}^{(1)}_{n'm'}(\boldsymbol{r}) \cdot \\
&\qquad \left. \hat{\boldsymbol{n}} \times \boldsymbol{q}^{(1\epsilon)}_{nm}(\boldsymbol{r}) ds \int_S \boldsymbol{p}^{(2\epsilon)}_{n,-m}(\boldsymbol{r}'') \cdot \hat{\boldsymbol{n}}'' \times \boldsymbol{u}^{(2)}_{n''m''}(\boldsymbol{r}'') ds'' \right).
\end{aligned}$$

Due to the orthogonality relationship [(72)-(77) in [60]], the contribution of the second term involving $\hat{\boldsymbol{n}} \times \boldsymbol{q}$ vanishes, which leads to the following simplification of matrix element $\mathcal{Z}^{S_1,S_2}_{m\epsilon}$

$$\begin{aligned}
\mathcal{Z}^{S_1,S_2}_{m\epsilon\ n'm',n''m''} &= -ik_\epsilon^2 \sum_{n,m} d_{nm} \left(\int_S \overline{\boldsymbol{u}}^{(1)}_{n'm'}(\boldsymbol{r}) \cdot \right. \\
&\qquad \left. \hat{\boldsymbol{n}} \times \boldsymbol{p}^{(1\epsilon)}_{nm}(\boldsymbol{r}) ds \int_S \boldsymbol{q}^{(2\epsilon)}_{n,-m}(\boldsymbol{r}'') \cdot \hat{\boldsymbol{n}}'' \times \boldsymbol{u}^{(2)}_{n''m''}(\boldsymbol{r}'') ds'' \right).
\end{aligned} \tag{4.19}$$

Employing expressions (47) and (76) from [60] and recalling the fact that $\hat{\boldsymbol{n}}\times\boldsymbol{u}^{(2)}_{n''m''} = -\boldsymbol{u}^{(1)}_{n''m''}$, we get

$$\begin{aligned}\mathcal{Z}^{S_1,S_2}_{m\epsilon\ n'm',n''m''} = -ik_\epsilon^2 \sum_{n,m} d_{nm} \Big(a j_n(k_\epsilon a) \\ \delta_{nn'}\delta_{mm'} d_{nm}^{-1/2}\ (-1) d_{nm}^{-1} \frac{1}{k_\epsilon}[k_\epsilon a h_n^{(2)}(k_\epsilon a)]' \\ \delta_{nn''}\delta_{m,m''} d^{1/2}_{n''m''}\Big) \\ = ik_\epsilon a j_{n'}(k_\epsilon a)[k_\epsilon a h^{(2)}_{n'}(k_\epsilon a)]' \delta_{n'n''}\delta_{m'm''}. \quad (4.20)\end{aligned}$$

Similarly, we obtain the other matrix element due to the interactions of the basis functions $\boldsymbol{u}^{(1)}_{n''m''}$ with the test functions $\boldsymbol{u}^{(2)}_{n'm'}$ via the integral operator $\mathcal{T}^{S,S}_{m\epsilon}$

$$\begin{aligned}\mathcal{Z}^{S_2,S_1}_{m\epsilon\ n'm',n''m''} = \left\langle \mathcal{T}^{S,S}_{m\epsilon} \circ \hat{\boldsymbol{n}} \times \boldsymbol{u}^{(1)}_{n''m''}, \boldsymbol{u}^{(2)}_{n'm'} \right\rangle_{L^2(S)} \\ = -ik_\epsilon^2 \sum_{n,m} d_{nm} \left(\int_S \overline{\boldsymbol{u}}^{(2)}_{n'm'}(\boldsymbol{r}) \cdot \hat{\boldsymbol{n}} \times \boldsymbol{p}^{(1\epsilon)}_{nm}(\boldsymbol{r}) ds \right. \\ \int_S \boldsymbol{q}^{(2\epsilon)}_{n,-m}(\boldsymbol{r}'') \cdot \hat{\boldsymbol{n}}'' \times \boldsymbol{u}^{(1)}_{n''m''}(\boldsymbol{r}'') ds'' + \int_S \overline{\boldsymbol{u}}^{(2)}_{n'm'}(\boldsymbol{r}) \cdot \\ \left. \hat{\boldsymbol{n}} \times \boldsymbol{q}^{(1\epsilon)}_{nm}(\boldsymbol{r}) ds \int_S \boldsymbol{p}^{(2\epsilon)}_{n,-m}(\boldsymbol{r}'') \cdot \hat{\boldsymbol{n}}'' \times \boldsymbol{u}^{(1)}_{n''m''}(\boldsymbol{r}'') ds'' \right). \quad (4.21)\end{aligned}$$

Using the orthogonality relationship [60], we determine that contributions from first term vanish, hence, producing

$$
\begin{aligned}
\mathcal{Z}^{S_2,S_1}_{m\epsilon\ n'm',n''m''} = & -ik_\epsilon^2 \sum_{n,m} d_{nm} \bigg(\int_S \overline{\boldsymbol{u}}^{(2)}_{n'm'}(\boldsymbol{r}) \cdot \\
& \hat{\boldsymbol{n}} \times \boldsymbol{q}^{(1\epsilon)}_{nm}(\boldsymbol{r}) ds \int_S \boldsymbol{p}^{(2\epsilon)}_{n,-m}(\boldsymbol{r}'') \cdot \hat{\boldsymbol{n}}'' \times \boldsymbol{u}^{(1)}_{n''m''}(\boldsymbol{r}'') ds'' \bigg) \\
= & -ik_\epsilon^2 \sum_{n,m} d_{nm} \bigg(\int_S d^{1/2}_{n'm'} \hat{\boldsymbol{r}} \times \nabla^t \overline{Y}^{m'}_{n'}(\boldsymbol{r}) \cdot \\
& \frac{1}{k_\epsilon} [k_\epsilon a j_n(k_\epsilon a)]' \hat{\boldsymbol{r}} \times \nabla^t Y^m_n(\hat{\boldsymbol{r}}) ds \\
& \int_S \boldsymbol{p}^{(2\epsilon)}_{n,-m}(\boldsymbol{r}'') \cdot d^{1/2}_{n''m''} \hat{\boldsymbol{n}}'' \times \nabla^t Y^{m''}_{n''}(\boldsymbol{r}'') ds'' \bigg) . \qquad (4.22)
\end{aligned}
$$

Employing (73) from [60] in addition to the orthogonality condition, we get the following closed-form expression

$$
\begin{aligned}
\mathcal{Z}^{S_2,S_1}_{m\epsilon\ n'm',n''m''} = & -ik_\epsilon^2 \frac{1}{k_\epsilon} \sum_{n,m} d_{nm} \Big(d^{-1/2}_{nm} [k_\epsilon a j_n(k_\epsilon a)]' \\
& \delta_{nn'} \delta_{mm'} \ [-a h^{(2)}_n(k_\epsilon a)] \delta_{nn''} \delta_{mm''} d^{-1}_{nm} d^{1/2}_{n''m''} \Big) \\
= & \ ik_\epsilon [k_\epsilon a j_{n'}(k_\epsilon a)]' [a h^{(2)}_{n'}(k_\epsilon a)] \delta_{n'n''} \delta_{m'm''}. \qquad (4.23)
\end{aligned}
$$

Arranging (4.16), (4.17), (4.20), and (4.23), the following hollow matrix representation of the surface-to-surface operator resulting from MoM discretization is obtained

$$
\boldsymbol{\mathcal{Z}}^{S,S}_{m\epsilon} = \begin{bmatrix} 0 & \boldsymbol{\mathcal{Z}}^{S_1,S_2}_{m\epsilon} \\ \boldsymbol{\mathcal{Z}}^{S_2,S_1}_{m\epsilon} & 0 \end{bmatrix} . \qquad (4.24)
$$

4.3.5 Discretization of the Surface-to-Volume Operator $\mathcal{T}^{V,S}_{m\epsilon}$

The MoM discretization of the integral operator $\mathcal{T}^{V,S}_{m\epsilon}$ performing translation of the surface current distribution to volumetric current distribution is obtained by testing with the functions $\boldsymbol{v}^{(i)}_{n'm'}$ of the electric field produced by the basis functions $\hat{\boldsymbol{n}} \times \boldsymbol{u}^{(j)}_{n''m''}$. The following matrix elements $\mathcal{Z}^{V_i,S_j}_{m\epsilon}$ are formed using the expansion of the magnetic dyadic Green's function (4.13)

$$\begin{aligned}\mathcal{Z}^{V_i,S_j}_{m\epsilon\ n'm',n''m''} &= \left\langle \mathcal{T}^{V,S}_{m\epsilon} \circ \hat{\boldsymbol{n}} \times \boldsymbol{u}^{(j)}_{n''m''}, \boldsymbol{v}^{(i)}_{n'm'} \right\rangle_{L^2(V)} = \\ &- ik_\epsilon^2 \sum_{n,m} d_{nm} \left(\int_V \overline{\boldsymbol{v}}^{(i)}_{n'm'}(\boldsymbol{r}) \cdot \boldsymbol{p}^{(1\epsilon)}_{nm}(\boldsymbol{r}) dv \right. \\ &\int_S \boldsymbol{q}^{(2\epsilon)}_{n,-m}(\boldsymbol{r}'') \cdot \hat{\boldsymbol{n}}'' \times \boldsymbol{u}^{(j)}_{n''m''}(\boldsymbol{r}'') ds'' + \int_V \overline{\boldsymbol{v}}^{(i)}_{n'm'}(\boldsymbol{r}) \cdot \\ &\left. \boldsymbol{q}^{(1\epsilon)}_{nm}(\boldsymbol{r}) dv \int_S \boldsymbol{p}^{(2\epsilon)}_{n,-m}(\boldsymbol{r}'') \cdot \hat{\boldsymbol{n}}'' \times \boldsymbol{u}^{(j)}_{n''m''}(\boldsymbol{r}'') ds'' \right). \qquad (4.25)\end{aligned}$$

In order to get the matrix element $\mathcal{Z}^{V_1,S_1}_{m\epsilon\ n'm',n''m''}$, we have

$$\begin{aligned}\mathcal{Z}^{V_1,S_1}_{m\epsilon\ n'm',n''m''} &= -ik_\epsilon^2 \sum_{n,m} d_{nm} \left(\int_V \overline{\boldsymbol{v}}^{(1)}_{n'm'}(\boldsymbol{r}) \cdot \right. \\ &\boldsymbol{p}^{(1\epsilon)}_{nm}(\boldsymbol{r}) dv \int_S \boldsymbol{q}^{(2\epsilon)}_{n,-m}(\boldsymbol{r}'') \cdot \hat{\boldsymbol{n}}'' \times \boldsymbol{u}^{(1)}_{n''m''}(\boldsymbol{r}'') ds'' + \int_V \\ &\left. \overline{\boldsymbol{v}}^{(1)}_{n'm'}(\boldsymbol{r}) \cdot \boldsymbol{q}^{(1\epsilon)}_{nm}(\boldsymbol{r}) dv \int_S \boldsymbol{p}^{(2\epsilon)}_{n,-m}(\boldsymbol{r}'') \cdot \hat{\boldsymbol{n}}'' \times \boldsymbol{u}^{(1)}_{n''m''}(\boldsymbol{r}'') ds'' \right). \qquad (4.26)\end{aligned}$$

Employing the orthogonality relations [(75) in [60]] and accounting for the orthogonality $\left\langle \boldsymbol{q}^{(1\epsilon)}_{nm}, \boldsymbol{v}^{(1)}_{n'm'} \right\rangle = \left\langle \boldsymbol{q}^{(1\epsilon)}_{nm}, \boldsymbol{p}^{(1\epsilon)}_{n'm'} \right\rangle = 0$ we obtain vanishing result for the element of $\mathcal{Z}^{V_1,S_1}_{m\epsilon\ n'm',n''m''}$ leading to

$$\boldsymbol{\mathcal{Z}}^{V_1,S_1}_{m\epsilon} = \mathbf{0}. \qquad (4.27)$$

For the matrix element $\mathcal{Z}^{V_1,S_2}_{m\epsilon\ n'm',n''m''}$

$$\begin{aligned}\mathcal{Z}^{V_1,S_2}_{m\epsilon\ n'm',n''m''} = -ik_\epsilon^2 \sum_{n,m} d_{nm} \Bigg(\int_V \overline{\boldsymbol{v}}^{(1)}_{n'm'}(\boldsymbol{r}) \cdot \boldsymbol{p}^{(1\epsilon)}_{nm}(\boldsymbol{r}) \\ dv \int_S \boldsymbol{q}^{(2\epsilon)}_{n,-m}(\boldsymbol{r}'') \cdot \hat{\boldsymbol{n}}'' \times \boldsymbol{u}^{(2)}_{n''m''}(\boldsymbol{r}'') ds'' + \int_V \overline{\boldsymbol{v}}^{(1)}_{n'm'}(\boldsymbol{r}) \cdot \\ \boldsymbol{q}^{(1\epsilon)}_{nm}(\boldsymbol{r}) dv \int_S \boldsymbol{p}^{(2\epsilon)}_{n,-m}(\boldsymbol{r}'') \cdot \hat{\boldsymbol{n}}'' \times \boldsymbol{u}^{(2)}_{n''m''}(\boldsymbol{r}'') ds'' \Bigg). \end{aligned} \tag{4.28}$$

Employing integral relation (72) in [60], the second term of the above equation disappear, and with aid of (74) in [60] and (113) in [35] the resultant expression becomes

$$\begin{aligned}\mathcal{Z}^{V_1,S_2}_{m\epsilon\ n'm',n''m''} &= -ik_\epsilon^2 \sum_{n,m} d_{nm} \Bigg(\int_0^a j_n(k_\epsilon r) j_{n'}(k_\epsilon r) \\ &\quad r^2 dr \delta_{nn'} \delta_{mm'} d_{nm}^{-1/2} d_{n'm'}^{-1/2} \frac{-1}{k_\epsilon} [(k_\epsilon a h_n^{(2)}(k_\epsilon a)]' \\ &\quad d^{1/2}_{n''m''} d^{-1}_{nm} \delta_{nn''} \delta_{mm''} \Bigg) \\ &= ik_\epsilon \Bigg(\int_0^a j_{n'}(k_\epsilon r) j_{n''}(k_\epsilon r) r^2 dr \cdot \\ &\quad [(k_\epsilon a h_{n'}^{(2)}(k_\epsilon a)]' d^{-1/2}_{n''m''} \delta_{n'n''} \delta_{m'm''} \Bigg). \end{aligned} \tag{4.29}$$

In the case of element $\mathcal{Z}^{V_2,S_1}_{m\epsilon\ n'm',n''m''}$ we have

$$\begin{aligned}\mathcal{Z}^{V_2,S_1}_{m\epsilon\ n'm',n''m''} = -ik_\epsilon^2 \sum_{n,m} d_{nm} \Bigg(\int_V \overline{\boldsymbol{v}}^{(2)}_{n'm'}(\boldsymbol{r}) \cdot \\ \boldsymbol{p}^{(1\epsilon)}_{nm}(\boldsymbol{r}) dv \int_S \boldsymbol{q}^{(2\epsilon)}_{n,-m}(\boldsymbol{r}'') \cdot \hat{\boldsymbol{n}}'' \times \boldsymbol{u}^{(1)}_{n''m''}(\boldsymbol{r}'') ds'' + \\ \int_V \overline{\boldsymbol{v}}^{(2)}_{n'm'}(\boldsymbol{r}) \cdot \boldsymbol{q}^{(1\epsilon)}_{nm}(\boldsymbol{r}) dv \int_S \boldsymbol{p}^{(2\epsilon)}_{n,-m}(\boldsymbol{r}'') \\ \cdot \hat{\boldsymbol{n}}'' \times \boldsymbol{u}^{(1)}_{n''m''}(\boldsymbol{r}'') ds'' \Bigg). \end{aligned} \tag{4.30}$$

Using relation (25) in [35], element of matrix $\mathcal{Z}_{m\epsilon}^{V_2,S_1}$ becomes

$$\mathcal{Z}_{m\epsilon\ n'm',n''m''}^{V_2,S_1} = -ik_\epsilon^2 \sum_{n,m} d_{nm} \Bigg(\int_V \boldsymbol{q}_{n',-m'}^{(1\epsilon)}(\boldsymbol{r}) \cdot$$
$$\boldsymbol{p}_{nm}^{(1\epsilon)}(\boldsymbol{r}) dv \int_S \boldsymbol{q}_{n,-m}^{(2\epsilon)}(\boldsymbol{r}'') \cdot d_{n''m''}^{1/2} \hat{\boldsymbol{n}}'' \times \nabla^t Y_{n''}^{m''}(\boldsymbol{r}'') ds''$$
$$+ \int_V \boldsymbol{q}_{n',-m'}^{(1\epsilon)}(\boldsymbol{r}) \cdot \boldsymbol{q}_{nm}^{(1\epsilon)}(\boldsymbol{r}) dv \int_S \boldsymbol{p}_{n,-m}^{(2\epsilon)}(\boldsymbol{r}'')$$
$$\cdot d_{n''m''}^{1/2} \hat{\boldsymbol{n}}'' \times \nabla^t Y_{n''}^{m''}(\boldsymbol{r}'') ds'' \Bigg) . \quad (4.31)$$

Because of orthogonality of $\left\langle \boldsymbol{q}_{n',-m'}^{(1\epsilon)}, \boldsymbol{p}_{nm}^{(1\epsilon)} \right\rangle = 0$ first term in (4.31) vanishes. Using (114) in [35] and (73) in [60] [1] we get

$$\mathcal{Z}_{m\epsilon\ n'm',n''m''}^{V_2,S_1} = -ik_\epsilon^2 \sum_{n,m} d_{nm} \Bigg(\frac{n(n+1)}{k_\epsilon^2} \int_0^a j_n(k_\epsilon r)$$
$$j_{n'}(k_\epsilon r) dr \cdot a^2 + \frac{1}{k_\epsilon^2} \int_0^a [k_\epsilon r j_n(k_\epsilon r)]' [k_\epsilon r j_{n'}(k_\epsilon r)]' dr \Bigg)$$
$$\delta_{nn'} \delta_{mm'} d_{nm}^{-1/2} d_{n'm'}^{-1/2} [-a h_n^{(2)}(k_\epsilon a)] d_{nm}^{-1} \delta_{nn''} \delta_{mm''} d_{n''m''}^{1/2}$$
$$= ik_\epsilon^2 \Bigg(\frac{n'(n'+1)}{k_\epsilon^2} a^2 \int_0^a j_{n'}(k_\epsilon r) j_{n''}(k_\epsilon r) dr$$
$$+ \frac{1}{k_\epsilon^2} \int_0^a [k_\epsilon r j_{n'}(k_\epsilon r)]' [k_\epsilon r j_{n''}(k_\epsilon r)]' dr \Bigg)$$
$$\cdot [a h_{n'}^{(2)}(k_\epsilon a)] \delta_{n'n''} \delta_{m'm''} d_{n''m''}^{-1/2} . \quad (4.32)$$

Finally, for the element of matrix $\mathcal{Z}_{m\epsilon}^{V_2,S_2}$ we have

$$\mathcal{Z}_{m\epsilon\ n'm',n''m''}^{V_2,S_2} = -ik_\epsilon^2 \sum_{n,m} d_{nm} \Bigg(\int_V \overline{\boldsymbol{v}}_{n'm'}^{(2)}(\boldsymbol{r}) \cdot \boldsymbol{p}_{nm}^{(1\epsilon)}(\boldsymbol{r})$$
$$dv \int_S \boldsymbol{q}_{n,-m}^{(2\epsilon)}(\boldsymbol{r}'') \cdot \hat{\boldsymbol{n}}'' \times \boldsymbol{u}_{n''m''}^{(2)}(\boldsymbol{r}'') ds'' + \int_V \overline{\boldsymbol{v}}_{n'm'}^{(2)}(\boldsymbol{r})$$
$$\cdot \boldsymbol{q}_{nm}^{(1\epsilon)}(\boldsymbol{r}) dv \int_S \boldsymbol{p}_{n,-m}^{(2\epsilon)}(\boldsymbol{r}'') \cdot \hat{\boldsymbol{n}}'' \times \boldsymbol{u}_{n''m''}^{(2)}(\boldsymbol{r}'') ds'' \Bigg) , \quad (4.33)$$

[1] Note that (73) in [60] has a mistake and should contain $z_n^{(j)}(ka)$ instead of $z_n^{(j)}(a)$

leading to vanishing of first term due to (25) in [35] and orthogonality $\left\langle \boldsymbol{q}^{(1\epsilon)}_{n',-m'}, \boldsymbol{p}^{(1\epsilon)}_{nm} \right\rangle = 0$ and second term due to (72) [60], which results in

$$\mathcal{Z}^{V_2,S_2}_{m\epsilon\ n'm',n''m''} = 0. \tag{4.34}$$

Combining (4.27), (4.29), (4.32), and (4.34), MoM discretization of the surface-to-volume operator corresponds to the following hollow matrix:

$$\boldsymbol{\mathcal{Z}}^{V,S}_{m\epsilon} = \begin{bmatrix} 0 & \boldsymbol{\mathcal{Z}}^{V_1,S_2}_{m\epsilon} \\ \boldsymbol{\mathcal{Z}}^{V_2,S_1}_{m\epsilon} & 0 \end{bmatrix}. \tag{4.35}$$

4.3.6 Discretization of the Volume-to-Surface Operator $\mathcal{T}^{S,V}_{e0}$

The MoM discretization of the integral operator $\mathcal{T}^{S,V}_{e0}$ which translates volumetric current distribution to surface current distribution is obtained by testing with the surface functions $\boldsymbol{u}^{(i)}_{n'm'}$ of the electric field produced by the volumetric vector basis functions $\boldsymbol{v}^{(j)}_{n''m''}$. Here we use the expansion of free space electric field dyadic Green's function as in (68) of [60], which is involved in the definition of the integral operator $\mathcal{T}^{S,V}_{e0}$ in (4.9)

$$\begin{aligned}
\mathcal{Z}^{S_i,V_j}_{e0\ n'm',n''m''} &= \left\langle \mathcal{T}^{S,V}_{e0} \circ \boldsymbol{v}^{(j)}_{n''m''}, \boldsymbol{u}^{(i)}_{n'm'} \right\rangle \\
&= k_0^2(\epsilon-1)(-ik_0)\sum_{n,m} d_{nm} \left(\int_S \overline{\boldsymbol{u}}^{(i)}_{n'm'}(\boldsymbol{r}) \cdot \hat{\boldsymbol{n}} \times \boldsymbol{q}^{(20)}_{nm}(\boldsymbol{r}) ds \right. \\
&\qquad \int_V \boldsymbol{q}^{(10)}_{n,-m}(\boldsymbol{r}'') \cdot \boldsymbol{v}^{(j)}_{n''m''}(\boldsymbol{r}'') dv'' + \int_S \overline{\boldsymbol{u}}^{(i)}_{n'm'}(\boldsymbol{r}) \\
&\qquad \left. \cdot\, \hat{\boldsymbol{n}} \times \boldsymbol{p}^{(20)}_{nm}(\boldsymbol{r}) ds \int_V \boldsymbol{p}^{(10)}_{n,-m}(\boldsymbol{r}'') \cdot \boldsymbol{v}^{(j)}_{n''m''}(\boldsymbol{r}'') dv'' \right).
\end{aligned} \tag{4.36}$$

Matrix block $\mathcal{Z}^{S,V}_{e0}$ corresponding to the case of $i = 1$, $j = 1$ has zero contribution from the term containing vector function $\boldsymbol{q}$ according to (48) and (77) in [60]. Using

(21) and (113) in [35] and (76) in [60] we get

$$\mathcal{Z}^{S_1,V_1}_{e0\;n'm',n''m''} = k_0^2(\epsilon-1)(-ik_0)\sum_{n,m} d_{nm}\Bigg(\int_S \overline{\boldsymbol{u}}^{(1)}_{n'm'}(\boldsymbol{r})\cdot\hat{\boldsymbol{n}}\times\boldsymbol{p}^{(20)}_{nm}(\boldsymbol{r})ds\int_V \boldsymbol{p}^{(10)}_{n,-m}(\boldsymbol{r}'')\cdot\boldsymbol{p}^{(1\epsilon)}_{n''m''}(\boldsymbol{r}'')dv''\Bigg)$$
$$= k_0^2(\epsilon-1)(-ik_0)\sum_{n,m} d_{nm}\Bigg(ah^{(2)}_n(k_0a)\int_S d^{1/2}_{n'm'}\nabla^t Y^m_n(\boldsymbol{r})\cdot\nabla^t\overline{Y}^{m'}_{n'}(\boldsymbol{r})ds\int_V \boldsymbol{p}^{(10)}_{n,-m}(\boldsymbol{r}'')\cdot\boldsymbol{p}^{(1\epsilon)}_{n''m''}(\boldsymbol{r}'')dv''\Bigg)$$
$$= k_0^2(\epsilon-1)(-ik_0)ah^{(2)}_{n'}(k_0a)d^{-1/2}_{n'm'}\delta_{n'n''}\delta_{m'm''}\int_0^a j_{n'}(k_0r)j_{n''}(k_\epsilon r)r^2dr. \quad (4.37)$$

Matrix blocks $\mathcal{Z}^{S_1,V_2}_{e0}$ and $\mathcal{Z}^{S_2,V_1}_{e0}$ are zero because of the fact that we have relations (48), (76), (77) in [60] as well as $\left\langle \boldsymbol{v}^{(2)}_{n'',m''},\boldsymbol{p}^{(10)}_{nm}\right\rangle = 0$ and $\left\langle \boldsymbol{v}^{(1)}_{n'',m''},\boldsymbol{q}^{(10)}_{nm}\right\rangle = 0$

$$\mathcal{Z}^{S_1,V_2}_{e0\;n'm',n''m''} = \left\langle \mathcal{T}^{S,V}_{e0}\circ\boldsymbol{v}^{(2)}_{n''m''},\boldsymbol{u}^{(1)}_{n'm'}\right\rangle = 0, \quad (4.38)$$

$$\mathcal{Z}^{S_2,V_1}_{e0\;n'm',n''m''} = \left\langle \mathcal{T}^{S,V}_{e0}\circ\boldsymbol{v}^{(1)}_{n''m''},\boldsymbol{u}^{(2)}_{n'm'}\right\rangle = 0. \quad (4.39)$$

With aid of (48), (76), and (77) in [60] and (114) from [35] the matrix elements $\mathcal{Z}^{S_2,V_2}_{e0\ n'm',n''m''}$ become

$$
\begin{aligned}
\mathcal{Z}^{S_2,V_2}_{e0\ n'm',n''m''} = k_0^2(\epsilon-1)(-ik_0)\sum_{n,m} d_{nm}\Bigg(\int_S d^{1/2}_{n'm'} \\
\hat{\boldsymbol{r}} \times \nabla^t \overline{Y}^{m'}_{n'}(\hat{\boldsymbol{r}}) \cdot \frac{1}{k_0}[k_0 a h^{(2)}_n(k_0 a)]' \hat{\boldsymbol{r}} \times \nabla^t Y^m_n(\hat{\boldsymbol{r}}) ds \\
\int_V \boldsymbol{q}^{(10)}_{n,-m}(\boldsymbol{r}'') \cdot \boldsymbol{q}^{(1\epsilon)}_{n''m''}(\boldsymbol{r}'') dv''\Bigg) = k_0^2(\epsilon-1)(-ik_0) \\
\sum_{n,m} d_{nm}\left(d^{-1/2}_{n'm'}\frac{1}{k_0}[k_0 a h^{(2)}_n(k_0 a)]'\right) \\
\delta_{nn'}\delta_{mm'}\left(\frac{n(n+1)}{k_0 k_\epsilon}a^2\int_0^a j_n(k_0 r) j_{n''}(k_\epsilon r) dr + \right. \\
\left.\frac{1}{k_0 k_\epsilon}\int_0^a [k_0 r j_n(k_0 r)]'[k_\epsilon r j_{n''}(k_\epsilon r)]' dr\right) \\
\delta_{nn''}\delta_{mm''} d^{-1/2}_{nm} d^{-1/2}_{n''m''} = k_0^2(\epsilon-1)(-ik_0) \\
\left(d^{-1/2}_{n'm'}\frac{1}{k_0}[k_0 a h^{(2)}_{n'}(k_0 a)]'\right) \\
\delta_{n'n''}\delta_{m'm''}\left(\frac{n'(n'+1)}{k_0 k_\epsilon}a^2\int_0^a j_{n'}(k_0 r) j_{n''}(k_\epsilon r) dr + \right. \\
\left.\frac{1}{k_0 k_\epsilon}\int_0^a [k_0 r j_{n'}(k_0 r)]'[k_\epsilon r j_{n''}(k_\epsilon r)]' dr\right). \qquad (4.40)
\end{aligned}
$$

Unfortunately, integrals in (4.40) over r do not bring us any closed-form expression [63].

Arranging expressions (4.37), (4.38), (4.39) and (4.40) together, the following block diagonal impedance matrix for the MoM discretization of the volume-to-surface operator $\mathcal{T}^{S,V}_{e0}$ is obtained

$$
\boldsymbol{\mathcal{Z}}^{S,V}_{e0} = \begin{bmatrix} \boldsymbol{\mathcal{Z}}^{S_1,V_1}_{e0} & 0 \\ 0 & \boldsymbol{\mathcal{Z}}^{S_2,V_2}_{e0} \end{bmatrix}. \qquad (4.41)
$$

4.4 Matrix Assembly for the MoM Discretization of the Integral Operators

The MoM discretization of the integral operators $\mathcal{T}_{m\epsilon}^{S,S}$, $\mathcal{T}_{m\epsilon}^{V,S}$, $\mathcal{T}_{e0}^{S,V}$ discussed in the previous section, can be arranged together to form the impedance matrix and the incident field based excitation vector for the proposed SVS-EFIE-M formulation (4.4). These can be used to form the following system of linear algebraic equations (SLAE) with respect to the unknown coefficients $b_{n,m}$ and $c_{n,m}$ in the current expansion (4.11)

$$\boldsymbol{\mathcal{Z}}_{\text{SVS}} \cdot \mathbf{I} = \mathbf{E}, \tag{4.42}$$

where

$$\mathbf{I} = [\mathbf{b}, \mathbf{c}]^t, \tag{4.43}$$

$$\mathbf{E} = \begin{bmatrix} \left\langle \hat{\boldsymbol{n}} \times \boldsymbol{E}^{inc}, \boldsymbol{u}_{n'm'}^{(1)} \right\rangle_{L^2(S)} \\ \left\langle \hat{\boldsymbol{n}} \times \boldsymbol{E}^{inc}, \boldsymbol{u}_{n'm'}^{(2)} \right\rangle_{L^2(S)} \end{bmatrix}, \tag{4.44}$$

and $\boldsymbol{\mathcal{Z}}_{\text{SVS}}$ is the hollow matrix defined as

$$\begin{gathered} \boldsymbol{\mathcal{Z}}_{\text{SVS}} = \begin{bmatrix} 0 & \boldsymbol{\mathcal{Z}}_{\text{SVS}}^1 \\ \boldsymbol{\mathcal{Z}}_{\text{SVS}}^2 & 0 \end{bmatrix} = \begin{bmatrix} 0 & \boldsymbol{\mathcal{Z}}_{m\epsilon}^{S_1,S_2} \\ \boldsymbol{\mathcal{Z}}_{m\epsilon}^{S_2,S_1} & 0 \end{bmatrix} - \\ \begin{bmatrix} \boldsymbol{\mathcal{Z}}_{e0}^{S_1,V_1} & 0 \\ 0 & \boldsymbol{\mathcal{Z}}_{e0}^{S_2,V_2} \end{bmatrix} \cdot \begin{bmatrix} \mathbf{\Gamma}_1 & 0 \\ 0 & \mathbf{\Gamma}_2 \end{bmatrix}^{-1} \cdot \begin{bmatrix} 0 & \boldsymbol{\mathcal{Z}}_{m\epsilon}^{V_1,S_2} \\ \boldsymbol{\mathcal{Z}}_{m\epsilon}^{V_2,S_1} & 0 \end{bmatrix}. \end{gathered} \tag{4.45}$$

The Gram matrix blocks $\mathbf{\Gamma}_j$ are defined as in (57) of [35].

The above multiplications of the matrices lead to the two groups of equations. The first group is associated with the unknown expansion coefficients c_{nm}

$$\begin{aligned}\boldsymbol{\mathcal{Z}}^{1}_{\mathrm{SVS}} \cdot \mathbf{c} = [\boldsymbol{\mathcal{Z}}^{S_1,S_2}_{m\epsilon} - \boldsymbol{\mathcal{Z}}^{S_1,V_1}_{e0} \cdot \boldsymbol{\Gamma}^{-1}_{1} \cdot \boldsymbol{\mathcal{Z}}^{V_1,S_2}_{m\epsilon}] \cdot \mathbf{c} = ik_\epsilon \\ \sum_{n'',m''} c_{n''m''} \Big([aj_{n'}(k_\epsilon a)][(k_\epsilon a)h^{(2)}_{n'}(k_\epsilon a)]' \\ \delta_{n'n''}\delta_{m'm''}\Big) - k_0^2(\epsilon-1) \left(\sum_{n'',m''} c_{n''m''} \right. \\ (-k_0)ah^{(2)}_{n'}(k_0 a) \int_0^a j_{n'}(k_0 r) j_{n''}(k_\epsilon r) r^2 dr \delta_{n'n''}\delta_{m'm''} \\ \left(\int_0^a j_{n'}(k_\epsilon r) j_{n''}(k_\epsilon r) r^2 dr \right)^{-1} \\ \left. (i^2 k_\epsilon)[(k_\epsilon a)h^{(2)}_{n'}(k_\epsilon a)]' \int_0^a j_{n'}(k_\epsilon r) j_{n''}(k_\epsilon r) r^2 dr \right). \quad (4.46)\end{aligned}$$

The diagonal form of the impedance matrix block $\boldsymbol{\mathcal{Z}}^{1}_{\mathrm{SVS}}$ allows us to solve SLAE (4.42) explicitly for c_{nm}, giving these unknown coefficients in the following closed-form

$$c_{nm} = \frac{E_{1,nm}}{\Lambda^{(2)}_{n}}, \quad (4.47)$$

where

$$\Lambda^{(2)}_{n} = \Lambda^{S,S}_{2,m\epsilon,n} + \Lambda^{S,V}_{2,e0,n} \hat{\Gamma}^{-1}_{1,n} \Lambda^{V,S}_{2,m\epsilon,n}, \quad (4.48)$$

$$\Lambda^{S,S}_{2,m\epsilon,n} = (ik_\epsilon)[aj_n(k_\epsilon a)][(k_\epsilon a)h^{(2)}_{n}(k_\epsilon a)]'. \quad (4.49)$$

$\Lambda^{S,V}_{2,e0,n}$ [(62) of [35]] and $\Lambda^{V,S}_{2,m\epsilon,n}$ have closed-form [63] as

$$\Lambda^{V,S}_{2,m\epsilon,n} = -k_\epsilon[(k_\epsilon a)h^{(2)}_{n'}(k_\epsilon a)]' \int_0^a j_n(k_\epsilon r)j_n(k_\epsilon r)r^2 dr = \\ - k_\epsilon[(k_\epsilon a)h^{(2)}_{n}(k_\epsilon a)]' \frac{a^3}{2}[j_n(k_\epsilon a)^2 - j_{n-1}(k_\epsilon a)j_{n+1}(k_\epsilon a)], \quad (4.50)$$

and the closed-form of Gram matrix elements $\hat{\Gamma}_{1,n}$ is given in (64) of [35].

Similarly, the second group of linear algebraic equations is formed due to the process of multiplication and addition of the matrix elements (4.45). Multiplication of the resultant matrix with the vector of unknown coefficients $\mathbf{b}$ is, as follows:

$$\begin{aligned}
\boldsymbol{\mathcal{Z}}^2_{\mathrm{SVS}} \cdot \mathbf{b} = [&\boldsymbol{\mathcal{Z}}^{S_2,S_1}_{m\epsilon} - \boldsymbol{\mathcal{Z}}^{S_2,V_2}_{e0} \cdot \boldsymbol{\Gamma}_2^{-1} \cdot \boldsymbol{\mathcal{Z}}^{V_2,S_1}_{m\epsilon}] \cdot \mathbf{b} \\
&= (ik_\epsilon) \sum_{n'',m''} b_{n''m''}(ah^{(2)}_{n'}(k_\epsilon a)]) \\
&[k_\epsilon a j_{n'}(k_\epsilon a)]' \delta_{n'n''}\delta_{m'm''} - (ik_\epsilon)^2 k_0^2(\epsilon - 1) \\
&\sum_{n'',m''} b_{n''m''}(-1)[k_0 a h^{(2)}_{n'}(k_0 a)]' \\
&\left(\frac{n'(n'+1)}{k_0 k_\epsilon} a^2 \int_0^a j_{n'}(k_0 r) j_{n''}(k_\epsilon r) dr + \frac{1}{k_0 k_\epsilon}\right. \\
&\left.\int_0^a [k_0 r j_{n'}(k_0 r)]'[k_\epsilon r j_{n''}(k_\epsilon r)]' dr\right) \delta_{n'n''}\delta_{m'm''} \\
&\left(\frac{n'(n'+1)}{k_\epsilon^2} a^2 \int_0^a j_{n'}(k_\epsilon r) j_{n''}(k_\epsilon r) dr\right. \\
&\left.+ \frac{1}{k_\epsilon^2} \int_0^a [k_\epsilon r j_{n'}(k_\epsilon r)]'[k_\epsilon r j_{n''}(k_\epsilon r)]' dr\right)^{-1} \\
&[ah^{(2)}_{n'}(k_\epsilon a)] \left(\frac{n'(n'+1)}{k_\epsilon^2} a^2 \int_0^a j_{n'}(k_\epsilon r) j_{n''}(k_\epsilon r) dr\right. \\
&\left.+ \frac{1}{k_\epsilon^2} \int_0^a [k_\epsilon r j_{n'}(k_\epsilon r)]'[k_\epsilon r j_{n''}(k_\epsilon r)]' dr\right). \quad (4.51)
\end{aligned}$$

The above diagonal impedance matrix $\boldsymbol{\mathcal{Z}}^2_{\text{SVS}}$ allows to determine the unknown coefficients b_{nm} in the following closed-form

$$b_{nm} = \frac{E_{2,nm}}{\Lambda_n^{(1)}}, \tag{4.52}$$

where

$$\Lambda_n^{(1)} = \Lambda^{S,S}_{1,m\epsilon,n} + \Lambda^{S,V}_{1,e0,n}\hat{\Gamma}^{-1}_{2,n}\Lambda^{V,S}_{1,m\epsilon,n}, \tag{4.53}$$

and the eigenvalues $\Lambda^{S,S}_{1,m\epsilon,n}$ and $\Lambda^{V,S}_{1,m\epsilon,n}$ are[1]

$$\Lambda^{S,S}_{1,m\epsilon,n} = ik_\epsilon(ah_n^{(2)}(k_\epsilon a))[k_\epsilon a j_n(k_\epsilon a)]', \tag{4.54}$$

$$\begin{aligned}\Lambda^{V,S}_{1,m\epsilon,n} = -(ik_\epsilon)^2 a h_n^{(2)}(k_\epsilon a)\Bigg(&\frac{n(n+1)}{k_\epsilon^2}a^2\int_0^a j_n(k_\epsilon r) \\ & j_n(k_\epsilon r)dr + \frac{1}{k_\epsilon^2}\int_0^a [(k_\epsilon r)j_n(k_\epsilon r)]'[(k_\epsilon r)j_n(k_\epsilon r)]'dr\Bigg).\end{aligned} \tag{4.55}$$

$\Lambda^{S,V}_{1,e0,n}$ and the Gram matrix $\hat{\Gamma}_{2,n}$ are expressed in (69) and (71) in [35], respectively.

4.5 Behavior of SVS-EFIE-M Spectrum

4.5.1 Spectra of SVS-EFIE-M operators

The following section describes the spectral properties of the integral operators in SVS-EFIE-M formulation. It can be shown (see (4.87) in Appendix I for details)

[1]We could not find a closed-form expression for the integrals in (4.55). It appears that neither could the authors of [63]. Lack of a closed-form expression for these integrals is the reason why we cannot establish analytically the equivalence of the proposed analytic MoM solution of the SVS-EFIE-M and Mie series despite both being exact solutions of the same boundary value problem.

that $\Lambda^{S,S}_{2,m\epsilon,n}$ are the eigenvalues of the operator $\mathcal{T}^{S,S}_{m\epsilon}$ since

$$\mathcal{T}^{S,S}_{m\epsilon} \circ (\nabla^t Y^m_n) = -\Lambda^{S,S}_{2,m\epsilon,n} \nabla^t Y^m_n, \tag{4.56}$$

and the product $\Lambda^{S,V}_{2,e0,n}\hat{\Gamma}^{-1}_{1,n}\Lambda^{V,S}_{2,m\epsilon,n}$ represents eigenvalues of the product of the integral operators $\mathcal{T}^{S,V}_{e0} \circ \mathcal{T}^{V,S}_{m\epsilon}$ per (4.92)

$$\mathcal{T}^{S,V}_{e0} \circ \mathcal{T}^{V,S}_{m\epsilon} \circ (\nabla^t Y^m_n) = \Lambda^{S,V}_{2,e0,n}\hat{\Gamma}^{-1}_{1,n}\Lambda^{V,S}_{2,m\epsilon,n} \nabla^t Y^m_n. \tag{4.57}$$

Thus, $\Lambda^{(2)}_n = \Lambda^{S,S}_{2,m\epsilon,n} + \Lambda^{S,V}_{2,e0,n}\hat{\Gamma}^{-1}_{1,n}\Lambda^{V,S}_{2,m\epsilon,n}$ the eigenvalues of the total SVS-EFIE-M operators $\mathcal{T}_{SVS} = \mathcal{T}^{S,S}_{m\epsilon} - \mathcal{T}^{S,V}_{e0} \circ \mathcal{T}^{V,S}_{m\epsilon}$

$$\mathcal{T}^{S,S}_{m\epsilon} \circ (\nabla^t Y^m_n) - \mathcal{T}^{S,V}_{e0} \circ \mathcal{T}^{V,S}_{m\epsilon} \circ (\nabla^t Y^m_n) = -\Lambda^{(2)}_n \nabla^t Y^m_n. \tag{4.58}$$

Similarly, eigenvalues of the integral operator $\mathcal{T}^{S,S}_{m\epsilon}$ are $\Lambda^{S,S}_{1,m\epsilon,n}$ (see (4.88) in Appendix I), since

$$\mathcal{T}^{S,S}_{m\epsilon} \circ (\hat{\boldsymbol{r}} \times \nabla^t Y^m_n) = \Lambda^{S,S}_{1,m\epsilon,n}(\hat{\boldsymbol{r}} \times \nabla^t Y^m_n). \tag{4.59}$$

The product $\Lambda^{S,V}_{1,e0,n}\hat{\Gamma}^{-1}_{2,n}\Lambda^{V,S}_{1,m\epsilon,n}$ forms the eigenvalues of the product of the operators $\mathcal{T}^{S,V}_{e0} \circ \mathcal{T}^{V,S}_{m\epsilon}$ according to

$$\mathcal{T}^{S,V}_{e0} \circ \mathcal{T}^{V,S}_{m\epsilon} \circ (\hat{\boldsymbol{r}} \times \nabla^t Y^m_n) = -\Lambda^{S,V}_{1,e0,n}\hat{\Gamma}^{-1}_{2,n}\Lambda^{V,S}_{1,m\epsilon,n}(\hat{\boldsymbol{r}} \times \nabla^t Y^m_n). \tag{4.60}$$

This makes $\Lambda^{(1)}_n = \Lambda^{S,S}_{1,m\epsilon,n} + \Lambda^{S,V}_{1,e0,n}\hat{\Gamma}^{-1}_{2,n}\Lambda^{V,S}_{1,m\epsilon,n}$ the eigenvalues of the total SVS-EFIE-M operator $\mathcal{T}_{SVS}$

$$\mathcal{T}^{S,S}_{m\epsilon} \circ (\hat{\boldsymbol{r}} \times \nabla^t Y^m_n) - \mathcal{T}^{S,V}_{e0} \circ \mathcal{T}^{V,S}_{m\epsilon} \circ (\hat{\boldsymbol{r}} \times \nabla^t Y^m_n) = \Lambda^{(1)}_n \hat{\boldsymbol{r}} \times \nabla^t Y^m_n. \tag{4.61}$$

4.5.2 Spectrum of Galerkin MoM matrix

Spectral behavior of the MoM matrix is demonstrated in this section. The integral operators produce two sets of eigenvalues as it was shown in previous section. These eigenvalues form the diagonal matrix elements and relate to the unknowns and the right hand side of SLAE as stated in (4.47) and (4.52). Hence, we can reveal spectral properties of the MoM matrix resulting from the discretization of new SVS-EFIE-M formulation in $L^2(S)$ space by stating the SLAE as

$$\left\langle \mathcal{T}_{SVS} \circ \hat{\boldsymbol{n}} \times \boldsymbol{J}, \boldsymbol{u}^{(1)}_{n'm'} \right\rangle_{L^2(S)} = \sum_{n,m} c_{nm} \Lambda^{(2)}_n \delta_{nn'} \delta_{mm'} = \left\langle \hat{\boldsymbol{n}} \times \boldsymbol{E}^{inc}, \boldsymbol{u}^{(1)}_{n'm'} \right\rangle_{L^2(S)}, \quad (4.62)$$

$$\left\langle \mathcal{T}_{SVS} \circ \hat{\boldsymbol{n}} \times \boldsymbol{J}, \boldsymbol{u}^{(2)}_{n'm'} \right\rangle_{L^2(S)} = \sum_{n,m} b_{nm} \Lambda^{(1)}_n \delta_{nn'} \delta_{mm'} = \left\langle \hat{\boldsymbol{n}} \times \boldsymbol{E}^{inc}, \boldsymbol{u}^{(2)}_{n'm'} \right\rangle_{L^2(S)}, \quad (4.63)$$

and computing the eigenvalues of the diagonal matrix in its left hand side.

4.5.3 Absence of oversampling breakdown

The behaviour of the eigenvalues of the operators forming the SVS-EFIE-M at significant value of n can be shown to be, as follows:

$$\Lambda^{(1)}_n = \Lambda^{S,S}_{1,m\epsilon,n} + \Lambda^{S,V}_{1,e0,n} \hat{\Gamma}^{-1}_{2,n} \Lambda^{V,S}_{1,m\epsilon,n} \sim O(n^0), \quad (4.64)$$

$$\Lambda^{(2)}_n = \Lambda^{S,S}_{2,m\epsilon,n} + \Lambda^{S,V}_{2,e0,n} \hat{\Gamma}^{-1}_{1,n} \Lambda^{V,S}_{2,m\epsilon,n} \sim O(n^0). \quad (4.65)$$

That is, the eigenvalues $\Lambda^{(1)}_n$ and $\Lambda^{(2)}_n$ of the Galerkin MoM impedance matrix tend to constants. This will be also numerically demonstrated in Fig. 4.11 in Section VII. Hence, the condition number upon the increased order of discretization n remains constant. This means that the proposed formulation does not suffer from oversampling breakdown. This is a result of Galerkin MoM solution of the SVS-EFIE-M sought in $L^2(S)$ space by analogy with the solution of the S-MFIE [60] as both SVS-EFIE-M and S-MFIE feature the magnetic field surface operator.

4.5.4 Absence of low frequency breakdown

Unlike the earlier J-formulation of SVS-EFIE, its proposed M-formulation does not suffer from the low frequency breakdown either. At low frequencies, eigenvalues can be shown to behave as

$$\Lambda_n^{(1)} \sim \omega^0, \quad \Lambda_n^{(2)} \sim \omega^0, \tag{4.66}$$

as also shown numerically in Fig. 4.10. As a result, SVS-EFIE-M is free from low frequency breakdown formulation.

Overall, the SVS-EFIE-M formulation is inherently immune to the low frequency and oversampling breakdowns[1] unlike its SVS-EFIE-J predecessor due to its surface-to-surface operator being in the desired form of sum of a constant operator and a compact operator and its MoM discretization being performed in the $L^{(2)}(S)$ functional space.

4.5.5 Internal resonances breakdown

At certain discrete frequencies $\omega = \omega_n^{(1)}$ when

$$\Lambda_{1,m\epsilon,n}^{S,S} = -\Lambda_{1,e0,n}^{S,V} \hat{\Gamma}_{2,n}^{-1} \Lambda_{1,m\epsilon,n}^{V,S}, \tag{4.67}$$

[1]For simply connected smooth objects

nth eigenvalue $\Lambda_n^{(1)}$ becomes zero. Similarly, nth eigenvalue $\Lambda_n^{(2)}$ becomes zero at frequencies $\omega = \omega_n^{(2)}$, when

$$\Lambda^{S,S}_{2,m\epsilon,n} = -\Lambda^{S,V}_{2,e0,n}\hat{\Gamma}^{-1}_{1,n}\Lambda^{V,S}_{2,m\epsilon,n}. \tag{4.68}$$

Frequencies $\omega_n^{(1)}$ and $\omega_n^{(2)}$ are not equal to each other. At each such frequency $\omega_n^{(1)}$ or $\omega_n^{(2)}$, solution of the SVS-EFIE-M (4.4) loses its uniqueness and experiences the internal resonance breakdown similarly with the SVS-EFIE-J (3.4) formulation. Notice, these resonance frequencies $\omega_n^{(1)}$ and $\omega_n^{(2)}$ do not coincide with the resonant frequencies of the surface-to-surface operator eigenvalues $\Lambda^{S,S}_{1,m\epsilon,n}$ or $\Lambda^{S,S}_{2,m\epsilon,n}$.

Neither SVS-EFIE-J nor SVS-EFIE-M formulation eliminate spurious resonances as tangential components of electric field vanishes at the surface of the sphere due to the boundary conditions. Solution of those two formulations result unknown electric current $\boldsymbol{J}$ and magnetic current M at the boundary manifesting PEC and PMC like sphere. In both formulations tangential component of the electric field exists on the right-hand-side which produces the same nth resonance frequencies of the cavity at which those eigenvalues become zero. Hence, this current version of the SVS-EFIE formulations do not guarantee for the elimination of the spurious resonances even though we make linear combination of those two formulations. Exploring possibilities for elimination of these spurious resonances through the combination of different SVS-EFIE formulations will be a subject of future work.

4.6 Evaluation of Electric Field Inside the Sphere

Having the solution for the unknown coefficients b_{nm} and c_{nm} in the MoM expansion for the fictitious current $\hat{\boldsymbol{n}}\times\boldsymbol{J}$ on the boundary S the electric field $\boldsymbol{E}$ in the scatterer volume V can be readily obtained from the single-source representation (4.2) in case of $\mathtt{a} = 0$ and $\mathtt{b} = 1$, i.e.

$$\boldsymbol{E}(\mathbf{r}) = \int_S \bar{\bar{\boldsymbol{G}}}_{m\epsilon}(\boldsymbol{r}, \boldsymbol{r'}) \cdot \hat{\boldsymbol{n}}' \times \boldsymbol{J}(\boldsymbol{r'})ds', \quad \boldsymbol{r} \in V. \tag{4.69}$$

Substituting the expression (4.13) for $\bar{\bar{\boldsymbol{G}}}_{m\epsilon}$ into (4.69) we have

$$\begin{aligned}\boldsymbol{E}(\boldsymbol{r}) = -ik_\epsilon^2 \sum_{n,m} d_{nm} \Bigg(\boldsymbol{p}_{nm}^{(1\epsilon)}(\boldsymbol{r}) \int_S \boldsymbol{q}_{n,-m}^{(2\epsilon)}(\boldsymbol{r'}) \cdot \hat{\boldsymbol{n}}' \times \\ \boldsymbol{J}(\boldsymbol{r'})ds' + \boldsymbol{q}_{nm}^{(1\epsilon)}(\boldsymbol{r}) \int_S \boldsymbol{p}_{n,-m}^{(2\epsilon)}(\boldsymbol{r'}) \cdot \hat{\boldsymbol{n}}' \times \boldsymbol{J}(\boldsymbol{r'})ds' \Bigg), \\ \boldsymbol{r} \in V.\end{aligned} \tag{4.70}$$

Using the expansion for current $\hat{\boldsymbol{n}} \times \boldsymbol{J}$ (4.11) in the above field definition produces the following expression for the field inside the sphere

$$\begin{aligned}\boldsymbol{E}(\boldsymbol{r}) = -ik_\epsilon^2 \sum_{n,m} d_{nm} \Big(\boldsymbol{p}_{nm}^{(1\epsilon)}(\boldsymbol{r}) \sum_{n'',m''} b_{n''m''} \\ \int_S \boldsymbol{q}_{n,-m}^{(2\epsilon)}(\boldsymbol{r'}) \cdot \hat{\boldsymbol{n}}' \times \boldsymbol{u}_{n''m''}^{(1)}(\boldsymbol{r'})ds' + \boldsymbol{p}_{nm}^{(1\epsilon)}(\boldsymbol{r}) \sum_{n'',m''} c_{n''m''} \\ \int_S \boldsymbol{q}_{n,-m}^{(2\epsilon)}(\boldsymbol{r'}) \cdot \hat{\boldsymbol{n}}' \times \boldsymbol{u}_{n''m''}^{(2)}(\boldsymbol{r'})ds' + \boldsymbol{q}_{nm}^{(1\epsilon)}(\boldsymbol{r}) \sum_{n'',m''} b_{n''m''} \\ \int_S \boldsymbol{p}_{n,-m}^{(2\epsilon)}(\boldsymbol{r'}) \cdot \hat{\boldsymbol{n}}' \times \boldsymbol{u}_{n''m''}^{(1)}(\boldsymbol{r'})ds' + \boldsymbol{q}_{nm}^{(1\epsilon)}(\boldsymbol{r}) \sum_{n'',m''} c_{n''m''} \\ \int_S \boldsymbol{p}_{n,-m}^{(2\epsilon)}(\boldsymbol{r'}) \cdot \hat{\boldsymbol{n}}' \times \boldsymbol{u}_{n''m''}^{(2)}(\boldsymbol{r'})ds' \Big).\end{aligned} \tag{4.71}$$

Orthogonality relations (75) and (72) in [60] zero out first and fourth terms in (4.71), yielding

$$\boldsymbol{E}(\boldsymbol{r}) = -ik_\epsilon^2 \sum_{n,m} d_{nm} \Big(\boldsymbol{p}_{nm}^{(1\epsilon)}(\boldsymbol{r}) \sum_{n'',m''} c_{n''m''} \int_S \boldsymbol{q}_{n,-m}^{(2\epsilon)}(\boldsymbol{r}') \cdot \hat{\boldsymbol{n}}' \times \boldsymbol{u}_{n''m''}^{(2)}(\boldsymbol{r}') ds' + \boldsymbol{q}_{nm}^{(1\epsilon)}(\boldsymbol{r}) \sum_{n'',m''} b_{n''m''} \int_S \boldsymbol{p}_{n,-m}^{(2\epsilon)}(\boldsymbol{r}') \cdot \hat{\boldsymbol{n}}' \times \boldsymbol{u}_{n''m''}^{(1)}(\boldsymbol{r}') ds' \Big), \quad (4.72)$$

which leads to the following expression for the field inside (see (73)-(74) in [60], with mistake in (73) of [60] fixed)

$$\boldsymbol{E}(\boldsymbol{r}) = -ik_\epsilon^2 \sum_{n,m} d_{nm} \Big(\boldsymbol{p}_{nm}^{(1\epsilon)}(\boldsymbol{r}) \sum_{n'',m''} c_{n''m''} \frac{-1}{k_\epsilon} [k_\epsilon a h_n^{(2)}(k_\epsilon a)]' \delta_{nn''} \delta_{mm''} d_{nm}^{-1} d_{n''m''}^{1/2} + \boldsymbol{q}_{nm}^{(1\epsilon)}(\boldsymbol{r}) \sum_{n'',m''} b_{n''m''} (-a h_n^{(2)}(k_\epsilon a)) \delta_{nn''} \delta_{mm''} d_{nm}^{-1} d_{n''m''}^{1/2} \Big). \quad (4.73)$$

4.6.1 Electric field inside sphere due to radial electric dipole

In case of the radial electric dipole excitation coefficients c_{nm} in (4.73) are zero (since $E_{1,nm} = 0$ in (4.47) per (93) in [35]) and only terms containing b_{nm} with $m = 0$ are non-zero. This gives the following expression for the field

$$\boldsymbol{E}(\boldsymbol{r}) = -ik_\epsilon^2 \sum_{n=1}^{\infty} d_{n0}^{1/2} \Big(b_{n0} \boldsymbol{q}_{n0}^{(1\epsilon)}(\boldsymbol{r}) [-a h_n^{(2)}(k_\epsilon a)] \Big). \quad (4.74)$$

Using definitions of the function $\boldsymbol{q}$ in (22) of [35] (see it also in [61]) we get components of the field inside the sphere

$$E_r = -ik_\epsilon^2 \sum_{n=1}^{\infty} d_{n0}^{1/2} b_{n0} \frac{n(n+1)}{k_\epsilon r} j_n(k_\epsilon r) P_n(\cos\theta)\ [-ah_n^{(2)}(k_\epsilon a)], \tag{4.75}$$

$$E_\theta = -ik_\epsilon^2 \sum_{n=1}^{\infty} d_{n0}^{1/2} b_{n0} \frac{1}{k_\epsilon r} [k_\epsilon r j_n(k_\epsilon r)]' \frac{d}{d\theta} P_n(\cos\theta) [-ah_n^{(2)}(k_\epsilon a)], \tag{4.76}$$

$$E_\phi = 0. \tag{4.77}$$

4.6.2 Electric field inside sphere due to tangential electric dipole

In the case of sphere excited by the tangential dipole situated above it, both coefficients b_{nm} and c_{nm} in (4.73) are non-zero. This gives the following expressions for the components of the field inside the sphere after using the expansion over functions $\boldsymbol{p}$ and $\boldsymbol{q}$ in (21)-(22) of [35] (see also [61]) and the fact that only $|m| = 1$ terms survive per (100) and (102) in [35]

$$E_r = -ik_\epsilon^2 \sum_{n=1}^{\infty} \sum_{m=-1,1} d_{nm}^{1/2} b_{nm} \left(\frac{n(n+1)}{k_\epsilon r} j_n(k_\epsilon r) P_n^{|m|}(\cos\theta) e^{im\phi} \right) [-ah_n^{(2)}(k_\epsilon a)], \tag{4.78}$$

$$\begin{aligned} E_\theta = -ik_\epsilon^2 \sum_{n=1}^{\infty} \sum_{m=-1,1} d_{nm}^{1/2} \Big[b_{nm} \left(\frac{1}{k_\epsilon r} [k_\epsilon r j_n(k_\epsilon r)]' \frac{d}{d\theta} P_n^{|m|}(\cos\theta) e^{im\phi} \right) [-ah_n^{(2)}(k_\epsilon a)] \\ + c_{nm} \left(\frac{im}{\sin\theta} P_n^{|m|}(\cos\theta) j_n(k_\epsilon r) e^{im\phi} \right) \left(\frac{-1}{k_\epsilon} [(k_\epsilon a) h_n^{(2)}(k_\epsilon a)]' \right) \Big], \end{aligned} \tag{4.79}$$

$$E_\phi = -ik_\epsilon^2 \sum_{n=1}^{\infty} \sum_{m=-1,1} d_{nm}^{1/2} \Big[b_{nm} \left(\frac{im}{k_\epsilon r \sin\theta} [k_\epsilon r j_n(k_\epsilon r)]' P_n^{|m|}(\cos\theta) e^{im\phi} \right) \left(-a h_n^{(2)}(k_\epsilon a) \right)$$
$$+ c_{nm} \left(-\frac{d}{d\theta} P_n^{|m|}(\cos\theta) j_n(k_\epsilon r) e^{im\phi} \right) \left(\frac{-1}{k_\epsilon} [(k_\epsilon a) h_n^{(2)}(k_\epsilon a)]' \right) \Big]. \quad (4.80)$$

4.7 Numerical Results

Validation of the proposed SVS-EFIE-M formulation and its analytical Galerkin MoM solution are presented in this section. The analytically obtained electric field components inside the dielectric sphere due to radiation of an electric dipole are compared against classical Mie series [52]. Various numerical experiments examine the rigorous nature of our novel magnetic current based SVS-EFIE, its spectral properties, as well as the accuracy of its MoM solution.

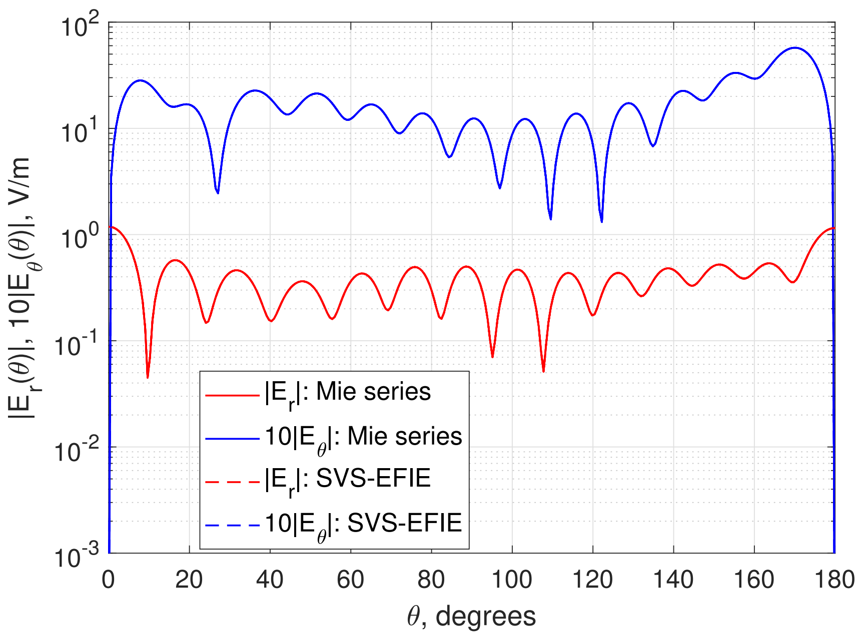

FIGURE 4.1: Electric field components on the surface of the sphere versus angle θ in the case of radial dipole excitation. Mie series results are shown by solid lines and SVS-EFIE-M solution is shown by dashed lines.

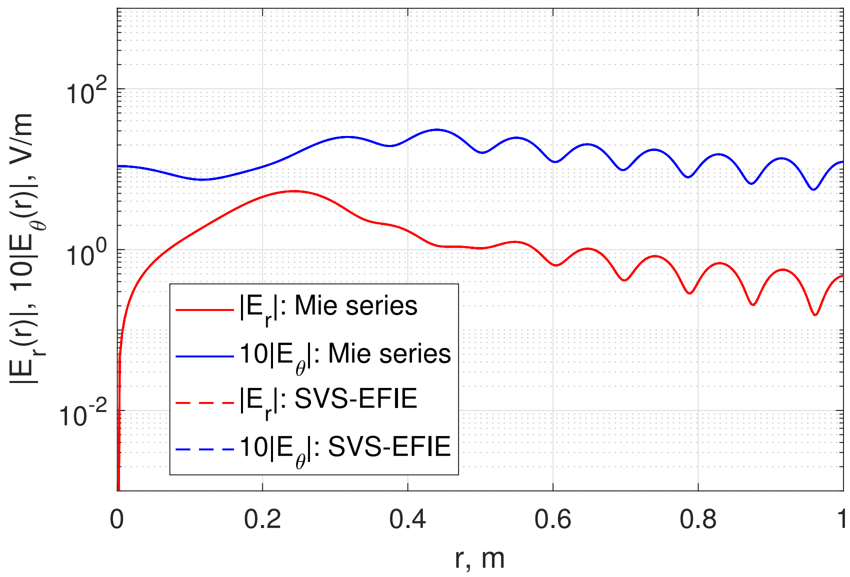

FIGURE 4.2: Electric field components inside the sphere versus radial coordinate r at $\theta = \pi/2$ in the case of radial dipole excitation. Mie series results are shown by solid lines and SVS-EFIE-M solution is shown by dashed lines.

Our first numerical example is a homogeneous dielectric sphere having radius $a = 1$m and relative permittivity $\epsilon = 10$. The sphere is excited by the radial electric dipole situated on the z-axis at location[1] $\boldsymbol{r}_0 = \hat{\boldsymbol{z}}10$m. It has a dipole moment $Il = 1[A \cdot m]$.

The magnitude of E_r and E_θ components of the electric field inside the dielectric sphere are demonstrated on the surface of the sphere as functions of angle θ and of radial coordinate r in Fig. 4.1 and Fig. 4.2, respectively. Only TM_r-waves are excited by the radial dipole. Due to symmetry the field is independent on the azimuthal angle ϕ. In Fig. 4.1 and Fig. 4.2 both the field components evaluated using the Galerkin MoM of the SVS-EFIE-M and those evaluated using Mie series are shown. The solution was evaluated with 50 terms. The frequency of analysis is 599.584916MHz. The maximum and average value of relative error between the

[1] Spherical harmonic representations of the field (4.75), (4.76) become extremely slowly convergent, when observation point comes close to the dipole location. Hence, in this work we take the dipole sufficiently far from the sphere surface to ensure that direct computation of the Mie series harmonics in (4.76) forming the right-hand-side (4.44) are machine precision accurate on the sphere and do not encounter numerical instabilities associated with computation of Bessel functions with indexes greatly exceeding their arguments.

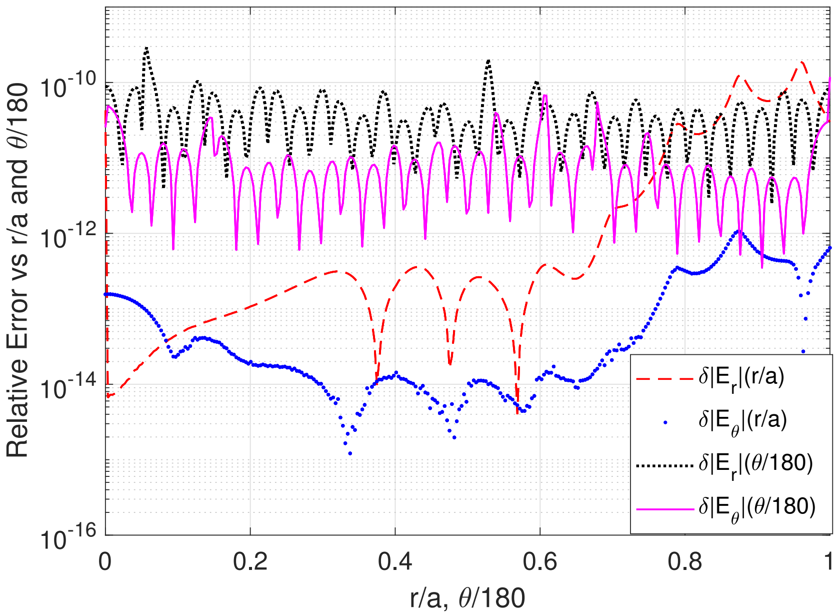

FIGURE 4.3: Relative error δE in the electric field components obtained by SVS-EFIE-M (compared to Mie series) on the surface of the sphere versus normalized angle $\theta/180$ corresponding to the curves in Fig. 4.1 (dashed lines) and relative error in the electric inside the sphere versus radial normalized coordinate r/a at $\theta = \pi/2$ corresponding to the curves in Fig. 4.2 (solid lines).

SVS-EFIE-M and Mie series solutions depicted in Fig. 4.3 with 50 terms each are in the range of 10^{-10} to 10^{-13}, respectively. The standard deviation for the E_r and E_θ components of the electric field was found to be 1.45×10^{-11} and 7.56×10^{-11} [V/m].

Our second numerical example is for the dielectric sphere with relative permittivity of $\epsilon = 10$ and excited with the tangential θ-directed electric dipole. In this case, both the TE_r- and TM_r-waves are produced, all components of electric field are present, and they are functions of all three spherical coordinates. The tangential electric dipole is placed on z-axis at the radial distance $r_0 = 10$m. The frequency of analysis is 599.584916MHz. In Fig. 4.4, the magnitude of E_r, E_θ, and E_ϕ components of the electric field as function of elevation angle θ is shown for both MoM solution of the SVS-EFIE-M and Mie series. In Fig. 4.5, the magnitude of the electric field components is shown as a function of the radial coordinate r for both MoM solution

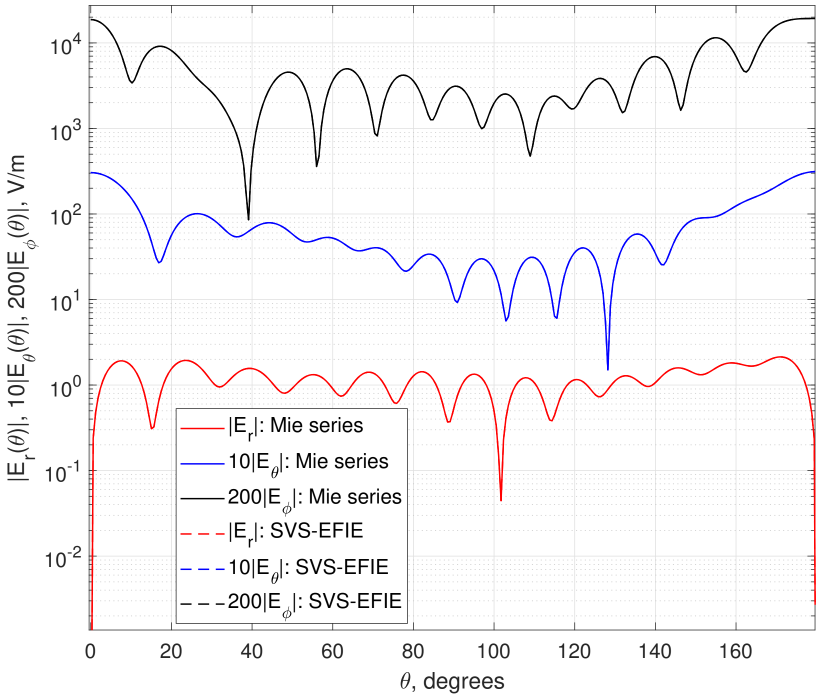

FIGURE 4.4: Electric field components on the surface of the sphere versus angle θ at $\phi = 0.4\pi$ in the case of tangential θ-directed dipole excitation. Mie series results are shown by solid lines and SVS-EFIE-M solution is shown by dashed lines.

of the SVS-EFIE-M and Mie series. The relative error between the analytic MoM solution of the SVS-EFIE-M and Mie series solutions is shown in Fig. 4.6. The maximum and average value of relative error between the SVS-EFIE-M and Mie series solutions evaluated with 50 terms each are in the range of 10^{-12} to 10^{-13}, respectively. The standard deviation for the E_r, E_θ and E_ϕ components of the electric field as functions of angle θ was found to be 6.285×10^{-11}, 5.24×10^{-11} and 1.26×10^{-11} [V/m], respectively.

The expansion of the magnetic current density on the boundary of the dielectric sphere over the spherical basis functions and determined expansion coefficients enable us to calculate the electric field components inside the dielectric sphere. This

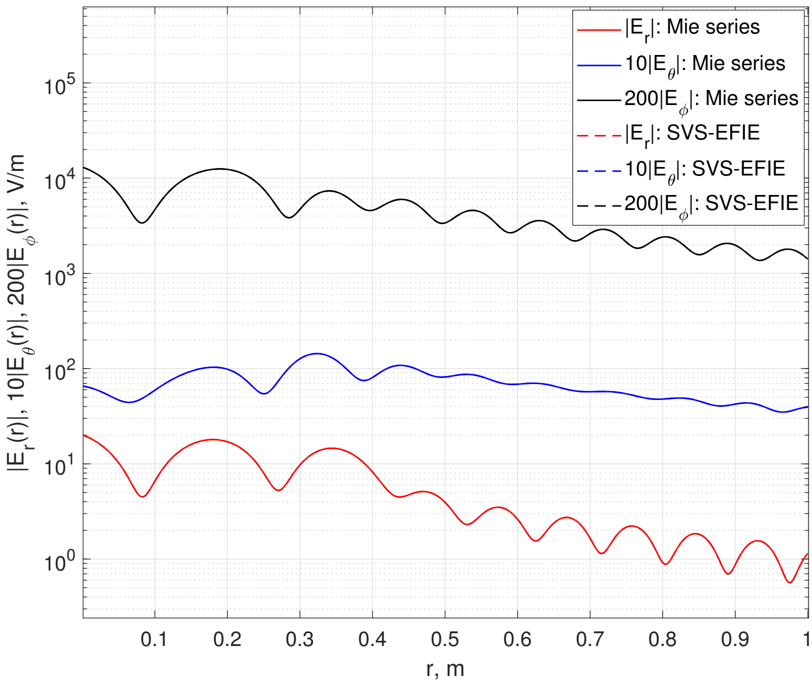

FIGURE 4.5: Electric field components inside the sphere versus radial coordinate r at $\theta = 0.4\pi$ at $\phi = 0.4\pi$ in the case of tangential θ-directed dipole excitation. Mie series results are shown by solid lines and SVS-EFIE-M solution is shown by dashed lines.

magnetic current density components M_θ and M_ϕ shown in Fig. 4.7 are both computed at $\phi = 0.4\pi$ for the case of tangential dipole excitation.

All the computations were performed in MathCAD 15 software with integrals computed numerically to 10^{-10} tolerance. The Legendre polynomials were defined in terms of the integrals and computed to the same 10^{-10} tolerance. This tolerance is seen to be forcing the maximum level of relative error between the analytic Galerkin MoM solution of the SVS-EFIE-M and Mie series in Fig. 4.3 and Fig. 4.6 below 10^{-10} and 10^{-12} levels respectively. The achieved level of relative error between the SVS-EFIE-M solution and Mie series undoubtedly validates both the rigorous nature of the proposed new integral equation formulation and exactness of its MoM solution.

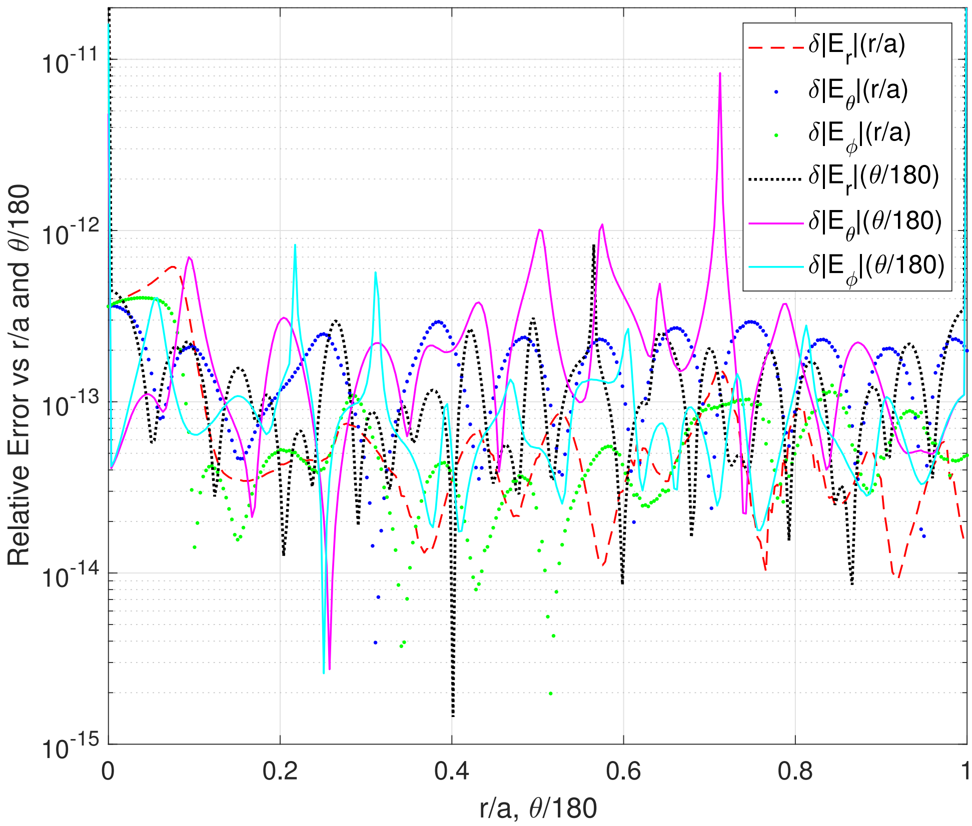

FIGURE 4.6: Relative error δE in the electric field components obtained by SVS-EFIE-M (compared to Mie series) on the surface of the sphere versus normalized angle $\theta/180$ at $\phi = 0.4\pi$ corresponding to the curves in Fig. 4.4 (dashed lines) and relative error in the electric inside the sphere versus radial normalized coordinate r/a at $\theta = 0.4\pi$ at $\phi = 0.4\pi$ corresponding to the curves in Fig. 4.5 (solid lines).

Next, we demonstrate the spectral properties of the SVS-EFIE-M formulation and show that performing MoM operations in the functional space $L^{(2)}(S)$ ensures boundedness in the condition number of the impedance matrix. In Fig. 4.12 and Fig. 4.9, the eigenvalues $\Lambda^{S,S}_{1,m\epsilon,n}$, $\Lambda^{S,S}_{2,m\epsilon,n}$, the products of the eigenvalues $\Lambda^{S,V}_{1,e0,n}\hat{\Gamma}^{-1}_{2,n}\Lambda^{V,S}_{1,m\epsilon,n}$, $\Lambda^{S,V}_{2,e0,n}\hat{\Gamma}^{-1}_{1,n}\Lambda^{V,S}_{2,m\epsilon,n}$ and their sums are shown under condition of the Galerkin MoM testing performed in $L^2(S)$ space. The eigenvalues depicted in Figs. 4.12-4.9 correspond to the solution under the tangential dipole radiation problem in Figs. 4.4-4.5. In order to have sufficient number of sampling points, we consider the solution at 599.584916MHz with 50 terms.

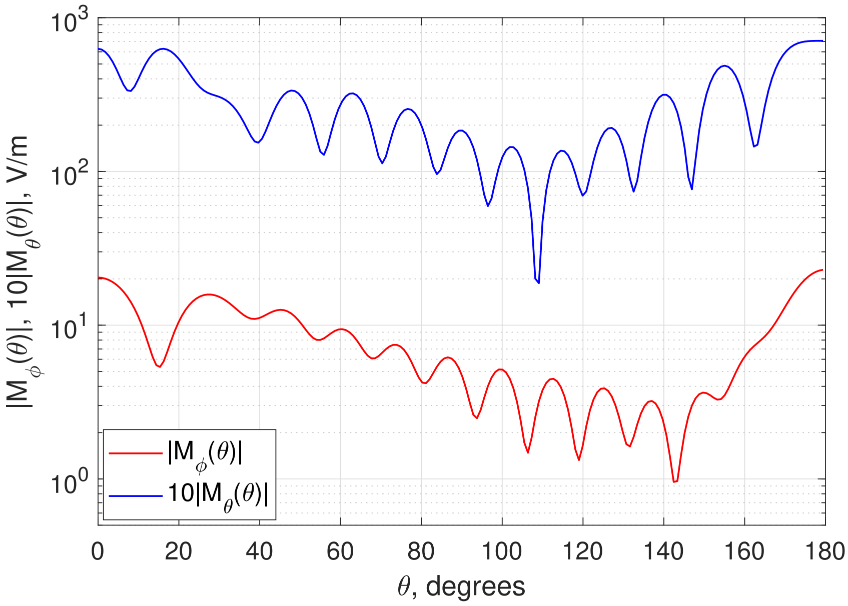

FIGURE 4.7: Absolute values of the magnetic current components computed through the MoM solution (4.14) upon solving for the unknowns on the boundary of the dielectric sphere. Both M_θ and M_ϕ are computed at $\phi = 0.4\pi$.

A representative eigenvalues $\Lambda_n^{(1)}$ and $\Lambda_n^{(2)}$ dependence on frequency is shown in Fig. 4.10 for $n = 2$. One can observe that eigenvalues $\Lambda_2^{(1)}$ and $\Lambda_2^{(2)}$ for SVS-EFIE-J formulation [35] tend to infinity and zero, respectively, as frequency tends to zero. This leads to a low frequency breakdown. The eigenvalue $\Lambda_2^{(1)}$ and $\Lambda_2^{(2)}$ in the proposed SVS-EFIE-M formulation remain constant at low frequencies and produce no such breakdown.

Behaviour of the eigenvalues $\Lambda_n^{(1)}$ and $\Lambda_n^{(2)}$ are also shown in Fig. 4.11 for increasing discretization order. One can observe that eigenvalues $\Lambda_n^{(1)}$ for SVS-EFIE-J formulation increases with the increasing discretization order while its eigenvalues $\Lambda_n^{(2)}$ decrease. Hence, SVS-EFIE-J formulation suffers from oversampling breakdown. In the proposed SVS-EFIE-M formulation, however, $\Lambda_n^{(1)}$ and $\Lambda_n^{(2)}$ tend to constants as the discretization order tends to infinity and, therefore, the formulation is free of the oversampling breakdown.

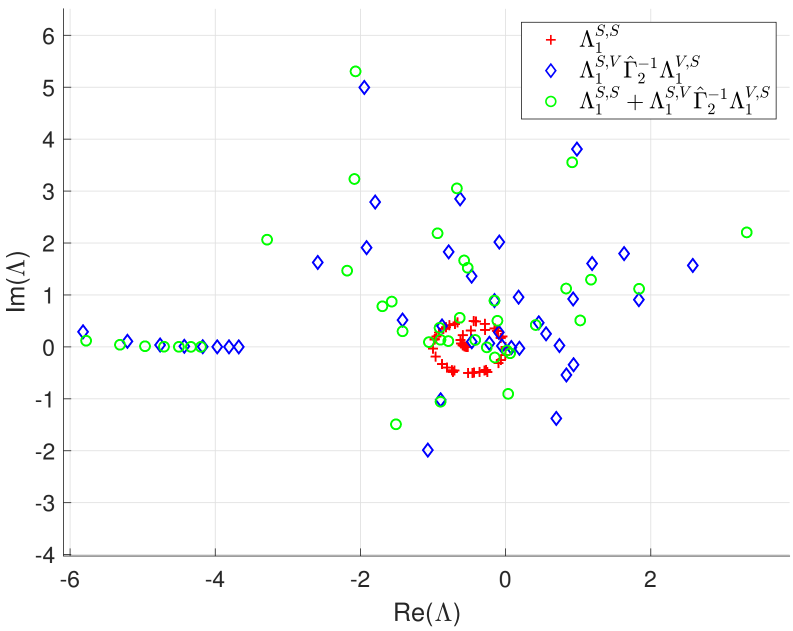

FIGURE 4.8: Eigenvalues $\Lambda^{S,S}_{1,m\epsilon,n}$ of the surface-to-surface operator, the product of eigenvalues $\Lambda^{S,V}_{1,e0,n}\hat{\Gamma}^{-1}_{2,n}\Lambda^{V,S}_{1,m\epsilon,n}$ corresponding to the product of the surface-to-volume and volume-to-surface operators and eigenvalues for the total SVS-EFIE-M operator $\Lambda^{(1)}_n = \Lambda^{S,S}_{1,m\epsilon,n} + \Lambda^{S,V}_{1e0,n}\hat{\Gamma}^{-1}_{1,n}\Lambda^{V,S}_{1,m\epsilon,n}$. One can observe the accumulation of those eigenvalues $\Lambda^{S,S}_{1,m\epsilon,n}$, $\Lambda^{S,V}_{1,e0,n}\hat{\Gamma}^{-1}_{2,n}\Lambda^{V,S}_{1,m\epsilon,n}$ and $\Lambda^{(1)}_n$ at constant values. We can also notice the behavior of the eigenvalues of surface-to-surface operator $\Lambda^{S,S}_{1,m\epsilon,n}$ encompassing a unit circle with centre at a constant of -1/2, which occurs due to their $-(1/2+\lambda_n)$ form stemming from the 'constant+compact' operator composition [60].

4.8 Conclusions

New Surface-Volume-Surface Electric Field Integral Equation of magnetic type (SVS-EFIE-M) is presented. Exact solutions of this SVS-EFIE-M with Galerkin Method of Moments (MoM) for the problems of radial and tangential electric dipole radiation in the presence of the homogeneous dielectric sphere are compared against the Mie series. The expansion of the unknown fictitious magnetic current in the single source SVS-EFIE-M is performed over the eigenfunctions of its integral operators. Spectral analysis of the integral operators forming the SVS-EFIE-M is also

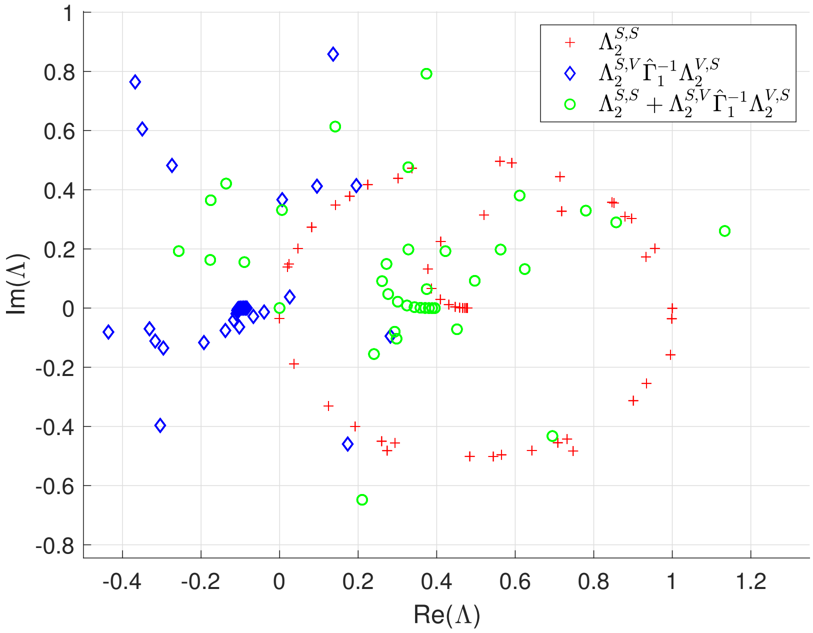

FIGURE 4.9: Eigenvalues $\Lambda^{S,S}_{2,m\epsilon,n}$ of the surface-to-surface operator, the product of eigenvalues $\Lambda^{S,V}_{2,e0,n}\hat{\Gamma}^{-1}_{1,n}\Lambda^{V,S}_{2,m\epsilon,n}$ corresponding to the product of the surface-to-volume and volume-to-surface operators, and eigenvalues $\Lambda^{(2)}_n = \Lambda^{S,S}_{2,m\epsilon,n} + \Lambda^{S,V}_{2e0,n}\hat{\Gamma}^{-1}_{1,n}\Lambda^{V,S}_{2,m\epsilon,n}$ for the total SVS-EFIE-M operator. One can observe the accumulation at constant values for all three sets of eigenvalues: $\Lambda^{S,S}_{2,m\epsilon,n}$, $\Lambda^{S,V}_{2,e0,n}\hat{\Gamma}^{-1}_{1,n}\Lambda^{V,S}_{2,m\epsilon,n}$ and $\Lambda^{(2)}_n$. We can also notice the behavior of the eigenvalues of surface-to-surface operator encompassing a unit circle centered at accumulation point of 1/2 due to the 'constant plus compact' operator structure resulting in $\Lambda^{S,S}_{2,m\epsilon,n} = 1/2 - \lambda_n$ [60].

conducted. The Galerkin testing of the SVS-EFIE-M is performed in $L^2(S)$ functional space and spectral properties of the resultant MoM impedance matrix are analyzed. It is shown that in order for the MoM impedance matrix condition number to remain bounded under condition of the increasing discretization order n or at low frequencies, the SVS-EFIE-M solution can be performed in conventional $L^2(S)$ space, which is easy to handle numerically. The MoM solution of the SVS-EFIE-M in $L^2(S)$ space produces an impedance matrix with condition number which remains constant under conditions of either oversampling or low frequency analysis making it an excellent candidate for solution of practical scattering and radiation problems.

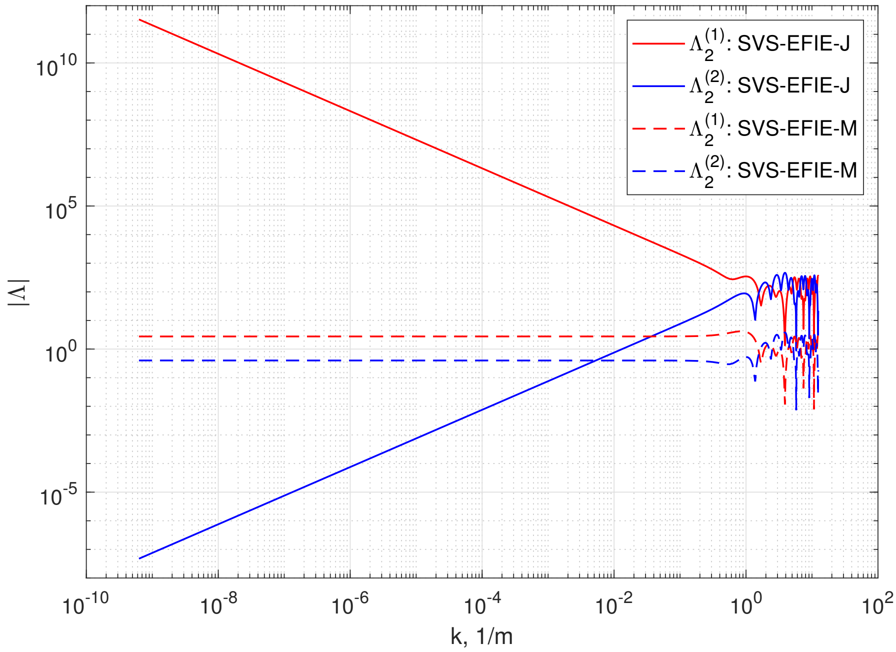

FIGURE 4.10: Eigenvalues $\Lambda_2^{(1)}$ and $\Lambda_2^{(2)}$ in a broad range of frequencies. Solid lines for the SVS-EFIE-J formulation and dashed lines corresponding to SVS-EFIE-M formulation. One can observe that eigenvalues $\Lambda_2^{(1)}$ in J-formulation tend to infinity while eigenvalues $\Lambda_2^{(2)}$ in J-formulation tend to zero, thus, causing the low frequency breakdown. The M-formulation features both sets of eigenvalues $\Lambda_2^{(1)}$ and $\Lambda_2^{(2)}$, which are constant as frequency tends to zero making formulation stable down to DC for simply connected smooth objects.

4.9 Appendix I: Eigenvalues of SVS-EFIE-M Operators

In this Appendix we demonstrate the following eigenvalue relations for the SVS-EFIE-M operator $\mathcal{T}_{SVS}$

$$\mathcal{T}_{SVS} \circ (\nabla^t Y_n^m) = -\Lambda_n^{(2)} (\nabla^t Y_n^m), \tag{4.81}$$

and

$$\mathcal{T}_{SVS} \circ (\hat{\boldsymbol{r}} \times \nabla^t Y_n^m) = \Lambda_n^{(1)} (\hat{\boldsymbol{r}} \times \nabla^t Y_n^m), \tag{4.82}$$

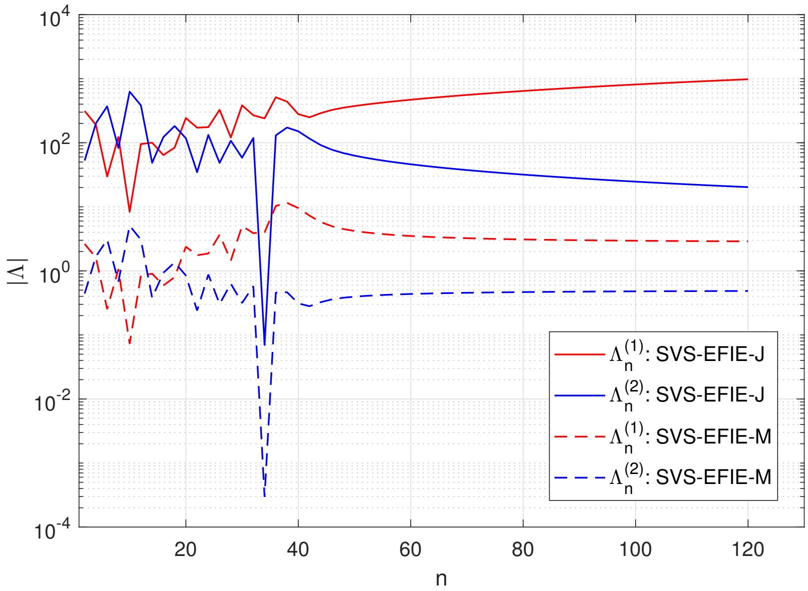

FIGURE 4.11: Eigenvalues $\Lambda_n^{(1)}$ and $\Lambda_n^{(2)}$ for discretization orders n from 1 to 120 at a fixed frequency of 599.584916MHz. Solid lines correspond to the SVS-EFIE-J formulation and dashed lines correspond to the proposed SVS-EFIE-M formulation. One can observe that eigenvalues $\Lambda_n^{(1)}$ for SVS-EFIE-J formulation increase with increasing discretization order n while its eigenvalues $\Lambda_n^{(2)}$ decrease. Such spectral behavior may lead to oversampling breakdown of SVS-EFIE-J formulation in practical discretizations. The proposed SVS-EFIE-M formulation has eigenvalues $\Lambda_n^{(1)}$ and $\Lambda_n^{(2)}$, which remain constant with increased discretization order n and do not cause growth of the MoM matrix condition number upon increased discretization order.

where

$$\mathcal{T}_{SVS} \circ \nabla^t Y_n^m = \mathcal{T}_{m\epsilon}^{S,S} \circ \nabla^t Y_n^m - \mathcal{T}_{e0}^{S,V} \circ \mathcal{T}_{m\epsilon}^{V,S} \circ \nabla^t Y_n^m. \tag{4.83}$$

We start with the surface-surface operator

$$\mathcal{T}_{m\epsilon}^{S,S} \circ \nabla^t Y_n^m = \hat{\boldsymbol{n}} \times \int_S \bar{\bar{\boldsymbol{G}}}_{m\epsilon}(\boldsymbol{r}, \boldsymbol{r}'') \cdot \nabla^t Y_n^m(\boldsymbol{r}'') ds'', \boldsymbol{r} \in S. \tag{4.84}$$

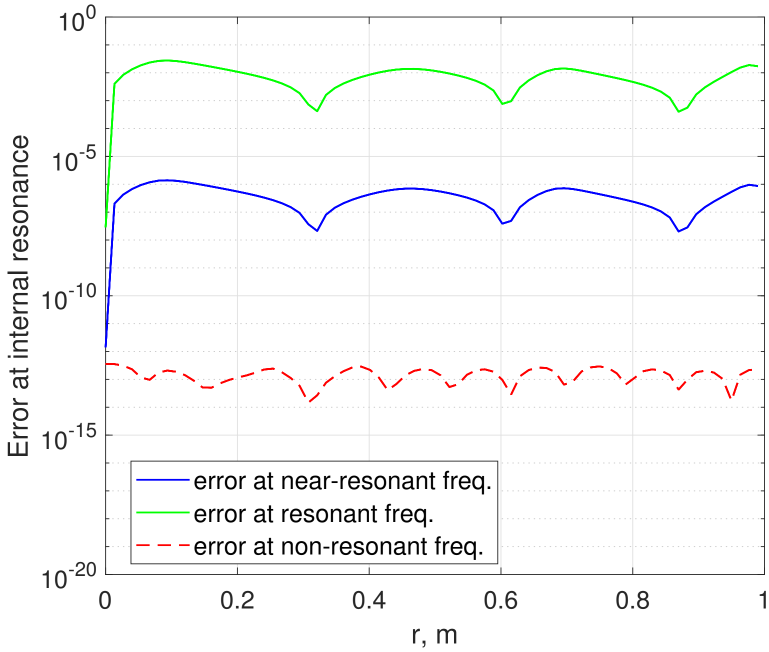

FIGURE 4.12: Eigenvalues $\Lambda_n^{(1)}$ and $\Lambda_n^{(2)}$ for the range of discretization order. Solid lines dictate SVS-EFIE-J formulations and dashed lines corresponding to SVS-EFIE-M formulations. One can observe that eigenvalues $\Lambda_n^{(1)}$ for SVS-EFIE-J formulation increases with the increasing of the discretization order hence suffer from oversampling breakdown whereas, $\Lambda_n^{(1)}$ is almost constant after certain range of the discretization order.

Recalling (4.13) and substituting it here for $|\boldsymbol{r}| < |\boldsymbol{r}''|$ we get

$$\begin{aligned}\mathcal{T}_{m\epsilon}^{S,S} \circ \nabla^t Y_n^m = \; & (-ik_\epsilon^2) \sum_{n'',m''} d_{n''m''} \Big(\hat{\boldsymbol{n}}\times \\ & \boldsymbol{p}_{n''m''}^{(1\epsilon)}(\boldsymbol{r}) \int_S \boldsymbol{q}_{n'',-m''}^{(2\epsilon)}(\boldsymbol{r}'') \cdot \nabla^t Y_n^m(\hat{\boldsymbol{r}}'') ds'' + \\ & \hat{\boldsymbol{n}} \times \boldsymbol{q}_{n''m''}^{(1\epsilon)}(\boldsymbol{r}) \int_S \boldsymbol{p}_{n'',-m''}^{(2\epsilon)}(\boldsymbol{r}'') \cdot \nabla^t Y_n^m(\hat{\boldsymbol{r}}'') ds'' \Big) . \end{aligned} \tag{4.85}$$

By virtue of (72), (74) and (76) in [60], we obtain

$$\begin{aligned}\mathcal{T}^{S,S}_{m\epsilon}\circ\nabla^t Y^m_n = \ & (-ik^2_\epsilon)\sum_{n'',m''} d_{n''m''}\,(\hat{\boldsymbol{n}}\times \\ & \boldsymbol{p}^{(1\epsilon)}_{n''m''}(\boldsymbol{r})\int_S \boldsymbol{q}^{(2\epsilon)}_{n'',-m''}(\boldsymbol{r}'')\cdot\nabla^t Y^m_n(\hat{\boldsymbol{r}}'')ds''\Big) \\ & = -ik^2_\epsilon\sum_{n'',m''} d_{n''m''}\left(aj_{n''}(k_\epsilon a)\nabla^t Y^m_n(\hat{\boldsymbol{r}})\right. \\ & \left. d^{-1}_{n''m''}\frac{1}{k_\epsilon}[k_\epsilon a h^{(2)}_{n''}(k_\epsilon a)]'\delta_{nn''}\delta_{mm''}\right) \\ & = -ik_\epsilon\left(aj_n(k_\epsilon a)[k_\epsilon a h^{(2)}_n(k_\epsilon a)]'\right)\nabla^t Y^m_n(\hat{\boldsymbol{r}}). \end{aligned}\tag{4.86}$$

Recalling (4.49), it follows from the above that

$$\mathcal{T}^{S,S}_{m\epsilon}\circ\nabla^t Y^m_n = -\Lambda^{S,S}_{2,m\epsilon,n}\nabla^t Y^m_n = -\left(\frac{1}{2}-\lambda_n\right)\nabla^t Y^m_n. \tag{4.87}$$

Similarly, recalling (4.84),

$$\mathcal{T}^{S,S}_{m\epsilon}\circ(\hat{\boldsymbol{r}}\times\nabla^t Y^m_n) = \Lambda^{S,S}_{1,m\epsilon,n}(\hat{\boldsymbol{r}}\times\nabla^t Y^m_n) = -\left(\frac{1}{2}+\lambda_n\right)(\hat{\boldsymbol{r}}\times\nabla^t Y^m_n), \tag{4.88}$$

where

$$\lambda_n = -\frac{ik_\epsilon a}{2}h^{(2)}_n(k_\epsilon a)[[k_\epsilon a j_n(k_\epsilon a)]' + j_n(k_\epsilon a)[k_\epsilon a h^{(2)}_n(k_\epsilon a)]'] \tag{4.89}$$

which is called compact factor. The relationships among λ_n and $1/2\pm\lambda_n$ can be found by using the Wronskian relation for Riccati-Bessel functions [(80)-(82) in [60]] and [62].

Next, we consider the surface-volume-surface operator in (4.83). Using definition of integral operators (4.8), (4.9) we have

$$
\begin{aligned}
\mathcal{T}_{e0}^{S,V} \circ \mathcal{T}_{m\epsilon}^{V,S} \circ \nabla^t Y_n^m = k_0^2(\epsilon - 1) \\
- ik_0 \sum_{n'',m''} d_{n''m''} \quad \hat{\boldsymbol{n}} \times \int_V dv' \Big(\boldsymbol{q}_{n''m''}^{(20)}(\boldsymbol{r}) \boldsymbol{q}_{n'',-m''}^{(10)}(\boldsymbol{r'}) + \boldsymbol{p}_{n''m''}^{(20)}(\boldsymbol{r}) \\
\boldsymbol{p}_{n'',-m''}^{(10)}(\boldsymbol{r'}) \Big) \cdot (-ik_\epsilon^2) \sum_{n',m'} d_{n'm'} \int_S \Big(\boldsymbol{p}_{n'm'}^{(1\epsilon)}(\boldsymbol{r'}) \boldsymbol{q}_{n',-m'}^{(2\epsilon)}(\boldsymbol{r''}) \\
+ \boldsymbol{q}_{n'm'}^{(1\epsilon)}(\boldsymbol{r'}) \boldsymbol{p}_{n',-m'}^{(2\epsilon)}(\boldsymbol{r''}) \Big) \cdot \nabla^t Y_n^m(\hat{\boldsymbol{r}}'') ds'' \\
= k_0^2(\epsilon - 1) ik_0 \sum_{n'',m''} d_{n''m''} ik_\epsilon^2 \sum_{n',m'} d_{n'm'} \Big(\hat{\boldsymbol{n}} \times \boldsymbol{q}_{n''m''}^{(20)}(\boldsymbol{r}) \\
\int_V \boldsymbol{q}_{n'',-m''}^{(10)}(\boldsymbol{r'}) \cdot \boldsymbol{p}_{n'm'}^{(1\epsilon)}(\boldsymbol{r'}) dv' \int_S \boldsymbol{q}_{n',-m'}^{(2\epsilon)}(\boldsymbol{r''}) \cdot \nabla^t Y_n^m(\hat{\boldsymbol{r}}'') ds'' + \\
\hat{\boldsymbol{n}} \times \boldsymbol{p}_{n''m''}^{(20)}(\boldsymbol{r}) \int_V \boldsymbol{p}_{n'',-m''}^{(10)}(\boldsymbol{r'}) \cdot \boldsymbol{q}_{n'm'}^{(1\epsilon)}(\boldsymbol{r'}) dv' \\
\int_S \boldsymbol{p}_{n',-m'}^{(2\epsilon)}(\boldsymbol{r''}) \cdot \nabla^t Y_n^m(\hat{\boldsymbol{r}}'') ds'' + \\
\hat{\boldsymbol{n}} \times \boldsymbol{q}_{n''m''}^{(20)}(\boldsymbol{r}) \int_V \boldsymbol{q}_{n'',-m''}^{(10)}(\boldsymbol{r'}) \cdot \boldsymbol{q}_{n'm'}^{(1\epsilon)}(\boldsymbol{r'}) dv' \\
\int_S \boldsymbol{p}_{n',-m'}^{(2\epsilon)}(\boldsymbol{r''}) \cdot \nabla^t Y_n^m(\hat{\boldsymbol{r}}'') ds'' + \\
\hat{\boldsymbol{n}} \times \boldsymbol{p}_{n''m''}^{(20)}(\boldsymbol{r}) \int_V \boldsymbol{p}_{n'',-m''}^{(10)}(\boldsymbol{r'}) \cdot \boldsymbol{p}_{n'm'}^{(1\epsilon)}(\boldsymbol{r'}) dv' \\
\int_S \boldsymbol{q}_{n',-m'}^{(2\epsilon)}(\boldsymbol{r''}) \cdot \nabla^t Y_n^m(\hat{\boldsymbol{r}}'') ds'' \Big). \quad (4.90)
\end{aligned}
$$

After using [60], we can simplify the above to

$$
\begin{aligned}
\mathcal{T}_{e0}^{S,V} \circ \mathcal{T}_{m\epsilon}^{V,S} \circ \nabla^t Y_n^m = k_0^2(\epsilon - 1)(ik_0) \sum_{n'',m''} d_{n''m''} ik_\epsilon^2 \\
\sum_{n',m'} d_{n'm'} \hat{\boldsymbol{n}} \times \boldsymbol{p}_{n''m''}^{(20)}(\boldsymbol{r}) \int_V \boldsymbol{p}_{n'',-m''}^{(10)}(\boldsymbol{r'}) \cdot \boldsymbol{p}_{n'm'}^{(1\epsilon)}(\boldsymbol{r'}) dv' \\
\int_S \boldsymbol{q}_{n',-m'}^{(2\epsilon)}(\boldsymbol{r''}) \cdot \nabla^t Y_n^m(\hat{\boldsymbol{r}}'') ds''. \quad (4.91)
\end{aligned}
$$

With reference to (113) in [35] [see Appendix I], the above equation can be reorganized, as follows:

$$\begin{aligned}\mathcal{T}_{e0}^{S,V} \circ \mathcal{T}_{m\epsilon}^{V,S} \circ \nabla^t Y_n^m = k_0^2(\epsilon - 1)(ik_0)(ik_\epsilon)ah_n^{(2)}(k_0 a)\\ \int_0^a j_n(k_0 r)j_n(k_\epsilon r)r^2 dr[k_\epsilon a h_n^{(2)}(k_\epsilon a)]' \nabla^t Y_n^m(\hat{\boldsymbol{r}})\\ = \Lambda_{2,e0,n}^{S,V} \hat{\Gamma}_{1,n}^{-1} \Lambda_{2,m\epsilon,n}^{V,S} \nabla^t Y_n^m. \quad (4.92)\end{aligned}$$

Derived relation (4.92) is stated in abbreviated form as eigenvalue relation (4.57). Eigenvalue relation (4.60) can be proven in a similar manner.

Chapter 5

Conclusions and Future Work

5.1 Conclusions

This research presents exact solution of the Surface-Volume-Surface Electric Field Integral Equations (SVS-EFIE) with Galerkin Method of Moments (MoM) for the problem of the radial or tangential electric dipole radiating in the vicinity of a homogeneous non-magnetic dielectric sphere. The solution is obtained by utilizing rotational and irrotational complete sets of orthogonal vector spherical harmonics as basis and test functions according to the Helmholtz decomposition. In this work, we studied the electric current based Surface-Volume-Surface Electric Field Integral Equation (SVS-EFIE-J) and the novel magnetic current based Surface-Volume-Surface Electric Field Integral Equation (SVS-EFIE-M) for a non-magnetic penetrable scatterer.

In the developed analytic MoM solution the expansion of the unknown fictitious current in the single-source SVS-EFIE is performed over the eigenfunctions of its integral operator. Spectral analysis of the integral operators forming the SVS-EFIE is conducted. The Galerkin testing of the SVS-EFIE-J and SVS-EFIE-M are performed in different functional spaces and spectral properties of the resultant MoM impedance matrices are analyzed. It is shown that in order for the MoM impedance matrix condition number to remain bounded under condition of the increasing discretization order the SVS-EFIE-J must be tested in Sobolev space $H_{div}^{-1/2}(S)$ and SVS-EFIE-M must be tested in $L^2(S)$.

The analytic MoM solution of the SVS-EFIE-J and SVS-EFIE-M are compared against Mie series and are shown to match the latter to 12 significant digits, hence, proving the rigorous nature of the SVS-EFIE formulations and exactness of their MoM solutions. Moreover, both the spectrum of the continuous integral operator of this new magnetic current based SVS-EFIE-M and the spectrum of its MoM matrix remain bounded at low frequencies and upon oversampling. Although the presented analysis shows how performing MoM solution in the proper functional space can eliminate the oversampling breakdown and the low frequency breakdown for a spherical scatterer, it is reasonable to expect that similar spectral behaviour of the SVS-EFIE-J and SVS-EFIE-M operators will take place for the sufficiently smooth simply connected scatterers of arbitrary shape.

The main contribution of the presented analytic MoM solution of the SVS-EFIE-M is in demonstration of its superior spectral properties to the alternative integral equations formulations for dielectric objects such as PMCHWT, Muller, EFIE, MFIE, CFIE, and SVS-EFIE-J. Specifically, it is shown that for smooth simply connected objects SVS-EFIE-M formulation leads to MoM solution with no low-frequency or oversampling breakdowns within easy to handle $L^2(S)$ space inner products. Note that alternative formulations such as PMCHWT, Muller, EFIE, MFIE, CFIE, and SVS-EFIE-J do not possess such desired spectral properties and suffer from the above breakdowns upon discretization.

In case of the MoM solution of the surface EFIE or MFIE on a sphere (PEC or PMC), the surface spherical harmonics taken as both the basis and test functions are the eigenfunctions of the EFIE and MFIE operators on the sphere. They also have desired orthogonality properties (see [45] for details). As a result, Galerkin

MoM casts impedance matrices into the diagonal form. Such MoM formulation also exhibits exponential converge to the solution. Because of this, the Galerkin MoM is the most convenient formulation for solving EFIE, MFIE as well as SVS-EFIE-J and SVS-EFIE-M on a sphere. That is the reason it was the formulation of choice in [60]) and in our work.

The Galerkin RWG MoM solution of the SVS-EFIE-M equation for the practical engineering problems with smooth simply connected dielectric objects is expected to produce similar spectral properties of the matrix equation and be free of the low-frequency and oversampling breakdowns.

5.2 Future Work

- It is important to emphasize that MoM testing of SVS-EFIE-J in the Sobolev space $H_{div}^{-1/2}(S)$, eliminates the oversampling and low-frequency breakdowns, while the MoM solution of the SVS-EFIE-M in the simpler $L^2(S)$ space eliminates such breakdowns also. However, internal resonances of SVS-EFIE remain unaltered. Remedies for this internal resonance breakdown require further investigation.

- The spectral properties of the MoM solution of regular EFIE and MFIE on a PEC sphere in [45] mimic those of RWG MoM solution for arbitrary smooth PEC objects. Similarly, spectrum of the matrix equation resultant from the MoM discretization of the SVS-EFIE is expected to mimic that of its continuous operator. Indeed, this is yet to be demonstrated numerically, which is subject of future work.

Bibliography

[1] J.-M. Jin, “The Finite Element Method in Electromagnetics,” 2nd ed. New York: Wiley, 2002.

[2] A. Taflove and S.C. Hagness, “The Finite-Difference Time-Domain Method,” 3rd ed. Norwood: Artech House, 2005.

[3] J. Aronsson, F. Ling, A. Menshov, S. Zheng, and V. Okhmatovski, “New trends in analysis of electromagnetic field in multilayered media,” in *New Trends in Computational Electromagnetics*, Ergul, Ozgur (ed.), IET, 2019.

[4] P. Kristensen, J. Mork, P Lodahl, and S. Hughes, “Decay dynamics of radiatively coupled quantum dots in photonic crystal slabs,” *Phys. Rev. B*, vol. 83, no. 7, pp. 075305–1075305-10, Feb. 2011.

[5] S. Li et al., ”Performance of V-band on-chip antennas in GlobalFoundries 45nm CMOS SOI process for mm-wave 5G applications,” *IEEE MTT-S Int. Microw. Symp.*, Philadelphia, PA, 2018, pp. 1593–1596.

[6] N. Firoozy, et al., “A controlled experiment on oil release beneath thin sea ice and its electromagnetic detection,” *IEEE Trans. Geosci. Remote Sens.*, vol. 56, no. 8, pp. 4406–4419, Aug. 2018.

[7] S. Sadeghi, K. Mohammadpour-Aghdam, K. Ren, R. Faraji-Dana and R. J. Burkholder, "A pole-extraction algorithm for wall characterization in through-the-wall imaging systems," *IEEE Trans. Antennas Propag.*, vol. 67, no. 11, pp. 7106–7113, Nov. 2019.

[8] Y. Baba and V. Rakov, "Electromagnetic models of the lightning return stroke," *J. Geophys. Res.*, vol. 112, pp. 1–17, Feb. 2007.

[9] R. F. Harrington, " Time-Harmonic Electromagnetic Fields, New York: McGraw-Hill 1961.

[10] A. Kishk and L. Shafai, "Different formulations for numerical solution of single or multibodies of revolution with mixed boundary conditions," *IEEE Trans. Antennas Propag.,* vol. 34, no. 5, pp. 666–673, May 1986.

[11] O. Ergul and L. Gurel, "Comparison of integral-equation formulations for the fast and accurate solution of scattering problems involving dielectric objects with MLFMA," *IEEE Trans. Antennas Propag.,* vol. 57, no. 1, pp. 176–187, Jan. 2009.

[12] A. Colliander and P. Yla-Oijala," Electromagnetic scattering from rough surface using single integral equation and adaptive integral method, *IEEE Trans. Antennas Propag.*, vol. 55, pp. 363–3646, 2007.

[13] P. Yla-Oijala and M. Taskinen, "Well-conditioned Muller formulation for electromagnetic scattering by dielectric objects," *IEEE Trans. Antennas Propag.,* vol. 53, pp. 3316– 3323, Oct. 2005.

[14] F. Valdes, F. P. Andriulli, H. Bagci, and E. Michielssen, "On the discretization of single source integral equations for analyzing scattering from homogeneous penetrable objects," in *IEEE Antennas Propag. Soc. Int. Symp.*, San-Diego, CA, pp. 1–4, Jul. 2008.

[15] A. W. Glisson, " Integral equation for electromagnetic scattering from homogeneous dielectric bodies," *IEEE Transactions on Antennas and Propag.*, vol. AP-32, no. 2, pp.173–175, 1984.

[16] J. R. Mautz and R. F. Harrington,"H-field E-field and combined-field solutions for conducting bodies of revolution," *Int. J. Electron. Commun.*, vol. 32, no. 4, pp. 157–164, 1978.

[17] J. Kornprobst and T. F. Eibert, "A combined source integral equation with weak form combined source condition," *IEEE Trans. Antennas Propag.*, vol. 66, no. 14, pp. 2151–2155, Apr. 2018.

[18] D. De Zutter and L. Knockaert, "Skin effect modeling based on a differential surface admittance operator", *IEEE Trans. Microw. Theory Techn.*, vol. 53, no. 8, pp. 2526–2538, Aug. 2005.

[19] T. Demeester and D. De Zutter, "Construction of the Dirichlet to Neumann boundary operator for triangles and applications in the analysis of polygonal conductors", *IEEE Trans. Microw. Theory Techn.*, vol. 58, no. 1, pp. 116–127, Jan. 2010.

[20] M. Huynen, M. Gossye, D. De Zutter and D. V. Ginste, "A 3-D differential surface admittance operator for lossy dipole antenna analysis", *IEEE Antennas Wireless Propag. Lett.*, vol. 16, pp. 1052–1055, 2017.

[21] M. Huynen, D. De Zutter and D. V. Ginste, "Rigorous full-wave resistance and inductance computation of 3-D interconnects," *IEEE Microw. Wireless Compon. Lett.*, vol. 28, no. 6, pp. 455–457, Jun. 2018.

[22] U. R. Patel and P. Triverio, "Skin effect modeling in conductors of arbitrary shape through a surface admittance operator and the contour integral method," *IEEE Trans. Microw. Theory Techn.*, vol. 64, no. 9, pp. 2708–2717, Sep. 2016.

[23] U. R. Patel, P. Triverio and S. V. Hum, “A novel single-source surface integral method to compute scattering from dielectric objects”, *IEEE Antennas Wireless Propag. Lett.*, vol. 16, pp. 1715–1718, 2017.

[24] S. Sharma and P. Triverio, ”SLIM: A Well-Conditioned Single-Source Boundary Element Method for Modeling Lossy Conductors in Layered Media,” *EEE Antennas Wireless Propag. Lett.*, vol. 19, no. 12, pp. 2072-2076, Dec. 2020, doi: 10.1109/LAWP.2020.3022593.

[25] D. Marek, S. Sharma and P. Triverio, ”A Parallel Boundary Element Method for the Electromagnetic Analysis of Large Structures With Lossy Conductors,” *IEEE Trans. Antennas Propag.*, vol. 70, no. 11, pp. 10736-10750, Nov. 2022, doi: 10.1109/TAP.2022.3188403.

[26] M. Huynen et al., ”Entire Domain Basis Function Expansion of the Differential Surface Admittance for Efficient Broadband Characterization of Lossy Interconnects,” *IEEE Transactions on Microwave Theory and Techniques*, vol. 68, no. 4, pp. 1217-1233, April 2020, doi: 10.1109/TMTT.2019.2957485.

[27] D. Bosman et al., ”Interconnect Modeling using a Surface Admittance Operator Derived with the Fokas Method,” *2022 IEEE 31st Conference on Electrical Performance of Electronic Packaging and Systems (EPEPS)*, 2022, pp. 1-3, doi: 10.1109/EPEPS53828.2022.9947108.

[28] A. Menshov and V. Okhmatovski, “Novel surface integral equation formulation for accurate broadband RL extraction in transmission lines of arbitrary cross-section,” *2012 IEEE/MTT-S International Microwave Symposium Digest*, Montreal, QC, 2012, pp. 1–3, doi: 10.1109/MWSYM.2012.6259361.

[29] A. Menshov and V. Okhmatovski, “New single-source surface integral equations for scattering on penetrable cylinders and current flow modeling in two-dimensional conductors,” *IEEE Trans. Microwave Theory Tech.*, vol. 61, pp. 341–350, No. 1, Jan. 2013.

[30] F. S. Hosseini Lori, A. Menshov, and V. Okhmatovski, "New vector single-source surface integral equation for scattering problems on dielectric objects in 2D," *IEEE Trans. Antennas Propag.,* vol. 65, no. 7, pp. 3794–3799, July, 2017.

[31] F. S. Hosseini Lori, A. Menshov, R. Gholami, J. Mojolagbe, and V. Okhmatovski, "Novel single-source integral equation for scattering problems by 3D dielectric objects," *IEEE Trans. Antennas Propag.* vol. 66, no. 2, pp. 797–807, Feb. 2018.

[32] Z. Chen, R. Gholami, J. Mojolagbe, V. Okhmatovski, "Formulation of surface-volume-surface EFIE for solution of three-dimensional scattering problems on composite dielectric objects," *IEEE Antennas Wireless Propag. Lett.,* vol. 17, no. 6, pp. 1043–1047, 2018.

[33] R. Gholami, A. Menshov, and V. Okhmatovski, "H-matrix accelerated solution of Surface-Volume-Surface EFIE for fast electromagnetic analysis of 3-D composite dielectric objects," *IEEE J. Multiscale Multiphys. Comp. Tech.,* vol. 4, pp. 152–162, May 2019.

[34] R. Gholami and V. Okhmatovski, "Surface-Volume-Surface EFIE for fast direct solution of scattering problems on general 3D composite metal-dielectric objects," *IEEE Trans. Antennas Propag.* vol. 68, no. 7, pp. 5742–5747, July 2020.

[35] O. Goni and V. Okhmatovski, "Analytic solution of Surface-Volume-Surface Electric Field Integral Equation on dielectric sphere and analysis of its spectral properties," *IEEE Trans. Antennas Propag., vol. 69, no. 12, pp. 8479-8493, Dec. 2021.*

[36] O. Goni and V. Okhmatovski, "Exact solution of new magnetic current based Surface-Volume-Surface EFIE and analysis of its spectral properties," *IEEE J. Multiscale Multiphys. Comp. Tech., vol. 7, pp. 102-116, 2022.*

[37] S. Zheng, R. Gholami, and V. Okhmatovski, "Surface-Volume-Surface EFIE for solution of scattering problems on 3D dielectric objects in multilayered media," *IEEE Trans. Microwave Theory Tech.,* vol. 66, no. 12, pp. 5399–5414, Dec. 2018.

[38] R. Gholami, S. Zheng, and V. Okhmatovski, "Surface-Volume-Surface EFIE for electromagnetic analysis of 3D composite dielectric objects in multilayered media," *IEEE J. Multiscale Multiphys. Comp. Tech.,* vol. 4, pp. 364–372, Dec. 2019.

[39] S. Zheng, R. Gholami, and V. Okhmatovski, "Surface-Volume-Surface EFIE for analysis of 3-D microwave circuits in multilayered substrates with finite dielectric inclusions," *2020 IEEE/MTT-S International Microwave Symposium Digest*, Los Angeles, CA, 2020, pp. 143–145, doi: 10.1109/IMS30576.2020.9223829

[40] D. Maystre and P. Vincent, "Diffraction d'une onde electromagnetique plane par un object cylindrique non inniniment conducteur de section arbitraire," (in French), *Optics Comm.,* vol. 5, no. 5, pp. 327–330, 1972.

[41] E. Marx, "Integral equation for scattering by a dielectric," *IEEE Trans. Antennas Propag.,* vol. 32, no. 2, pp. 166–172, Feb. 1984.

[42] L. F. Knockaert and D. De Zutter, "Integral equations for fields inside a dielectric cylinder immersed in an incident E-wave," *IEEE Trans. Antennas Propag.,* vol. 34, no. 8, pp. 1065–1067, Aug. 1984.

[43] R. E. Kleinman and P. A. Martin, "On the single integral equation for the transmission problem of acoustics," *SIAM J. Appl. Math.,* vol. 48, no. 2, pp. 307–325, 1988.

[44] P. A. Martin and P. Ola, "Boundary integral equations for the scattering of electromagnetic waves by a homogeneous dielectric obstacle," *Proc. Roy. Soc. Minburgh Sect. A,* vol. 123, pp. 185–208, 1993.

[45] D. Swatek, "Investigation of single source surface integral equation for electromagnetic wave scattering by dielectric bodies," Ph.D. dissertation, Dept. Elect. Comput. Eng., Univ. Manitoba, Winnipeg, MB, Canada, 1999. [Online]. Available: http://hdl.handle.net/1993/1699.

[46] M. S. Yeung, "Single integral equation for electromagnetic scattering by three-dimensional homogeneous dielectric objects," *IEEE Trans. Antennas Propag.*, vol. 47, no. 10, pp. 1615–1622, Oct. 1999.

[47] Z. G. Qian, W. C. Chew, and R. Suaya, "Generalized impedance boundary condition for conductor modeling in surface integral equation," *IEEE Trans. Microw. Theory Tech.,* vol. 55, no. 11, pp. 2354–2364, Nov. 2007.

[48] E. Jorgensen, J. L. Volakis, P. Meincke, and O. Breinbjerg, "Higher order hierarchical Legendre basis functions for electromagnetic modeling," *IEEE Trans. Antennas Propag.*, vol. 52, no. 11, pp. 2985–2995, Nov. 2004.

[49] A. F. Peterson, C. F. Smith, and R. Mittra "Eigenvalues of the moment-method matrix and their effect on the convergence of the conjugate gradient algorithm," *IEEE Trans. Antennas Propag.*, vol. 36, no. 9, pp. 1177-1179, Aug. 1988.

[50] A. Peterson, S.Ray, and R. Mittra "Computational Methods for Electromagnetics," *New York : IEEE Press, 1998.*

[51] Weng Cho Chew, Mei Song Tong, and Bin Hu, *Integral Equation Methods for Electromagnetic and Elastic Waves,* Morgan and Claypool, 2009.

[52] W. C. Chew, *Waves and Fields in Inhomogeneous Media,* Wiley-IEEE Press, 1999.

[53] C. T. Tai, *Dyadic Green Functions in Electromagnetic Theory,* 2nd ed. New York: IEEE bPress, 1994.

[54] D. Colton and R. Kress, (ed.) *Integral Equation Methods in Scattering Theory,* Malabar, Florida: Krieger Publishing Company, 1992.

[55] F. L. S. Hosseini, "Novel single source integral equation for analysis of electromagnetic scattering by penetrable objects," Ph.D. dissertation, Dept. Elect. Comput. Eng., Univ. Manitoba, Winnipeg, MB, Canada, 2017. [Online]. Available: https://mspace.lib.umanitoba.ca/handle/1993/32362.

[56] W. C. Chew, J.-M. Jin, E. Michielssen, and J. Song, (ed.) *Fast and Efficient Algorithms in Computational Electromagnetics,* Norwood: Artech House, 2001.

[57] J. Markkanen, C. C. Lu, X. Cao, and P. Yla-Oijala, "Analysis of volume integral equation formulations for scattering by high-contrast penetrable objects," *IEEE Trans. Antennas Propag.,* vol. 60, no. 5, pp. 2367–2374, May 2012.

[58] N. A. Khizhnyak, "Green's function of Maxwell equations in inhomogeneous media," *J. Tech. Phys.*, vol. 28, no. 7, pp. 1592–1609, 1958, (*in Russian*),

[59] E. N. Vasil'ev, *Excitation of bodies of revolution*, Moscow: Radio i Svyaz', 1987, (*in Russian*).

[60] G. C. Hsiao and R. E. Kleinman, "Mathematical foundations for error estimation in numerical solutions of integral equations in electromagnetics", *IEEE Trans. Antennas Propag.* vol. 45, no. 3, pp. 316–328, Mar. 1997.

[61] D. S. Jones, *Acoustic and Electromagnetic Waves*, Oxford University Press, 1989.

[62] M. Abramowitz and L. A. Stegun, "Handbook of Mathematical Functions with Formulas, Graphs, and Mathematical Tables ", *Nat. Bureau Standards*, 1964.

[63] J. K. Bloomfield, S. H. P. Face, and Z. Moss, "Indefinite integrals of spherical Bessel functions", *MIT-CTP/4872* , Mar. 2017.